

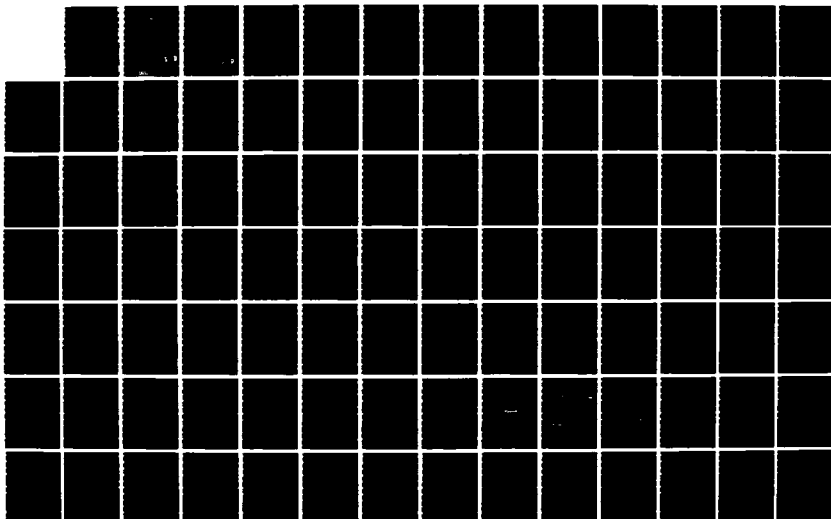
AD-A178 854

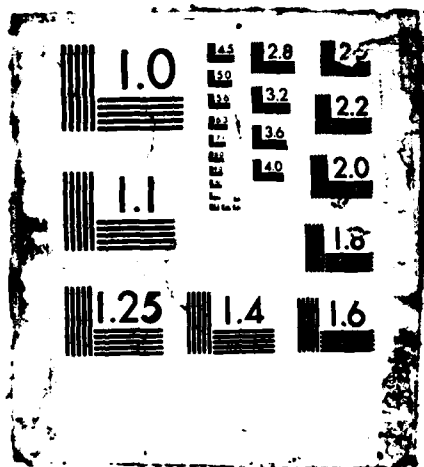
GENACS (GENERAL EM MODEL FOR THE ANALYSIS OF COMPUTER  
SYSTEMS) FREQUENCY- (U) AIR FORCE INST OF TECH  
WRIGHT-PATTERSON AFB OH SCHOOL OF ENGI F G TONKO  
DEC 86 AFIT/GE/ENG/86D-10 F/G 1/3

1/2

UNCLASSIFIED

NL





DTIC FILE COPY

AD-A178 854



GEMACS FREQUENCY-DOMAIN ANALYSIS  
TO DETERMINE THE LIGHTNING INDUCED  
ELECTROMAGNETIC SKIN CURRENT  
DISTRIBUTIONS ON AN AIRCRAFT

THESIS

Frank G. Tomko  
Captain, USAF

AFIT/GE/ENG/86D-10

DTIC  
ELECTE  
APR 13 1987  
S D E

DEPARTMENT OF THE AIR FORCE  
AIR UNIVERSITY

**AIR FORCE INSTITUTE OF TECHNOLOGY**

Wright-Patterson Air Force Base, Ohio

This document has been approved  
for public release and sale in  
unlimited quantities.

87 4 10 084

AFIT/GE/ENG/86D-10

GEMACS FREQUENCY-DOMAIN ANALYSIS  
TO DETERMINE THE LIGHTNING INDUCED  
ELECTROMAGNETIC SKIN CURRENT  
DISTRIBUTIONS ON AN AIRCRAFT

THESIS

Frank G. Tomko  
Captain, USAF

AFIT/GE/ENG/86D-10

DTIC  
ELECTE  
APR 13 1987  
S D E

Approved for public release; distribution unlimited

AFIT/GE/ENG/86D-10

GEMACS FREQUENCY-DOMAIN ANALYSIS TO DETERMINE THE LIGHTNING  
INDUCED ELECTROMAGNETIC SKIN CURRENT DISTRIBUTIONS  
ON AN AIRCRAFT

THESIS

Presented to the Faculty of the School of Engineering  
of the Air Force Institute of Technology

Air University

In Partial Fulfillment of the  
Requirements for the Degree of  
Master of Science in Electrical Engineering



Frank G. Tomko, B.S.  
Captain, USAF

December 1986

Accession For	
NTIS GRAM	<input checked="" type="checkbox"/>
DTIC TAB	<input type="checkbox"/>
Unannounced	<input type="checkbox"/>
Justification	
By	
Distribution/	
Availability Codes	
Dist	Avail and/or Special
A-1	

Approved for public release; distribution unlimited

## Acknowledgments

My thesis could not have been accomplished without the assistance and support of many dedicated individuals. The thanks begin with the sponsoring organization, AFWAL/FIESL, who created the thesis topic. CPT James Hebert, who was originally from that organization and further refined the research effort requirements, changed jobs in the middle of the thesis, but never failed to offer his assistance and expert advice. CPT Randy Jost, my thesis advisor, provided well defined thesis guidelines which allowed me to put the large thesis effort into proper perspective. His requirements were demanding, yet fair, and were the sole reason the thesis was completed with time to spare. MAJ Steve Woffinden, from the Computer Science Department, and Dr. Alan Lair, from the Mathematics Department, made up the rest of my thesis committee, and provided a refreshing outlook on my thesis approach and analysis. Special thanks go out to MAJ Woffinden for teaching me the difference between "code" and "program". Jeff D. Sweet and Teresa McKinney of AFWAL/AARI-3, deserve a note of thanks for all of their support. Finally, I could never have finished this effort without the love and support of my wife, Cindy, and the unknowing patience of my three children, Trae, Ben, and Sara.

Frank G. Tomko

## Table of Contents

	Page
Acknowledgments . . . . .	ii
List of Figures . . . . .	v
List of Tables . . . . .	vii
Abstract . . . . .	viii
1. Introduction . . . . .	1
Lightning . . . . .	3
Lightning and Aircraft . . . . .	4
Background . . . . .	5
Problem . . . . .	9
Scope . . . . .	9
Assumptions . . . . .	10
Analysis . . . . .	10
Synopsis . . . . .	11
2. Theory . . . . .	12
Field Integral Equations . . . . .	12
Method of Moments . . . . .	14
Banded Matrix Iteration . . . . .	16
Time-Domain Programs . . . . .	20
Actual Lightning Measurements . . . . .	22
Frequency-Domain Conversions and Comparisons . . . . .	22
Frequency and Length . . . . .	24
3. Analysis . . . . .	26
GEMACS Manuals . . . . .	26
GEMACS Installation and Testing . . . . .	28
Wire Grid Model . . . . .	29
Lightning Channel Models . . . . .	35
GEMACS Program File . . . . .	41
GEMACS Operations . . . . .	45
GEMACS Output . . . . .	47
4. Results and Conclusions . . . . .	55
Segments of Interest . . . . .	56
Ground Plane -vs- No Ground Plane . . . . .	58
MOM with BMI . . . . .	60
Results . . . . .	63
Actual Lightning Strike Results . . . . .	64
T3DFD Results . . . . .	72
GEMACS Results . . . . .	74

	Page
Comparisons with Airborne Results . . . . .	86
Comparisons with T3DFD Results . . . . .	89
Conclusions . . . . .	92
5. Summary and Recommendations . . . . .	95
Appendix: Constructing Wire Grid Models in GEMACS . .	99
Bibliography . . . . .	114
VITA . . . . .	120

## List of Figures

Figure	Page
1. Three View Drawing of the CV-580 Aircraft . . . .	31
2. 2-D Wire Grid Representations of the CV-580 . . .	32
3. 3-D Wire Grid Representation of the CV-580 . . .	33
4. Geometry Input Data for the CV-580 Model . . . .	36
5. Thin Wire Lightning Channel Model . . . . .	37
6. Equivalent Circuit Model of the nth Segment . . .	39
7. Current Source Circuit Representation . . . . .	40
8. Current Source Driving a Node Connected to m Segments . . . . .	40
9. Current Flow Diagram . . . . .	40
10. VMS Command File for GEMACS Operations . . . .	47
11. Sample INPUT Module Wire Segment Data . . . . .	49
12. End of INPUT Module Checkpoint . . . . .	48
13. MOM Module Start-Up Procedure . . . . .	50
14. MOM Module Task Execution . . . . .	51
15. Sample MOM Module Segment Current Data . . . . .	52
16. End of MOM Module Checkpoint . . . . .	53
17. Segments of Interest . . . . .	57
18. CV-580 MGL and FPD Sensor Locations . . . . .	65
19. Measured Aircraft Surface Current Waveforms . . .	67
20. Transformation of the Source Current . . . . .	68
21. Transformation of the Forward Fuselage Sensor Response . . . . .	68
22. Example of the Transfer Function Generation Procedure . . . . .	69
23. Linear Plot of the Forward Fuselage Transfer Function . . . . .	70

24.	Actual Aircraft Transfer Functions . . . . .	71
25.	T3DFD Generated Results . . . . .	73
26.	Lightning Channels Current Distribution at 5 MHz . . . . .	76
27.	Segments Representing Actual Sensor Locations . .	79
28.	Aft Fuselage Transfer Function . . . . .	81
29.	Forward Fuselage Transfer Function . . . . .	82
30.	Right Wing Transfer Function . . . . .	83
31.	Left Wing Transfer Function . . . . .	84
32.	Actual and Predicted Transfer Functions . . . . .	87
33.	GEMACS and T3DFD Predicted Transfer Functions . .	90

List of Tables

Table	Page
1. Comparison of Ground Plane and No Ground Plane Predicted Segment Currents . . . . .	59
2. Comparison of BMI and MOM Predicted Segment Currents . . . . .	62
3. Acronym Identifiers for Segments of Interest . .	80

Abstract

A frequency-domain electromagnetic (EM) analysis of an aircraft's EM interaction with lightning is performed by using the General EM Model for the Analysis of Complex Systems (GEMACS) to determine the EM skin current distributions on the surface of a FAA CV-580 aircraft. The Method of Moments (MOM) is incorporated in GEMACS to provide an approximate solution to Maxwell's integral equations and to determine the aircraft surface currents. A 384 segment wire grid model of the CV-580 and lightning channels is constructed for the analysis; two variations of modelling the channels are implemented. The GEMACS analysis is performed for frequencies of 0.5 MHz to 5.0 MHz, in 0.5 MHz increments. The GEMACS' predicted segment currents are used to derive wire grid frequency-domain transfer functions which are compared to: (1) actual aircraft transfer functions obtained from in-flight lightning measurements, and (2) transfer functions generated from a previously performed time-domain three-dimensional finite difference (T3DFD) EM program analysis. Results show that GEMACS can be implemented to adequately predict lightning induced aircraft skin current distributions and associated aircraft resonant frequencies. Also, GEMACS provides more EM interaction information than T3DFD and, based on CPU run times, predicts this information much more efficiently.

## 1. Introduction

This thesis compares the results of a frequency-domain electromagnetic (EM) analysis of an aircraft's EM interaction with lightning to in-flight, measured lightning data and to the results of a time-domain analysis. The frequency domain analysis is performed by using the General EM Model for the Analysis of Complex Systems (GEMACS), developed by the BDM Corporation and sponsored by Rome Air Development Center, to determine the skin current distribution throughout the surface of a CV-580 aircraft. The major tasks accomplished during this effort include:

- a. The GEMACS code was modified and installed on the AFIT VAX computer.
- b. The code was tested to verify proper installation and to assure all GEMACS modules were operating.
- c. A wire grid model of the CV-580 was constructed in accordance with the GEMACS Engineering and User Manuals (19; 20).
- d. Three methods of simulating the lightning channel were investigated; two were implemented.
- e. The GEMACS analysis was performed to validate the prediction of the EM coupling to the aircraft from an incident EM pulse wave at selected frequencies from near dc to a maximum of 5MHz, and from direct attachments at a set of the direct attachment/exit locations sampled at 10 frequencies.

The output data obtained from GEMACS were magnitudes of the current response at various locations on the CV-580, thereby providing discrete skin current distributions as a function of frequency due to the input lightning current.

f. The predicted aircraft skin currents were divided by the magnitude of the input current surge which provided predicted aircraft transfer functions.

g. The results of the analysis were compared to actual lightning data measured on a CV-580 aircraft during a two year in-flight characterization research program (36; 16) and to results of a time-domain three-dimensional finite difference computer program (T3DFD) analysis (15).

h. The efficiency of the GEMACS program relative to the T3DFD program efficiency was assessed.

The wire grid model of the CV-580 was simulated in computer code in a manner suitable for analysis by GEMACS. The actual lightning data was measured by the Air Force Wright Aeronautical Laboratories Atmospheric Electricity Hazards Group (AFWAL/FIESL), Wright-Patterson AFB, Ohio (36; 16). The Rymes' T3DFD program was used by CPT James Hebert at AFWAL/FIESL to perform a time-domain analysis of the CV-580 aircraft/lightning interaction. The end products of the analysis are graphs of several predicted aircraft skin current transfer functions as a function of frequency. A detailed investigation of GEMACS' capability to accurately predict aircraft skin current distributions was accomplished.

## Lightning

Thunderstorms produce visible electrical discharge known as lightning. Lightning may discharge between parts of the same cloud, from one cloud to another, or from a cloud to the ground (48:1). In each case, the air must be ionized before a discharge can occur (43:67). The process by which this ionization takes place in the free atmosphere is extremely complex. This is due to the irregular distributions of the charge source through a large, essentially non-conducting, cloud volume and the ion-density in any atmospheric path (30:90-1).

The sequence of events leading to common streak lightning begins when two charge sources attain a potential difference of the order of several thousand volts per centimeter (48:1). At that time, several stepped leaders begin making their way towards earth in an exploratory manner along irregular paths of least resistance between the charge sources, forming several highly ionized paths through the sky (30:90-1). These paths race towards the earth. One path wins. This path approaches the earth carrying the high potential of the cloud charge center. As the high potential nears the earth (at 100 to 200 feet), a streamer of opposite polarity forms and surges up from the earth to meet the downward streamer. When these two streamers join, the lightning channel is neutralized and the channel expands faster than the speed of sound causing the

characteristic clap of thunder (14). The branches which did not win the race to earth are also neutralized causing the brilliant light display across the sky. The neutralization process continues up into the cloud where main cloud charge centers (up to 100 Coulombs) are dissipated. If only one charge center is neutralized, the lightning flash may only consist of one lightning stroke. If more than one is neutralized, the entire flash may consist of several subsequent strokes following the already ionized main channel. Thus, lightning is a rapidly pulsating phenomenon in which all strokes in a given flash take essentially the same path.

#### Lightning and Aircraft

Aircraft between the charge sources can be "struck" by the lightning and become part of the high current channel (30:90-2). When lightning strikes good conductors that are properly grounded, damage is negligible. However, lightning poses a very serious threat to the airborne craft's instrumentation and other unprotected electronics (9:i). Since it is virtually impossible to determine when a lightning strike will occur, it is necessary to provide constant, reliable protection for the aircraft's flight-critical components (37). The increasing importance of characterizing lightning and its effects is indicated by the large number of publications concerning this topic (7; 18; 25; 30; 31; 32; 34; 35; 38; 39; 42; 43; 50). The fact that some aircraft may be unable to fly

after being struck by lightning (1:1) further increases the importance of studying and understanding these effects.

Aircraft skin currents caused by lightning strikes induce EM fields on and within the aircraft (8; 10; 11; 15). The first step in understanding and analyzing lightning EM interaction with aerospace vehicles is to understand how current and charge, induced by lightning, are distributed on the aircraft's surfaces (29:2,16). This information is then used to make further predictions of how the induced fields can affect the aircraft flight critical components as they enter the aircraft through apertures and joints (14; 25; 29; 32). Finally, steps can be taken to protect the sensitive electronic components (18; 27; 31; 35; 49).

#### Background

Several recent developments have resulted in an increased interest in the computer-aided analysis of the EM interaction of lightning with aircraft. Data from the recent WC-130 (39:2-4; 23:12) and CV-580 (40) in-flight lightning characterization programs have shown the lightning threat environment to have "significant spectral content in the aircraft resonant regions 2 - 20 MHz" (5:2). Lightning protection requirements are becoming better defined and organized with the introduction of a Military Standards draft, "Lightning Protection of Aerospace Vehicles and Hardware", currently under review by the U.S. Air Force (14). However,

EM analysts and aircraft designers are faced with the task of satisfying many different requirements other than those for lightning protection. Requirements for protection from other EM threats such as nuclear EM pulse (NEMP), as well as for EM compatibility (EMC) are combined with requirements for lighter aircraft (27; 28). Balanced protection from all EM threats must be provided with the minimum of additional weight and costs. These developments emphasize the necessity for accurate computer-aided EM interaction analysis tools for the design of protection for tomorrow's aerospace vehicles.

One method used to simplify the complicated EM analysis consists of dividing the interaction process into external and internal interactions (26; 33:173; 47). The external interaction consists of the lightning's distribution on the aircraft's surface. The internal interaction consists of the coupling, propagation, and penetration of the energy into the internal system circuits. Theoretically, these two processes are not independent, especially when apertures are electrically larger than the wavelength of the EM threat (47:62; 33:200). However, when the mutual coupling between the processes is weak, the internal components do not affect the external charge and current distributions. In these cases, the analysis is greatly simplified by decoupling the external and internal processes.

A large number of EM computer programs have been developed to assist in the analysis of external interaction of EM threats with aircraft using this "weak coupling" assumption

(3:156; 10). AFWAL/FIESL has reviewed and examined many of these programs for their suitability as a lightning protection analysis and design tool (27; 2:2-4). It was found that several programs exist which are applicable to lightning and EMP interaction and coupling. However, problems which the programs could address were too specific, as certain programs were better suited at solving one particular EM problem and poorly suited at solving others. To solve a series of related but slightly different problems, the user would need many different programs as well as the facilities and resources to maintain these programs. These factors have led many analysts to search for a centrally-maintained general purpose EM computer program applicable to a wide class of EM problems.

One possible candidate for the EM program is the GEMACS (12; 19; 20; 21; 44; 45). Many aspects of the program, make it particularly attractive for the analysis of the lightning/aircraft EM interaction event. Resident within the single GEMACS program are two widely used and fairly general physics formulations: the method of moments (MOM) and the geometrical theory of diffraction (GTD). These formulations have allowed wide applications of the GEMACS program to EM problems dealing with EMP, EMC, ECM, ECCM, radar cross section, jamming susceptibility, antenna performance, EM radiation and scattering, and, most recently, the analysis of the lightning/aircraft interaction event (45).

A recent preliminary analysis has demonstrated GEMACS' applicability to the aircraft/lightning external EM

interaction problem (5). The BDM Corporation, under supervision of the U.S. Air Force's Atmospheric Electricity Hazards Protection Advanced Development Program, modified and implemented GEMACS to predict the skin current distributions on an advanced composite helicopter testbed. The results emphasize GEMACS ease of use, including generation of structure geometry, selection and set-up of physics, and computation of surface currents (5:4). Although lightning induced skin currents were predicted on the helicopter, no measured, in-flight lightning data is available for this aircraft to validate the analysis predictions.

Other programs have been used to analyze the EM interaction of lightning with aircraft, but at a considerable cost in major mainframe CPU time. For example, the Rymes' T3DFD program (41) has been used to successfully predict the electromagnetic skin current distributions on the surface of the CV-580 (15). This time-domain program provides an accurate but very expensive prediction technique (14; 50:ii). In addition to the high cost disadvantage associated with time-domain programs, the majority of the present aperture diffusion and joint coupling EM models are frequency-domain models (14). It is believed that the frequency-domain based GEMACS program can be employed as effectively as the T3DFD program, but much more efficiently (14).

## Problem

The main objectives of this study are to determine the capability and efficiency of the GEMACS program to predict aircraft skin current distributions. The results of a GEMACS frequency-domain EM analysis of an aircraft's EM interaction with lightning will be compared to in-flight, measured, lightning data. Also, the efficiency of the GEMACS program will be compared to the T3DFD program efficiency.

## Scope

This study will use the GEMACS program to compute the EM skin current distribution on the surface of a CV-580 aircraft. The author will install a modified form of GEMACS Version 3 on the AFIT VAX computer system and implement the program for analysis of the EM interaction event. The GEMACS analysis will be performed, using a wire grid model of the CV-580, and will result in predicted current magnitudes on the surface of the model. The results of the analysis will be compared to data from actual CV-580 lightning strikes and to T3DFD results. The CPU run time efficiency of GEMACS will be assessed.

The study will not consider the problem of external to internal EM interaction. The induced fields on the surface of the aircraft will enter the vehicle through joints and apertures. Determination of the induced internal EM fields is

the next step in understanding ways to protect the aircraft from the EM threat of a lightning strike.

### Assumptions

One major assumption is necessary for this analysis to be performed. The assumption is that the aircraft's internal structures do not affect the external charge and current distributions. The analysis is then simplified by separating the external and internal interaction processes. This analysis will only consider the external interactions. The assumption is valid when aircraft's apertures are electrically small with respect to the wavelength of the induced EM fields.

### Analysis

This section provides an executive-type summary of the thesis analysis, results, and conclusions. A GEMACS analysis using a 384 segment CV-580 aircraft/lightning channel wire grid model was performed for frequencies of 0.5 MHz to 5.0 MHz, in 0.5 MHz steps. The results of the analysis included predicted segment currents as a function of the analysis frequencies. The predicted currents were divided by the predicted magnitude of the input current, representing the lightning source, to form wire grid current transfer functions with respect to frequency. These transfer functions were compared to aircraft transfer functions derived from actual

lightning measurements. The GEMACS program execution time was compared to the T3DFD program execution time. The results show that GEMACS can be implemented to adequately predict lightning induced aircraft skin currents and associated aircraft resonances. GEMACS was found to be much more efficient than the time-domain program.

### Synopsis

The thesis report consists of five chapters and an appendix. Chapter 2 describes the basic theory associated with the GEMACS program including: the MOM formulation and Banded Matrix Iteration approximation technique; time-domain programs; a lightning strike measurement method; and, frequency's relation to an object's length. Chapter 3 explains the GEMACS analysis including program installation and testing, problems with implementing the program for a lightning analysis, geometry generation, lightning channel implementation, program operations, and final output. Chapter 4 presents the results of the analysis, comparisons to the actual lightning strike data and T3DFD results, and conclusions. Chapter 5 provides a thesis summary and recommendations for follow-on efforts. The Appendix presents a detailed procedure for constructing wire grid models for implementation in GEMACS using the CV-580 as an example.

## 2. Theory

An understanding of several electromagnetic (EM) analysis concepts and techniques is necessary to allow an accurate comparison of GEMACS EM program results to actual lightning strike data and to the time-domain EM program results. Besides the theory associated with the GEMACS frequency-domain program, a discussion of how the time-domain program works as well as the method in which actual lightning strike data is converted into useable information is presented. Also, the relationship between frequency and a given structure's dimensions is discussed.

### Field Integral Equations

The GEMACS program is based on the numerical solution of integral equation representations of electric and magnetic fields. The integral equations result from applying boundary conditions to Maxwell's differential equations (50:13,14):

$$\mu \frac{\partial \vec{H}}{\partial t} = -\nabla \times \vec{E} \quad (2.1a)$$

$$\epsilon \frac{\partial \vec{E}}{\partial t} = \nabla \times \vec{H} - \sigma \vec{E} \quad (2.1b)$$

$$\nabla \cdot (\epsilon \vec{E}) = \rho \quad (2.1c)$$

$$\nabla \cdot (\mu \vec{H}) = 0 \quad (2.1d)$$

where

$H$  = magnetic field intensity [A/m]  
 $E$  = electric field intensity [V/m]  
 $t$  = time [s]  
 $\mu$  = (mu) permeability [H/m]  
 $\epsilon$  = (epsilon) permittivity [F/m]  
 $\rho$  = (rho) electric charge density [C/m<sup>3</sup>]  
 $\sigma$  = (sigma) conductivity [mho/m]  
 $\nabla \times$  = curl operator  
 $\nabla \cdot$  = divergence operator

The two most widely used integral equation formulations are the electric field integral equation (EFIE) and the magnetic field integral equation (MFIE) (20:4). The EFIE expresses structure currents in terms of a Green's function and incident electric fields. It is well suited to one-dimensional geometries such as those comprised of thin wires. The MFIE expresses surface currents in terms of the derivative of the Green's function and incident magnetic fields. It is well suited for smooth, closed surfaces. In the equations, "I" represents the magnitude of the current along a given length and "J" represents an object's surface current density.

$$\hat{r} \cdot \vec{E}^i = \frac{j\omega\mu}{4\pi} \hat{r} \cdot \int_1 IG(r, r') dl \quad (\text{EFIE})$$

$$\hat{n} \times \vec{H}^i = \frac{1}{2} \vec{J}_S - \frac{1}{4\pi} \hat{n} \times \oint_S (\vec{J}_S \times \nabla G(r, r')) d\vec{S} \quad (\text{MFIE})$$

where

$$\begin{aligned} G(r, r') &= e^{-jkr}/R && \text{; free space Green's function} \\ r' &= \text{distance from origin to observation point} \\ r &= \text{distance from origin to source point} \\ R &= |r - r'| && \text{; distance from observation to source point} \end{aligned}$$

The EFIE and MFIE equations form the foundation of most all solution methods used in exterior EM radiation and scattering problems (20:3). The solution methods provided by GEMACS are inherently based on the numerical solution of these equations.

#### Method of Moments

Of the solutions offered by GEMACS, a formulation called the Method of Moments (MOM) is particularly useful in solving general physical problems involving actual wires, wire grid models of conducting surfaces, or a combination of these. A detailed explanation of the MOM can be found in many references (6; 13; 19; 20; 46); a brief overview of the MOM formulation follows.

In linear field problems, an original functional equation is reduced to a matrix equation by a procedure called the Method of Moments (13:1). MOM is an approximation technique that relies on linearity and superposition. The MOM gives a general procedure for treating field problems, but the details of solution vary widely with the particular problem.

An important engineering problem is the EM behavior of thin wires and surface patches (13:8). These objects can be used to geometrically model various structures of interest. Within the domain of each object, a current of known functional form but unknown amplitude is proposed as the solution of the original integral equation (20:6). By linearity, the unknown amplitude constants are factored outside of the integral which can then be performed analytically or numerically (6; 22:497). Now, the field at any point in space, due to the current on any portion of the structure, can be computed. The total field at a point in space can then be found by superposition.

The surface of the structure provides the best location at which to compute the total field, since the surface boundary conditions are known (20:7). On each object the field distributions are weighted to obtain a scalar field value associated with that object. The unknown current coefficients are found by solving the resulting matrix problem. These coefficients are then used to determine the solution currents over the entire structure. Finally, the scattered fields are computed by inserting these currents into the EFIE and performing the integration numerically.

The MOM is inherently a low frequency technique (dc to about 100 MHz) that does not account for diffraction and reflection effects. This simplistic nature makes the MOM particularly suitable for lightning analysis, since potentially threatening lightning frequencies exist in the dc

to 20 MHz range. For the lightning/aircraft interaction problem, the MOM can be effectively applied if the wavelength of the EM phenomena is greater than the wavelength which corresponds to the aircraft's resonant regions. For the lightning frequency bandwidth, this criteria can be guaranteed.

#### Banded Matrix Iteration

The most time consuming operation in terms of computer resources (CPU time) in MOM programs is the decomposition of the interaction matrix. For a 384 element model, such as the one used in this analysis, the program must decompose a 384 by 384 element interaction matrix. The standard MOM solution implemented on mainframe computers may be too expensive for application to problems of this size (20:101). The Banded Matrix Iteration (BMI) technique was developed to reduce this cost. Exact solutions computed by standard methods were compared to the iterative solution generated by the BMI method (20:101). The BMI method was shown to be accurate, within a specified error, and the reduction in cost justified its use in the solution of large problems (20:101).

Before describing the BMI technique, it is necessary to address the topic of "relative efficiency". A program algorithm can be evaluated by a variety of criteria. Usually, either the rate of growth of time or the space required to solve larger and larger instances of a problem is of

particular interest. However, the efficiency can also be affected by the type of machine used to run the program. It is beyond the scope of this effort to adequately address and analyze the relative efficiency of the algorithm inherently employed by the GEMACS program. It is further assumed that computer memory requirements do not pose a problem for the user. Therefore, a program's run time will be the only measure used to compare the efficiency of the GEMACS program to the T3DFD program. It is suggested that future algorithm analyses be performed to derive the actual "relative efficiency" of the GEMACS program.

As discussed in the previous section, the MOM is a formalism for reducing an integral equation to a set of linear simultaneous equations

$$AX = b, \quad (2.2)$$

where  $A$  is the complex  $N \times N$  interaction matrix,  $X$  is the column vector of complex coefficients in the current expansion, and  $b$  is the complex excitation column vector. A variety of choices for the integral equation, expansion functions, and weighting functions are in use. It is assumed that the combination chosen leads to an nonsymmetric matrix  $A$ .

The BMI method for solving linear simultaneous equations is to decompose the matrix into a product of lower and upper triangular matrices using Gaussian elimination (20:102). The matrix elements correspond to interactions among wire and

patch segments. The interactions decrease with increasing distance between the segments. The segments can be renumbered such that the difference between segment numbers for all close-neighboring segment pairs is relatively small, say, one order of magnitude, compared to  $N$ , the number of total segments. The largest matrix elements can then be kept close to the principal diagonal of  $A$ . The matrix is separated into

$$A = L + B + U, \quad (2.3)$$

where  $B$  is a banded matrix with upper and lower bandwidths  $M$  (number of minor diagonals above and below the principal diagonal),  $L$  is the triangular portion of  $A$  below  $B$ , and  $U$  is the triangular portion of  $A$  above  $B$ . Eq (2.2) can be written as

$$BX = b - (L+U)X. \quad (2.4)$$

An iterative scheme is then

$$BX\{J+1\} = b - (L+U)X\{J\} \quad (2.5)$$

where  $X\{J\}$  denotes an approximation to the solution at the  $J$ th iteration, and  $X\{J+1\}$  denotes an approximation to the solution at the next iteration. Some starting value  $X\{0\}$  is chosen, and  $X\{1\}$  is computed from Eq (2.5). Then,  $X\{1\}$  is entered on the right-hand side, and  $X\{2\}$  is computed. If the sequence

converges, an approximate solution of Eq (2.2) is obtained.

Eq (2.5) must be solved at each iteration. The computing time is minimized by decomposing B into a product of upper triangular banded matrices,  $B_L$  and  $B_U$ . Eq (2.5) is then solved by forward elimination in

$$B_L X\{J\} = b - (L+U)X\{J\} \quad (2.6)$$

followed by back substitution in

$$B_U X\{J+1\} = Y\{J\}. \quad (2.7)$$

Since B can be a much smaller matrix than the original full matrix, A, decomposition of B results in less computing time.

Theoretically, convergence of the sequence is assured if the spectral radius (magnitude of the largest eigenvalue) of  $(L+U)/B$  is less than one. If the spectral radius is greater than one, the sequence may initially converge and then diverge. This behavior is called pseudoconvergence and has been observed in previous studies (20:104). The best approximated solution obtained during pseudoconvergence may be sufficiently accurate for some purposes, depending on the quantity of interest and the percent of error.

Once convergence has been reached, it is necessary to assess the accuracy of the resulting complex coefficients in the current expansion. The assessment employed in this thesis will consist of comparing results from the complete GEMACS MOM

solution technique for two analysis frequencies to the results obtained using the BMI technique at the same frequencies. If the error found is less than 5%, as suggested by Dr. Edgar Coffey, author of GEMACS, then the BMI generated current data will be considered valid for the entire range of operating frequencies (4). According to Dr. Coffey, the validation of results for a single resonant frequency coupled with attained convergence for all frequencies suggests accuracy and soundness of the structure geometry (4). The validity of the geometrical model itself provides confidence in the BMI method's results.

#### Time-Domain Programs

The approximate solution to the differential form of Maxwell's equations (Eq 2.1) can be obtained by using a time-domain finite difference approximation to the equations. Examples of computer programs which provide these approximate time-domain solutions include THREDE (17) and the Rymes' T3DFD program (41). The Rymes' program was originally used to analyze data from direct lightning strikes to a NOAA C-130. The program was modified for use in the analysis of data using an FAA CV-580 aircraft (15).

In the finite difference method, the derivatives found in Maxwell's equations, Eq (2.1), are replaced by a finite difference approximation. Two common approximations are:

forward differencing, given by

$$\frac{df(x)}{dx} = \frac{f(x+h) - f(x)}{h} \quad (2.8)$$

and central differencing given by

$$\frac{df(x)}{dx} = \frac{f(x+0.5h) - f(x-0.5h)}{h} \quad (2.9)$$

It can be shown that the forward differencing provides a first order approximation of the derivatives, while central differencing provides a more accurate second order approximation of the derivatives (15:9).

A decentralizing mesh is used to describe where electric and magnetic field points are located. An important aspect of the decentralizing grid is that these fields are not co-located. This provides the spatial separations required to form the derivatives which allow the fields to be alternately determined as the program advances step-wise through the grid in space and time.

The final output of the program offers magnitudes of the electric and magnetic fields as a function of space and time. Magnitudes of the current response as a function of space and time can be calculated. The CV-580 surface currents as a function of time have been accurately predicted using the T3DFD program, but at a considerable cost in CPU time (15).

One of the questions to be answered by this thesis is: Can GEMACS make these predictions more efficiently?

### Actual Lightning Measurements

The baseline purpose of any time- or frequency-domain program is to accurately predict results that would be expected from actual measurements. In-flight lightning strike data can be obtained by flying in or near active thunderstorms and then measuring and recording the EM fields and skin current distributions on the aircraft due to direct lightning attachments. Aircraft wing tips can be equipped with current shunts at the base of metal booms. The shunts can be oriented in such a way as to produce polarity waveforms when conventional current flows onto the aircraft. Skin current distributions can be measured by placing derivative magnetic field sensors at various locations on the aircraft surface (16). The measured boom current or response current can then be plotted as a function of time.

### Frequency-Domain Conversions and Comparisons

Two methods of comparing GEMACS output to that of the actual lightning strike measured data and to the time-domain results exist. One method includes converting the frequency-domain results to the time domain and directly comparing the results. This process is not trivial and would only be valid

if GEMACS is operated for a large sample of frequencies. Conversely, the second method consists of translating the actual lightning and T3DFD data, already in current-versus-time format, into the frequency domain. This straightforward procedure will be used as the method of comparison in this thesis.

The first step in the frequency domain conversion process is to remove the effects of the measurement system. For the actual lightning measurements, this process is detailed in a AFWAL report (16:4). This step is not necessary for the T3DFD analysis results since these data are predicted and not measured.

The next step is to produce the transfer function of the aircraft at the sensor locations. These transfer functions were formed using the following relationship:

$$T(f) = R(f)/S(f) \quad (2.10)$$

where  $f$  is the operating frequency in Hertz,  $T(f)$  is the frequency-domain transfer function,  $R(f)$  is the Fast Fourier Transform (FFT) of the sensor response, and  $S(f)$  is the FFT of the applied source current. Since  $R(f)$  and  $S(f)$  information is readily available from the GEMACS output, similar transfer functions can be derived for the aircraft wire grid and direct comparisons can be made.

## Frequency and Length

During the results and conclusion phase of this thesis, it will be necessary to relate operating frequency to differing segment lengths along the aircraft wire grid model. Many natural modes of resonance exist on and within the aircraft simply due to the aircraft dimensions. At very low operating frequencies, the entire aircraft will be smaller than a wavelength and the resulting current distribution will essentially be a static current distribution. As the frequency increases and wavelength decreases, the lengths of the aircraft wire grid model segments will have more affect on the segment current causing a less uniform, dynamic distribution. The transfer functions calculated for the frequency-domain analysis should illustrate that the interaction of lightning produces resonances which are more complex than those predicted by wing-to-wing dimensions (16:19-6). In fact, these resonances may closely correspond not only to direct aircraft dimensions but also to combinations of these dimensions. Careful consideration of these aircraft lengths, combinations of lengths, and their relation to the aircraft's resonant regions can provide a viable method of validating a reasonable frequency-domain analysis of lightning's interaction with aircraft.

The theoretical concepts discussed in this chapter allow comparisons of the GEMACS EM analysis data to actual lightning data and to time-domain EM program predictions. Before describing the results and comparisons, a detailed explanation of the GEMACS analysis is given in the next chapter.

### 3. Analysis

The GEMACS frequency-domain analysis to determine the lightning induced skin current distribution on the CV-580 aircraft was accomplished in several steps. The GEMACS program was installed on the AFIT VAX computer. The program was tested for simple geometries to insure that the modelling system was correctly installed and operating properly. A wire grid model of the CV-580 aircraft was constructed. Three ways of modelling the incident lightning channel were reviewed; two of the lightning channel models were implemented. A GEMACS analysis was then performed to determine the aircraft skin current distributions for selected frequencies as a result of direct attachment of lightning to a set of aircraft attachment/exit locations.

#### GEMACS Manuals

GEMACS is a well documented computer program which made it reasonably easy to use. The program is accompanied by a user manual (19), engineering manual (20), and four volume set of program documentation (21) capable of satisfying the most demanding program user.

The GEMACS User Manual contains instructions for using the program. The program is a highly user-oriented general purpose program designed for the gradual incorporation of a variety of techniques for performing electromagnetic analysis

of complex systems. The user is assumed to be an experienced electromagnetics analyst with a fair understanding of applied linear algebra. Version 3 supports all of the functions necessary for using a thin-wire/surface patch formalism with or without Geometrical Theory of Diffraction (GTD) interactions. GEMACS is implemented by sequentially calling several executable FORTRAN programs (called "modules"). The User Manual describes the commands and parameters needed to use the modules as well as commands needed to generate the structure geometry. The GEMACS program provides flexibility of control over the computational sequence by the user. Error messages, debug and trace options, and other features are included to aid the user in identifying sources of fatal errors.

The GEMACS Engineering Manual overviews the physical and mathematical methods used in the program to obtain solutions to exterior radiation and scattering problems. A variety of solution techniques are available in version 3 of GEMACS, and the relationships of these techniques to the fundamental physics of EM scattering are discussed. Also, the implementation of the physics into engineering models is given in detail. The manual has been written assuming that the reader is familiar with the parameters and theory that comprise Maxwell's equations, the method of moments formulation, and the concepts embodied in geometrical optics and diffraction. The manual is not a rigorous treatise on fundamental physics or well-known numerical techniques, but

rather it offers information on engineering concepts and models supported by GEMACS which could not easily be obtained elsewhere.

#### GEMACS Installation and Testing

The GEMACS program (version 3 dated July 1985) was installed and tested on the AFIT VAX computer running the VMS operating system. The program was sent from the Rome Air Development Center (RADC) on magnetic tape and mounted on the AFIT Information Systems Laboratory (ISL) network.

To simplify the transportation of GEMACS from one host computer to another, the source program was written in standard FORTRAN 77. This simplified the implementation of GEMACS onto the AFIT computer. However, the program in its entirety, is very large (about 100,000 lines of code including comments). Although there are only four GEMACS modules (input, MOM, GTD, output), there are over 500 other related subroutines called by these modules. Just the program itself required 10 million bytes of the VAX memory. An additional 2 million bytes were allotted for geometry generation and for the temporary files created by GEMACS as each of the modules is accessed.

Certain program characteristics are system unique and, as such, it took considerable time and effort to get the program operating properly. Version 3 was written for a 36 bit machine. Since the VAX is a 32 bit system, the program was

sent, already modified such that all GEMACS commands and user-defined variable names would consist of five characters or less. The Version 3 engineering and user manuals were not edited for these important modifications and a great deal of time was spent translating the "36-bit" commands into "32-bit" commands. A translation table was constructed and placed in each of the manuals for future GEMACS Version 3 users.

After GEMACS was installed on the AFIT VAX, the program was operated for two test cases. A sample program offered in the GEMACS Users Manual was run, and output from this first test case was in agreement with the given sample program output. The program was also tested for a simple dipole antenna. The results were as published by Harrington (13) and, as expected, gave confidence that the program was correctly installed on the AFIT computers.

#### Wire Grid Model

The GEMACS program was used to predict the current distribution on the surface of a CV-580 as a function of frequency. As stated, the MOM module, incorporating the BMI technique, was the solution method employed. Within the MOM module of GEMACS, there are two equivalent ways of modeling the CV-580, as either a wire grid model or a surface patch model can be used. Surface patch models are typically used for representations of small, smooth, uniform objects. A surface patch model for a structure of this complexity and

size was determined to be impractical. Wire gridding provides a more practical approach to modelling large structure geometries, and, as such, was the modelling method chosen for this thesis.

The method of generating a wire grid model for a complex object is given in detail in the GEMACS Engineering Manual. A step-by-step description of how the CV-580 wire grid used in this thesis was constructed is given in the Appendix. In general, before a wire grid model can be constructed, the actual dimensions of the structure geometry need to be known. Figure 1 shows a top, side, and front view of the actual dimensions of the CV-580. Figure 2 illustrates the wire grid representations of these views.

The following are some of the general guidelines, required by the GEMACS program to develop a wire grid model:

1. The length of each segment in the model should be less than one-tenth of a wavelength at the highest analysis frequency (for this case, 5 MHz).
2. The radius ( $r$ ) of a segment is related to the length ( $L$ ) by  $L/6 < r < L/5$ .
3. The length of connecting segments differ by no more than a factor of 2.

The wire grid model of the CV-580, shown in Figure 3, was developed within these guidelines and consists of 74 points and 161 segments. The maximum segment length was determined

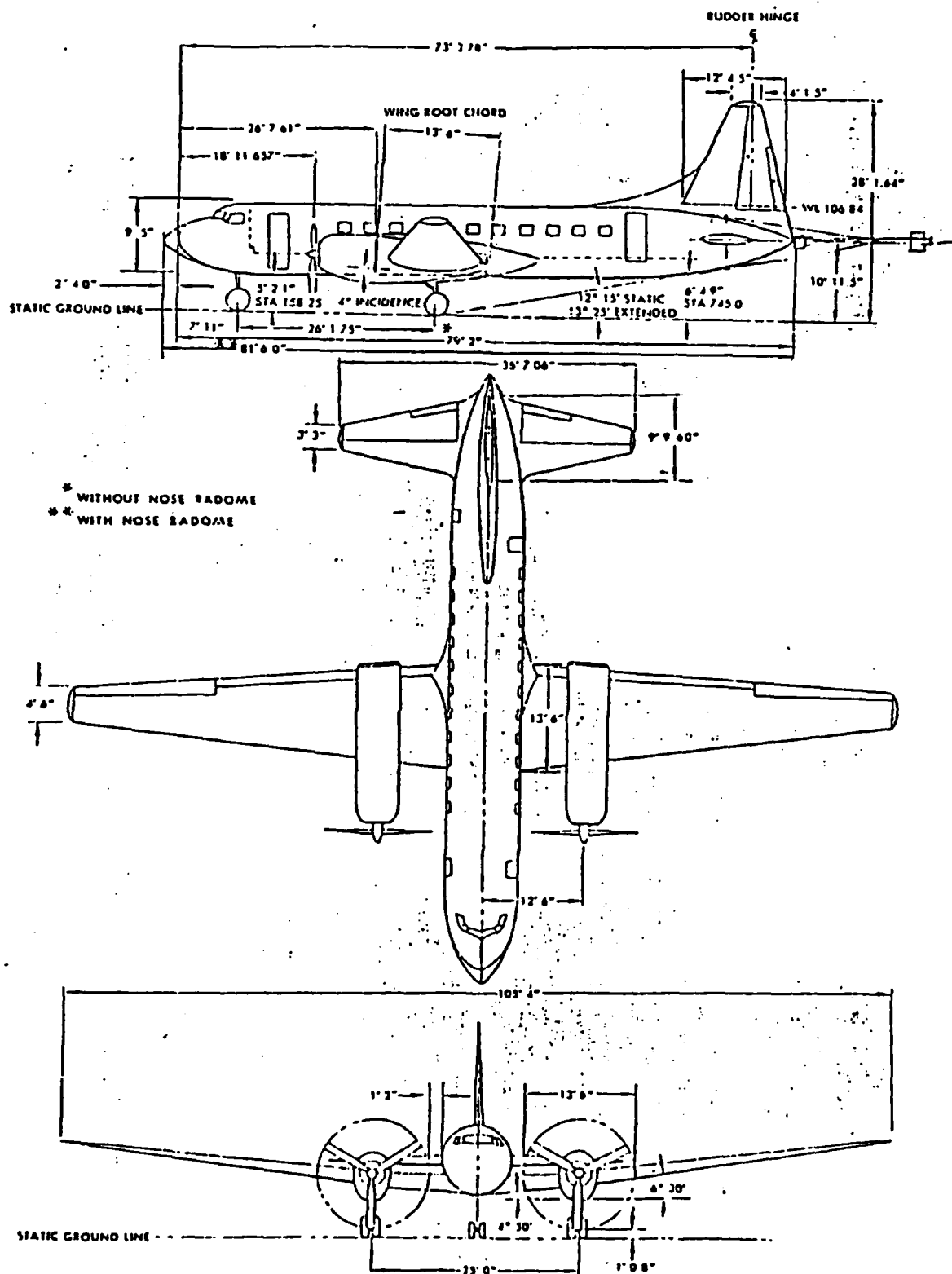


Figure 1. Three View Drawing of the CV-580 Aircraft

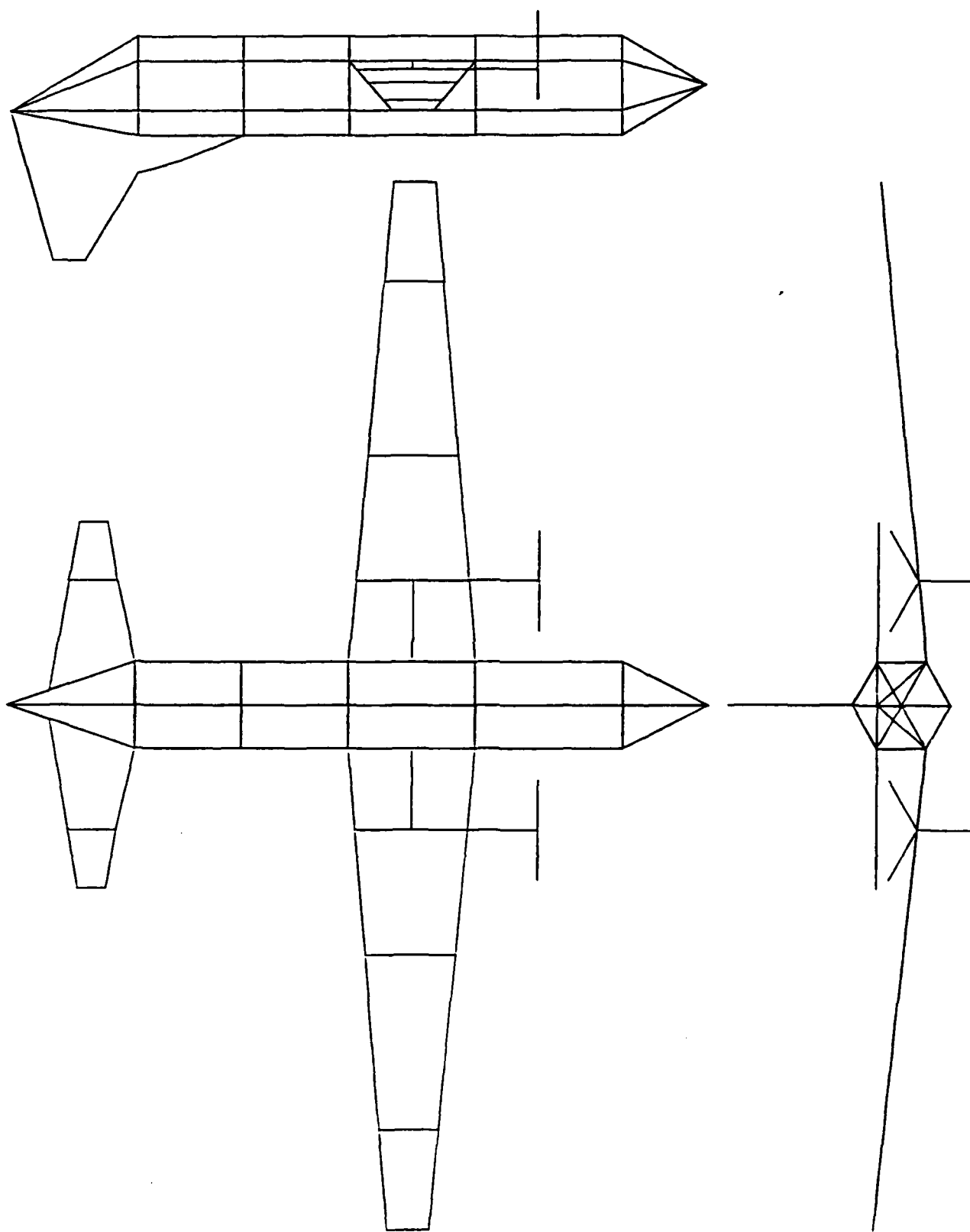


Figure 2. 2-D Wire Grid Representations of the CV-580

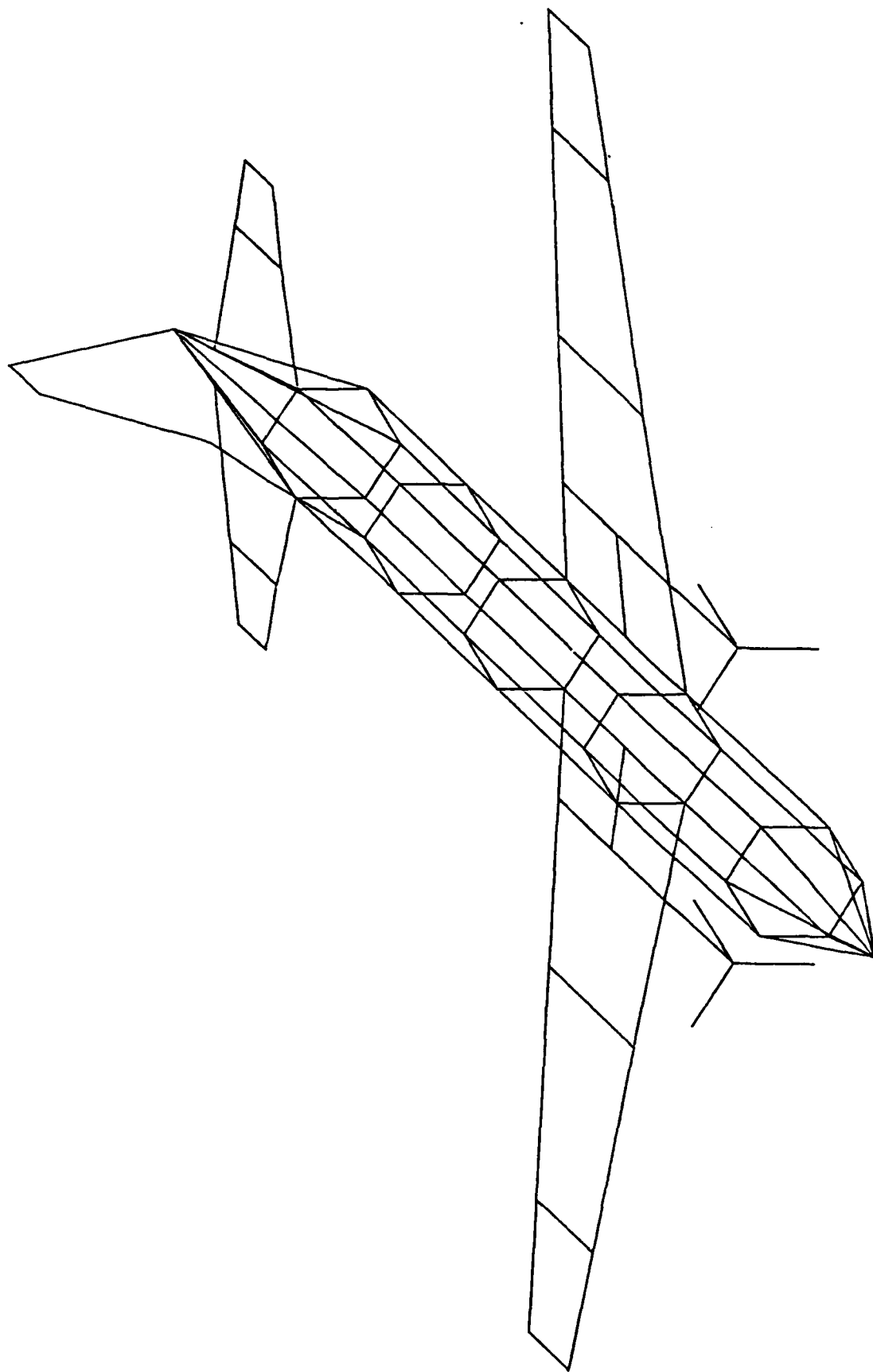


Figure 3. 3-D Wire Grid Representation of the CV-580

$$\text{max segment length} = \frac{c}{f} \times 0.1 \quad [\text{meters}] \quad (3.1)$$

to be 6 meters by using Eq 3.1. In the equation,  $c$  is the speed of light in meters per second, and  $f$  is the maximum analysis frequency in hertz (5 MHz for this analysis). The maximum segment length of 6 meters was then converted into 236 inches. The 2-D and 3-D wire grid patterns shown in Figures 2 and 3 were accomplished using the graphics capability of an Hewlett Packard HP-9000 owned and operated by the E-0 Sensor and Atmospheric Science Group of the AFWAL Avionics Laboratory (AFWAL/AARI-3), WPAFB, Dayton OH.

Geometry data is coded in GEMACS through its Geometry Input Processor (GIP). A nice feature of a strict wire grid pattern, as opposed to a hybrid wire/patch model, is that only four GIP commands are necessary to generate the entire wire model. These commands are summarized below:

SC - scale parameter. Command to scale all dimensions to a desired system of units. GEMACS then converts all units to the MKS system of units. Example: SC IN tells GEMACS that all geometry-related dimensions are given in inches.

PT - point specification. Example. PT 1 5 3 -2 places point 1 at  $(x,y,z) = (5,3,-2)$ .

RA - Radii specification. Example. RA 0.01 0.02 defines a sequential list of segment radii. The first radius called will have a value of 0.01, the second radius will be 0.02.

CP - connect points operation. The format for using the command is

CP P1 P2 S T R

where CP - connect points code.

P1 - first point

P2 - second point

S - number of segments between points

T - tag number identifying each segment

R - index to radii table entry

Example. CP 1 2 3 0 5 would result in connection of point 1 to point 2, three equal length segments with a tag of 0 between the points, and wire radius extracted from the fifth radii entry.

Figure 4 gives the GIP commands and data for the CV-580 wire grid model.

#### Lightning Channel Models

A MOM solution technique to a general EM problem requires an appropriate model for both the lightning channel and the object to be excited. A direct attachment of lightning onto an object involves two kinds of coupling phenomenon: field coupling due to the lightning channel in the atmosphere and current coupling at the attachment/exit points of the aircraft. Three lightning channel modelling methods were identified as acceptable in that they all account for these coupling phenomena. Two were actually implemented while the other is offered as an alternative method.

Before modelling the channel, it is necessary to identify

SC IN	PT 71 750.0 760.0 100.0	CP 22 25 1 0 2
PT 1 870.0 682.0 150.0	PT 72 750.0 720.0 135.0	CP 23 24 2 0 2
PT 2 870.0 682.0 90.0	PT 73 750.0 840.0 135.0	CP 23 26 1 0 2
PT 3 660.0 682.0 150.0	PT 74 750.0 760.0 30.0	CP 24 25 2 0 2
PT 4 660.0 682.0 90.0	PT 75 600.0 0.0 270.0	CP 24 26 2 0 2
PT 5 480.0 682.0 150.0	PT 76 600.0 0.0 25350.0	CP 25 27 2 0 7
PT 6 480.0 682.0 90.0	PT 77 420.0 1260.0 150.0	CP 26 28 2 0 7
PT 7 330.0 682.0 150.0	PT 78 -24660.0 1260.0 150.0	CP 27 29 2 0 5
PT 8 330.0 682.0 90.0	PT 79 -24660.0 1260.0 0.0	CP 28 30 2 0 5
PT 9 180.0 682.0 150.0	RA 7.16 10.82 11.94 16.0	CP 29 31 2 0 3
PT 10 180.0 682.0 90.0	RA 14.48 15.68 16.71 19.69	CP 30 32 2 0 3
PT 11 60.0 647.0 150.0	RA 24.03 36.29	CP 31 16.1 0 2
PT 12 0.0 630.0 150.0	CP 1 2 1 0 2	CP 31 33 2 0 3
PT 13 60.0 613.0 150.0	CP 1 3 2 0 7	CP 33 12 2 0 5
PT 14 180.0 578.0 150.0	CP 1 24 2 0 2	CP 32 34 2 0 3
PT 15 180.0 578.0 90.0	CP 1 25 1 0 2	CP 34 12 2 0 7
PT 16 330.0 578.0 150.0	CP 2 4 2 0 7	CP 35 36.1 0 3
PT 17 330.0 578.0 90.0	CP 2 24 2 0 2	CP 35 38 1 0 2
PT 18 480.0 578.0 150.0	CP 2 26 1 0 2	CP 36 37 1 0 1
PT 19 480.0 578.0 90.0	CP 3 4 1 0 2	CP 37 38 1 0 3
PT 20 660.0 578.0 150.0	CP 3 5 2 0 3	CP 38 13 1 0 9
PT 21 660.0 578.0 90.0	CP 3 27 1 0 2	CP 39 40 1 0 3
PT 22 870.0 578.0 150.0	CP 4 28 1 0 2	CP 39 42 1 0 2
PT 23 870.0 578.0 90.0	CP 4 57 1 0 5	CP 40 41 1 0 1
PT 24 990.0 630.0 120.0	CP 4 60 1 0 6	CP 41 42 1 0 3
PT 25 870.0 630.0 180.0	CP 5 6 1 0 2	CP 42 11 1 0 9
PT 26 870.0 630.0 60.0	CP 5 7 2 0 3	CP 43 44 1 0 1
PT 27 660.0 630.0 180.0	CP 5 29 1 0 2	CP 44 45 2 0 2
PT 28 660.0 630.0 60.0	CP 6 8 2 0 3	CP 45 46 1 0 2
PT 29 480.0 630.0 180.0	CP 6 30 1 0 2	CP 46 31 1 0 6
PT 30 480.0 630.0 60.0	CP 6 57 1 0 5	CP 47 48 1 0 6
PT 31 330.0 630.0 180.0	CP 6 59 1 0 6	CP 48 49 1 0 4
PT 32 330.0 630.0 60.0	CP 7 8 1 0 2	CP 48 50 1 0 4
PT 33 180.0 630.0 180.0	CP 7 9 2 0 3	CP 49 19 1 0 6
PT 34 180.0 630.0 60.0	CP 7 31 1 0 2	CP 49 51 1 0 9
PT 35 154.0 480.0 150.0	CP 8 10 2 0 3	CP 52 50 1 0 9
PT 36 140.0 410.0 150.0	CP 8 32 1 0 2	CP 50 21 1 0 6
PT 37 100.0 410.0 150.0	CP 9 10 1 0 2	CP 50 67 1 0 4
PT 38 86.0 480.0 150.0	CP 9 11 1 0 8	CP 51 52 1 0 9
PT 39 154.0 780.0 150.0	CP 9 33 1 0 2	CP 51 53 2 0 7
PT 40 140.0 850.0 150.0	CP 10 12 2 0 6	CP 53 54 1 0 5
PT 41 100.0 850.0 150.0	CP 10 34 1 0 2	CP 53 55 1 0 8
PT 42 86.0 780.0 150.0	CP 11 12 1 0 2	CP 55 56 1 0 2
PT 43 60.0 630.0 330.0	CP 12 13 1 0 2	CP 56 54 1 0 2
PT 44 105.0 630.0 330.0	CP 12 15 2 0 6	CP 54 52 2 0 7
PT 45 180.0 630.0 225.0	CP 12 43 2 0 6	CP 57 58 1 0 6
PT 46 240.0 630.0 210.0	CP 13 14 1 0 8	CP 58 59 1 0 4
PT 47 570.0 578.0 90.0	CP 9 39 1 0 7	CP 58 60 1 0 4
PT 48 570.0 480.0 100.0	CP 14 15 1 0 2	CP 59 61 1 0 9
PT 49 490.0 480.0 100.0	CP 14 16 2 0 3	CP 60 62 1 0 9
PT 50 650.0 480.0 100.0	CP 14 33 1 0 2	CP 60 71 1 0 4
PT 51 506.0 330.0 116.0	CP 14 35 1 0 7	CP 61 62 1 0 9
PT 52 634.0 330.0 116.0	CP 15 17 2 0 3	CP 61 63 2 0 7
PT 53 527.5 120.0 137.5	CP 15 34 1 0 2	CP 62 64 2 0 7
PT 54 612.5 120.0 137.5	CP 16 17 1 0 2	CP 63 64 1 0 5
PT 55 540.0 0.0 150.0	CP 16 18 2 0 3	CP 63 65 1 0 8
PT 56 600.0 0.0 150.0	CP 17 19 2 0 3	CP 64 66 1 0 8
PT 57 570.0 682.0 90.0	CP 17 32 1 0 2	CP 66 65 1 0 2
PT 58 570.0 780.0 100.0	CP 18 19 1 0 2	CP 67 66 1 0 3
PT 59 490.0 750.0 100.0	CP 18 20 2 0 5	CP 67 69 1 0 3
PT 60 650.0 780.0 100.0	CP 18 29 1 0 2	CP 67 70 1 0 3
PT 61 506.0 930.0 116.0	CP 19 30 1 0 2	CP 71 72 1 0 3
PT 62 634.0 930.0 116.0	CP 19 47 1 0 5	CP 71 73 1 0 3
PT 63 527.5 1140.0 137.5	CP 20 21 1 0 2	CP 71 74 1 0 3
PT 64 612.5 1140.0 137.5	CP 20 22 2 0 7	CP 76 75 110 0 10
PT 65 540.0 1260.0 150.0	CP 20 27 1 0 2	CP 75 56 1 0 8
PT 66 600.0 1260.0 150.0	CP 21 23 2 0 7	CP 65 77 1 0 8
PT 67 750.0 480.0 100.0	CP 21 28 1 0 2	CP 77 78 110 0 10
PT 68 750.0 420.0 135.0	CP 21 47 1 0 5	CP 78 79 1 0 9
PT 69 750.0 540.0 135.0	CP 22 23 1 0 2	END
PT 70 750.0 480.0 30.0	CP 22 24 2 0 2	

Figure 4. Geometry Input Data for CV-580 Wire Grid Model

where the aircraft will be excited, that is, where the lightning will attach and exit from the aircraft. Studies have shown (36; 16) there are many attachment/exit locations on the aircraft with two occurring most often: (1) the lightning strikes one wing tip and exits the other and (2) the attachment occurs at the nose of the craft and exits at the tail. The wing-to-wing configuration has been very well characterized in actual lightning strike studies (36; 16) as well as in T3DFD studies (15; 50); therefore, this scenario was chosen as the configuration to be modelled.

One of the two methods implemented in the analysis models the lightning entry and exiting channels as long thin conductors attached to the aircraft as illustrated in Figure 5. The model's channel attached to the right forward wing tip, exited the left aft wing tip, and continued until it was terminated into an infinite ground plane. Each of the two channels divided into at least 110 segments as dictated by the geometry generation guidelines.

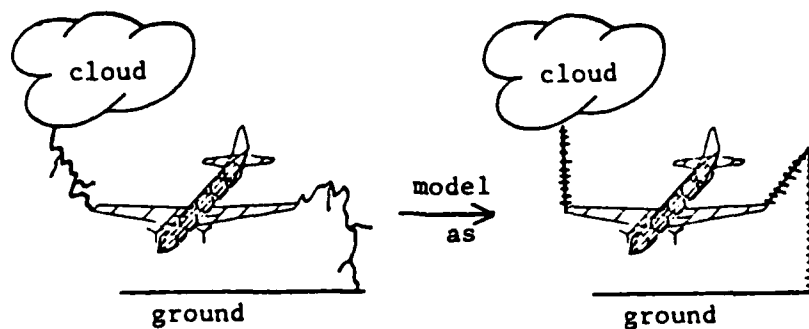


Figure 5. Thin Wire Lightning Channel Model

The lightning channels are easily created using the GEMACS geometry commands. The channel should typically be much longer than the largest dimension of the object to which it is attached (12:6), in order to assure minimal interaction between the excited segment and the aircraft segments. The length of both channels was chosen to be 20 times the length of the aircraft (12:7). Lightning currents were excited into the far ends of the lightning channel model by delta-gap voltage sources.

The second method implemented to model the lightning channel is a variation of the first and differs only by the exclusion of the ground plane. The method has a lightning channel attach to the craft and the second channel exit into free space. This scenario was used in the BDM analysis of lightning's EM interaction with an ACAP helicopter and described in their report (12). The "grounded" method better characterizes the actual lightning interaction event since the actual exiting channel attaches to an essentially infinite ground plane (earth). The main purpose of implementing the "ungrounded" method was to determine if it is a viable means of representing the lightning channel. Results of these two implemented methods are presented in the next chapter.

An alternative channel model is presented which may serve as a starting point for adding a current source to GEMACS without modification to the program, and may aid future users in similar analyses (5:3). In this method, illustrated for the nth segment in Figure 6, a current source is added to

GEMACS by finding the equivalent delta-gap voltages for each segment connected to a current driven node (source segments).

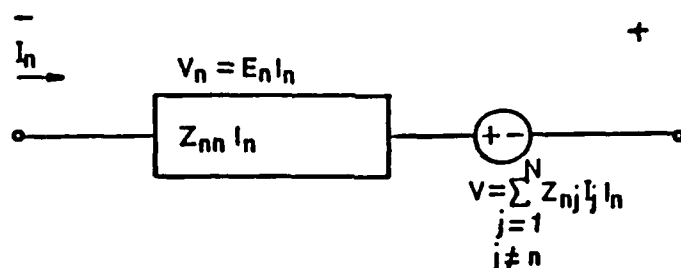


Figure 6. Equivalent Circuit Model of the nth Segment (5:7).

These delta-gap voltages are converted to an incident electric field at the center of each source segment. GEMACS can then use MOM to solve for the current in the segment and the resulting scattered fields based upon its interaction matrix. The  $Z_{nn}$  term is for the nth segment, and the  $Z_{nj}$  term is a current dependent voltage source in mutual terms. If one node of this segment is driven by a current source, it requires that an incident electric field be determined for that segment, as illustrated in Figure 7.

A more general case would be a current source exciting several segments at a node (Figure 8). The current in each segment is found by a current divider based on the admittance of the segments being driven. Figure 9 gives a current flow diagram for this case.

Delta-gap voltage sources and the incident electric field at the center of each term is determined by the segment's interaction matrix term  $Z_{ij}$ , the current to be injected  $J_j$ ,

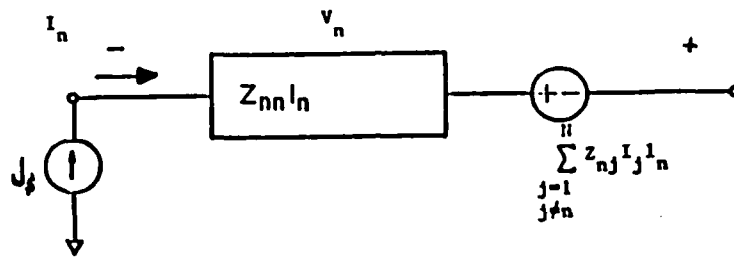


Figure 7. Current Source Circuit Representation, nth Segment Driven by Current Source,  $J_s$  (5:7).

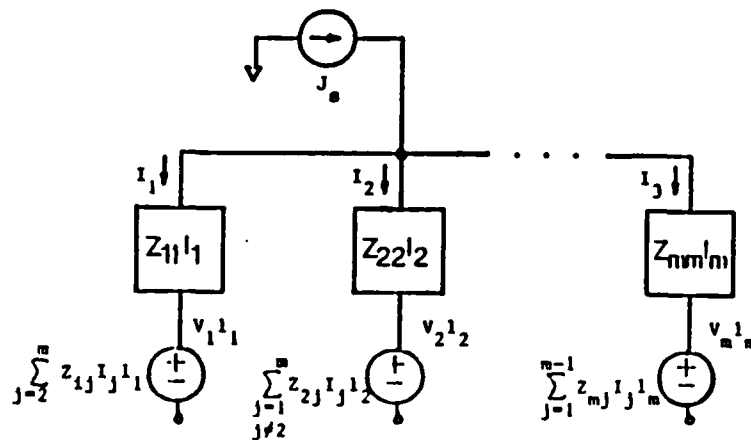


Figure 8. Current Source Driving a Node Connected to m Segments (5:7).

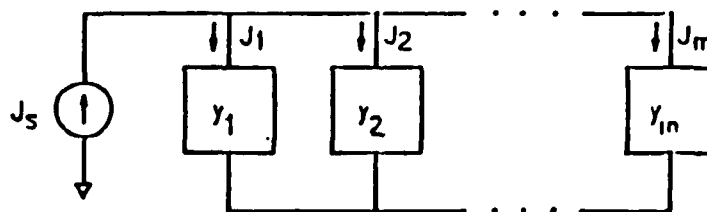


Figure 9. Current Flow Diagram (5:8).

and the mutual terms  $Z_{ij}$  as

$$-V_i = J_i Z_{ii} l_i + \sum_{j=1} Z_{ij} l_i J_j \quad (\text{delta-gap}) \quad (3.2)$$

and

$$E_i = J_j Z_{ij} \quad (\text{incident field}) \quad (3.3)$$

Once these delta-gap voltage sources are found for each driven segment, the current distribution is found on the aircraft by inputting voltage sources into the input deck of GEMACS. For other potential surface current injection techniques, the reader is referred to the report by Kunz (24).

#### GEMACS Program File

The GEMACS program permits the user to generate or define data sets and then perform operations on the data. The GEMACS inputs are in two categories. The command language directs the program execution while the geometry language describes the geometrical properties of the structure being analyzed. The wire grid model, including the lightning channels, was implemented using the geometry input processor (GIP). The GEMACS program file was written with the GEMACS command language and is described in this section.

The GEMACS command language is a free-field, keyword oriented input stream. All of the GEMACS commands are read by the INPUT module and checked for errors prior to execution of the MOM module. The only restrictions on symbolic names

provided by the user are that they have five (six on a 36 bit machine) characters or less, the first character be a letter, and other characters be strictly alphanumeric. In addition, the following reserved keywords may not be used for symbolic names:

A	C	D	N	O	R	V	X	Y	Z
CD	CR	CS	CW	CY	C1	C2	DC	DM	DP
DR	DT	DW	DX	DY	DZ	EC	ED	EI	ER
ES	EU	IS	LU	MM	NP	NR	ON	PC	PD
PL	PR	P1	P2	RC	RD	RR	R1	R2	SC
SW	T1	T2	VS	X1	X2	Y1	Y2	Z1	Z2
ABS	CDP	ECC	END	FRQ	GTD	ILP	INV	IRE	LUD
OFF	PDR	PHI	PRE	RDP	SEQ	SET	ASRC	AXIS	BAND
BCRE	BNDW	BSUB	CHPT	CLPE	CNVG	COND	EFLD	EPSR	ESRC
EXPD	FILE	GMDT	LGLG	LGLN	LGPL	LNLG	LNLN	LNPL	LOOP
MODL	MXIT	NFIL	OTPT	PLOT	PRLC	PSIN	READ	REDU	REFL
REPL	RSTT	SCDP	SEGS	SETI	SIZE	SNCS	SRDP	SRLC	SYMD
TAGS	TIME	TRSP	TYPE	VSRC	WIPO	ZCDS	ZGEN	ZIMP	ZLDS
ZMAT	CONJG	CPINC	CPNUM	DEBUG	INPUT	LABEL	PARTN	PIVOT	PRINT
PULSE	PURGE	SOLVE	STATS	TANG1	TANG2	THETA	TRACE	VALUE	WRITE

The actual program file for this GEMACS analysis was relatively short and straightforward. An example of the input deck for the long wire lightning channel with a ground plane is given with comments describing each of the GEMACS commands:

1. NFIL=23 - sets the number of temporary files, used to store intermediate program data, to 23.
2. TIME=1000 - sets the maximum execution time to 1000 CPU minutes.
3. FRQ=0.5 - sets initial analysis frequency to 0.5 MHz.
4. SETI MM - selects MOM solution technique.
5. GMDT=PLANE - names the geometry data set "PLANE".
6. LOOP 1,10 - cause commands within loop to be executed 10 times (i.e. for 10 frequencies).
7. VIN=VSRC(PLANE), V=1.,0., SEGS=162 - places a voltage of magnitude 1 V with phase 0 onto segment 162 (tip of the source channel) of the PLANE.
8. ZGEN ZMAT=ZPLNE GMDT=PLANE COND=-1 - generates an interaction matrix on PLANE, stores the decomposed matrix, ZMAT, in ZPLNE. COND=-1 sets a ground plane at  $z = 0$ .
9. BZP=BAND(ZPLNE), BNDW=161 - constructs a banded matrix from ZPLNE by banding the first 161 segments, which completely define the wire grid model of the aircraft without the lightning channels.
10. LBZ=LUD(BZP) - decomposes the banded matrix, stores the result in LBZ.
11. LBZ\*I=VIN-ZPLNE\*I, MXIT=5, CNVG=PRE, VALUE=10 - defines the equation to be solved by using the BMI method to solve for the current, I, on each segment. MXIT defines maximum number of banded

matrix iterations to 5. CNVG=PRE sets default convergence parameter and the value in percent which the CNVG parameter must be reached is 10.

12. PURGE ZPLNE,BZP,LBZ - after execution, unnecessary files are purged.
13. PRINT I - prints the calculated segment current.
14. FRQ=FRQ+0.5 - steps to next analysis frequency.
15. LABEL 1 - returns control to start of LOOP statement.
16. END - ends program execution.

This program file, in conjunction with the geometry data given earlier, represents all of the commands needed to perform the GEMACS analysis. The second lightning channel model was implemented by changing line 8 of the command file such that no ground plane was used. This was accomplished by setting the value of COND equal to zero.

An accuracy assessment of the BMI technique was performed by operating the program without the BMI approximation method at two frequencies, 0.5 MHz and 4.5 MHz. The new command file given below shows the changes necessary to accomplish the assessment:

1. NFIL=23
2. TIME=1000
3. FRQ=0.5
4. SETI=MM
5. GMDT=PLANE

```

6.  LOOP=1,2
7.  VIN=VSRC(PLANE), V=1.,0., SEGS=162
8.  ZGEN ZMAT=ZPLNE GMDT=PLANE COND=-1
9.  SOLVE ZPLNE*I=VIN - solves for the current using the
      MOM technique without BMI.
10. PURGE ZPLNE
11. PRINT I
12. FRQ=FRQ+4
13. LABEL 1
14. END

```

As shown, it is very simple to switch from one solution technique to the other. This fact alone makes GEMACS a very flexible analysis tool. Results of the accuracy assessment as well as comparisons of the two lightning channel models will be discussed in the next chapter.

### GEMACS Operations

Three GEMACS modules were used to complete this analysis: INPUT, MOM, and OUTPUT. The INPUT module reads in the GEMACS program file and geometry data. The MOM module solves for the current expansion using the MOM solution technique. The OUTPUT module prints and/or plots the resulting electric or magnetic field data. For this analysis, only segment current predictions were needed.

The GEMACS program file and geometry data may be directly

entered into the INPUT module. However, this module does not contain any type of editing features; hence, a simple typing mistake would force the user to re-enter all of the program and geometry data. Fortunately, the VMS operating system, used on the AFIT ISL VAX, allows the user to set up a command file in which system input and output control can be transferred from the keyboard/terminal to input and output files. This procedure enables the entire GEMACS analysis to be performed by one command allowing the user to input the entire analysis procedure at one time and then run the analysis to completion without constant monitoring by the user. This is necessary since about 99% of the total GEMACS run time is spent in the MOM module (GEMMOM) which, for this case, translates into over 9 CPU hours before the user can inspect the final GEMACS output data.

The VMS command file, RUNPLANE.COM, used in this analysis is shown in Figure 10. The dollar signs serve as VMS system command prompts and are necessary prior to each command in the file. All GEMACS program and geometry data, located in the PLANE.GEM file, are in accordance with the GEMACS User Manual. All output from GEMACS is placed in the PLANE.OUT file. The GEMACS INPUT, MOM, and OUTPUT modules are then executed sequentially. Finally, system I/O is transferred back to the user keyboard and terminal. The entire GEMACS analysis is accomplished by simply entering the command "@RUNPLANE" at the VMS dollar sign prompt.

```

$ ASSIGN PLANE.GEM SYSS$INPUT
$ ASSIGN PLANE.OUT SYSS$OUTPUT
$ TYPE PLANE.GEM
$ RUN GEMINP
$ RUN GEMMOM
$ RUN GEMOUT
$ DEASSIGN SYSS$INPUT
$ DEASSIGN SYSS$OUTPUT
$ TYPE PLANE.OUT

```

Figure 10. VMS Command File Used  
for GEMACS Operations

#### GEMACS Output

After RUNPLANE.COM is executed, the GEMACS output was obtained by printing the file PLANE.OUT. Samples of the output are presented below.

PLANE.GEM. The first portion of the PLANE.OUT file contains a data dump of all the program file and structure geometry commands. Program control is then transferred to the INPUT module.

INPUT Module. The function of the INPUT module is two-fold: (1) to check for errors in the input program file and GIP data and (2) to assimilate the GIP information into a useable structure geometry interaction matrix. If no errors are found in the input field, the interaction matrix is

constructed and a listing of the geometry elements with the exact coordinates and connection information for each segment in the wire grid is generated. A sample of this data is presented in Figure 11. All information is given in meters.

Upon termination, the INPUT module writes an end-of-module checkpoint, Figure 12, to be used in starting the MOM module.

GEMACS-IN EXECUTION COMPLETED ON 09/29/86 AT 10.05

TOTAL CPU TIME(SECONDS) = 32.97

CHECKPOINT NUMBER	1	STARTED AT TIME	0.553 ON LOGICAL UNIT 7
COMMON BLOCK ADEBUG WRITTEN OUT TO	CKFL.	1337 WORDS	
COMMON BLOCK AMPZIJ WRITTEN OUT TO	CKFL.	71 WORDS	
COMMON BLOCK ARGCOM WRITTEN OUT TO	CKFL.	104 WORDS	
COMMON BLOCK CSYSTH WRITTEN OUT TO	CKFL.	72 WORDS	
COMMON BLOCK DEFDAT WRITTEN OUT TO	CKFL.	506 WORDS	
COMMON BLOCK FLDCOM WRITTEN OUT TO	CKFL.	7 WORDS	
COMMON BLOCK GEODAT WRITTEN OUT TO	CKFL.	120 WORDS	
COMMON BLOCK IOFLES WRITTEN OUT TO	CKFL.	200 WORDS	
COMMON BLOCK JUNCOM WRITTEN OUT TO	CKFL.	205 WORDS	
COMMON BLOCK PARTAB WRITTEN OUT TO	CKFL.	3442 WORDS	
COMMON BLOCK SCNPAR WRITTEN OUT TO	CKFL.	755 WORDS	
COMMON BLOCK SEGMENT WRITTEN OUT TO	CKFL.	5531 WORDS	
COMMON BLOCK SYMSTR WRITTEN OUT TO	CKFL.	102 WORDS	
COMMON BLOCK SYSFIL WRITTEN OUT TO	CKFL.	36 WORDS	
COMMON BLOCK TEMPO1 WRITTEN OUT TO	CKFL.	5502 WORDS	
COMMON BLOCK GTDDAT WRITTEN OUT TO	CKFL.	14 WORDS	
COMMON BLOCK MODULE WRITTEN OUT TO	CKFL.	13 WORDS	
COMMON BLOCK INTMAT WRITTEN OUT TO	CKFL.	131 WORDS	
PERIPHERAL FILE 8 SYMBOL PLANE	NUMREC=	1	
CHECKPOINT COMPLETE AT	0.568		
ELAPSED TIME=	0.016		
CURRENT FILE LENGTH=	23704		

Figure 12. End of INPUT Module Checkpoint

MOM Module. Program control is then transferred to the MOM module which begins with a start-up procedure, Figure 13, which lists all subroutines to be called.

WIRE SEGMENT DATA

ENDPOINTS		CENTERPOINTS		RADIUS	LENGTH	END1	END2	NSEC	TAG
YN	YP	ZN	ZP	XC	YC	ZC			
22.1	17.3	3.81	2.29	22.1	17.3	3.05	0.275	1.52	0
22.1	17.3	3.81	3.81	20.8	17.3	3.81	0.424	2.67	0
19.4	17.3	3.81	3.81	18.1	17.3	3.81	0.424	2.67	0
22.1	17.3	3.81	3.43	22.9	17.0	3.62	0.275	1.70	0
23.6	16.7	3.81	3.05	24.4	16.3	3.24	0.275	1.70	0
22.1	16.0	3.81	4.57	22.1	16.7	4.19	0.275	1.52	0
22.1	17.3	2.29	2.29	20.8	17.3	2.29	0.424	2.67	0
19.4	17.3	2.29	2.29	18.1	17.3	2.29	0.424	2.67	0
22.1	16.7	2.29	2.67	22.9	17.0	2.48	0.275	1.70	0
23.6	15.0	2.67	3.05	24.4	16.3	2.86	0.275	1.70	0
22.1	16.0	2.29	1.52	22.1	16.7	1.90	0.275	1.52	0
16.8	17.3	3.81	2.29	16.8	17.3	3.05	0.275	1.52	0
14.5	17.3	3.81	3.81	15.6	17.3	3.81	0.368	2.29	0
14.5	17.3	3.81	3.81	13.3	17.3	3.81	0.368	2.29	0
16.8	16.0	3.81	4.57	16.8	16.7	4.19	0.275	1.52	0
16.8	16.0	2.29	1.52	16.8	16.7	1.90	0.275	1.52	0
14.5	17.3	2.29	2.29	15.6	17.3	2.29	0.368	2.29	0
16.8	17.3	2.29	2.54	16.6	18.6	2.41	0.398	2.51	0
12.2	17.3	3.81	2.29	12.2	17.3	3.05	0.275	1.52	0
12.2	17.3	3.81	3.81	11.2	17.3	3.81	0.303	1.90	0
10.3	17.3	3.81	3.81	9.33	17.3	3.81	0.303	1.90	0
12.2	16.0	3.81	4.57	12.2	16.7	4.19	0.275	1.52	0
10.3	17.3	2.29	2.29	11.2	17.3	2.29	0.303	1.90	0
12.2	17.3	2.29	2.29	9.33	17.3	2.29	0.303	1.90	0
12.2	16.0	2.29	1.52	12.2	16.7	1.90	0.275	1.52	0
12.2	17.3	2.29	2.29	13.3	17.3	2.29	0.368	2.29	0
12.4	19.8	2.29	2.54	12.3	18.6	2.41	0.398	2.51	0
8.38	17.3	3.81	2.29	8.38	17.3	3.05	0.275	1.52	0
8.38	17.3	3.81	3.81	7.43	17.3	3.81	0.303	1.90	0
8.38	17.3	3.81	3.81	5.52	16.7	4.19	0.275	1.52	0
8.38	16.0	2.29	4.57	8.38	16.7	4.19	0.275	1.52	0
6.48	17.3	2.29	2.29	7.43	17.3	2.29	0.303	1.90	0
6.48	17.3	2.29	2.29	5.52	17.3	2.29	0.303	1.90	0
8.38	17.3	2.29	1.52	8.38	16.7	1.90	0.275	1.52	0
4.57	17.3	3.81	2.29	4.57	17.3	3.05	0.275	1.52	0
4.57	16.4	3.81	3.81	3.05	16.9	3.81	0.505	3.18	0
4.57	16.0	3.81	4.57	4.57	16.7	4.19	0.275	1.52	0
2.29	16.7	3.05	3.05	3.43	17.0	2.67	0.398	2.50	0
0.000E+00	16.0	3.81	3.81	1.14	16.3	3.43	0.398	2.50	0
4.57	16.0	2.29	1.52	4.57	16.7	1.90	0.275	1.52	0
0.000E+00	16.4	3.81	3.81	0.762	16.2	3.81	0.275	1.58	0
0.000E+00	16.0	3.81	3.81	0.762	15.8	3.81	0.275	1.58	0
2.29	15.3	3.81	3.05	1.14	15.7	3.43	0.398	2.50	0
0.000E+00	16.0	3.81	2.29	3.43	15.0	2.67	0.398	2.50	0
0.762	16.0	3.81	6.10	0.381	16.0	4.95	0.398	2.41	0
1.52	16.0	6.10	8.38	1.14	16.0	7.24	0.398	2.41	0
0.000E+00	15.6	3.81	3.81	3.05	15.1	3.81	0.505	3.18	0
4.57	17.3	3.81	3.81	3.81	18.6	3.81	0.424	2.58	0
4.57	14.7	3.81	2.29	4.57	14.7	3.05	0.275	1.52	0
4.57	14.7	3.81	3.81	5.52	14.7	3.81	0.303	1.91	0

Figure 11. Sample INPUT Module Wire Segment Data

GEMACS START-UP PROCESSOR CALLED ON 09/29/86 AT 10.05

```
BEGIN START-UP PROCEDURE
COMMON ADEBUG READ WITH 1337 WORDS
COMMON AMPZIJ READ WITH 71 WORDS
COMMON ARGCOM READ WITH 104 WORDS
COMMON CSYSTM READ WITH 72 WORDS
COMMON DEFDAT READ WITH 506 WORDS
COMMON FLDCOM READ WITH 7 WORDS
COMMON GEODAT READ WITH 120 WORDS
COMMON IOFLES READ WITH 200 WORDS
COMMON JUNCOM READ WITH 205 WORDS
COMMON PARTAB READ WITH 3442 WORDS
COMMON SCNPAR READ WITH 755 WORDS
COMMON SEGMNT READ WITH 5531 WORDS
COMMON SYMSTR READ WITH 102 WORDS
COMMON SYSFIL READ WITH 36 WORDS
COMMON TEMPO1 READ WITH 5502 WORDS
COMMON GTDDAT READ WITH 14 WORDS
COMMON MODULE READ WITH 13 WORDS
COMMON INTMAT READ WITH 131 WORDS
PERIPHERAL FILE 8 SYMBOL PLANE NUMREC= 1
START-UP COMPLETE
MODULES PREVIOUSLY RUN: IN
```

Figure 13. MOM Module Start-Up Procedure

Execution of the module follows (Figure 14). During this stage, several tasks are accomplished. The analysis frequency is set, the source segment is excited, the interaction matrix is decomposed, and the MOM solution in conjunction with the BMI approximation technique is used to determine the complex segment current expansion. Once convergence of a solution is reached, the real, imaginary, magnitude, and phase components of the segments' currents are printed (Figure 15). Finally, an MOM end-of-module checkpoint is printed (Figure 16).

GENACS-MOM TASK EXECUTION STARTED ON 09/29/86 AT 10 05

NUMBER OF PERIPHERAL FILES AVAILABLE 23

RUN TIME SET TO 0 100E-04 CPU MINUTES

FREQUENCY SET TO 0 500 MEGAHERTZ  
WAVELENGTH 600. METERS

EXCITE GEOMETRY DATA PLANE  
EXCITATION VOLT  
EXCITATION DATA VIN

INTERACTIONS SET MM

REAL COMP 1.00 IMAG COMP 0 000E-00  
EXCITED SEGS  
162

FILL IMPEDANCE MATRIX ZPLNE  
USING BASIS FUNCTION SMCS  
ON GEOMETRY DATA SET PLANE  
SHADOWING MATRIX  
LOADS (IF SPECIFIED) IN  
FREQUENCY (MEGAHERTZ) 0.50000  
GROUND COND (PHOS/M) -1.0000  
RELATIVE PERMITIVITY 1.0000

INTERACTIONS SET MM  
END 2 SEGMENT 384 GROUNDED

EXTRACT BIZ FROM ZPLNE BANDWIDTH 161

BANDING SUB-MATRIX 1  
COLUMN 1 IN-BAND NORM= 0 1184E-05 OUT-OF-BAND NORM= 3.438  
BAND DOMINANCE FACTOR= 3443

COLUMN 384 IN-BAND NORM= 1008 OUT-OF-BAND NORM= 0.2352E-01  
BAND DOMINANCE FACTOR= 0 3950E-05

DECOMPOSE BIZ STORE RESULT IN LBZ PIVOT= N

MAX DIAG = 12781 MIN DIAG = 0.27065  
PIVOT RATIO = 34483 00

BIZ SOLUTION TO- LBZ \* I = VIN - ZPLNE \* I

MAXITR= 5 CONVRG ON PRE 8 AT  
ITERATION 1 PRED CONVR IN 0 ITERATIONS  
PRE= 100 00 IRE= 100.00 SCRE= 2.97

CONVERGENCE REACHED

FINAL VALUES-- PRE 2.68 IRE 16 37 SCRE 0 22

GEOMETRY DATA SET PLANE

\*\*\* NO LOAD FOR STRUCTURE \*\*\*

ANTENNA/LOAD PARAMETERS (SEE USERS MANUAL)

SEGMENT	INPUT (IMP(MAG))	INPUT (IMP(PHZ))	PWR INPUT	PWR LOAD	REAL Z	IMAG Z
162	3188.772	-88.949	0.287E-05	0 000E-00	5.8463622E+01	-3.1882366E+03

Figure 14. MOM Module Task Execution

(segment #)  
C6L

	REAL	IMAGINARY	MAGNITUDE	PHASE (DEG)	REAL	IMAGINARY	MAGNITUDE	PHASE (DEG)	
1	0.1369E-03	-0.7386E-04	0.1555E-03	-28.35	2	-0.5031E-04	0.2045E-04	0.5430E-04	157.9
3	-0.6126E-04	0.2399E-04	0.6579E-04	158.6	4	-0.1123E-03	0.5249E-04	0.1240E-03	154.9
5	-0.1163E-04	0.5376E-04	0.1281E-03	155.2	6	0.8744E-05	0.6750E-05	0.1105E-04	37.66
7	0.8999E-04	-0.3007E-04	0.9488E-04	-18.47	8	0.9078E-04	-0.2810E-04	0.9503E-04	-17.20
9	0.1359E-03	-0.4995E-04	0.1447E-03	-20.18	10	0.1319E-03	-0.4764E-04	0.1402E-03	-19.86
11	-0.8024E-04	0.5584E-05	0.8043E-04	176.0	12	0.5849E-04	-0.3286E-04	0.6709E-04	-29.33
13	0.1267E-03	0.4993E-04	0.1362E-03	158.5	14	-0.1321E-03	0.5109E-04	0.1416E-03	158.8
15	-0.3666E-05	0.1010E-04	0.1075E-04	109.9	16	-0.1084E-03	0.3025E-04	0.1125E-03	164.4
17	0.2277E-03	-0.8757E-04	0.2440E-03	-21.04	18	0.3623E-04	-0.3719E-05	0.3642E-04	-5.861
19	0.2378E-03	-0.7875E-04	0.2505E-03	-18.32	20	-0.4496E-03	0.1581E-03	0.4765E-03	160.6
21	-0.4483E-03	0.1573E-03	0.4751E-03	160.7	22	0.7613E-04	-0.2797E-04	0.8111E-04	-20.17
23	0.7277E-03	-0.2083E-03	0.7570E-03	-15.97	24	0.7153E-03	-0.2026E-03	0.7434E-03	-15.82
25	-0.3982E-03	0.1183E-03	0.4154E-03	163.5	26	0.6895E-04	-0.4076E-04	0.8009E-04	-30.59
27	-0.1609E-03	0.5353E-04	0.1696E-03	161.6	28	-0.4998E-03	0.1315E-03	0.5168E-03	165.3
29	0.6870E-03	-0.2435E-03	0.7289E-03	-19.52	30	0.6876E-03	-0.2441E-03	0.7297E-03	-19.54
31	-0.5968E-03	0.2554E-03	0.6492E-03	156.8	32	-0.4798E-03	0.9677E-04	0.4894E-03	168.6
33	-0.4938E-03	0.1032E-03	0.5044E-03	168.2	34	0.6402E-03	-0.1510E-03	0.6578E-03	-13.27
35	0.1411E-03	-0.4288E-04	0.1475E-03	-16.90	36	0.5131E-04	-0.1754E-04	0.5422E-04	-18.87
37	0.4544E-03	-0.1671E-03	0.4842E-03	-20.19	38	-0.1334E-03	0.4605E-04	0.1411E-03	161.0
39	-0.1365E-03	0.4985E-04	0.1453E-03	159.9	40	-0.2306E-03	0.2275E-04	0.2317E-03	174.4
41	0.4136E-05	-0.3143E-05	0.5195E-05	-37.23	42	0.1336E-04	-0.4497E-05	0.1409E-04	-18.61
43	-0.9755E-04	0.5103E-04	0.1101E-03	152.4	44	-0.8439E-04	0.4748E-04	0.9683E-04	150.6
45	0.2059E-04	0.1013E-04	0.2295E-04	26.20	46	0.6227E-05	0.1022E-04	0.1196E-04	58.64
47	-0.2604E-04	0.7825E-05	0.2719E-04	163.3	48	0.2941E-04	-0.1347E-04	0.3235E-04	-24.62
49	-0.1463E-04	0.2748E-04	0.3113E-04	118.0	50	-0.2932E-03	0.8584E-04	0.3055E-03	163.7
51	-0.2960E-03	0.8684E-04	0.3085E-03	163.6	52	0.2454E-03	-0.8997E-04	0.2614E-03	-20.14
53	0.2557E-04	-0.1264E-04	0.2852E-04	-26.31	54	0.3831E-03	-0.7193E-04	0.3898E-03	-10.63
55	0.3749E-03	-0.6782E-04	0.3810E-03	-10.25	56	-0.4655E-03	0.1429E-03	0.4869E-03	162.9
57	0.2168E-04	-0.6645E-04	0.6989E-04	-71.93	58	-0.3102E-04	0.4048E-04	0.5100E-04	127.5
59	-0.2865E-04	0.3924E-04	0.4859E-04	126.1	60	0.4156E-04	-0.1089E-03	0.1165E-03	-69.11
61	0.3260E-04	-0.1045E-03	0.1095E-03	-72.68	62	0.3318E-03	-0.2100E-04	0.3325E-03	-3.621
63	-0.1809E-03	0.1065E-03	0.2099E-03	149.5	64	0.1701E-04	-0.5268E-05	0.1781E-04	-17.21
65	0.2402E-04	-0.9236E-05	0.2573E-04	-21.03	66	0.1456E-03	-0.6770E-04	0.1606E-03	-24.93
67	0.2174E-03	-0.1295E-03	0.2530E-03	-30.78	68	-0.1069E-02	0.4508E-03	0.1160E-02	157.1
69	-0.7663E-04	0.3484E-04	0.8418E-04	155.6	70	0.2321E-04	-0.9297E-05	0.2500E-04	-21.83
71	0.2165E-04	-0.9443E-05	0.2362E-04	-23.57	72	0.8159E-04	-0.3766E-04	0.8986E-04	-24.78
73	0.1448E-03	-0.7174E-04	0.1615E-03	-26.35	74	0.1273E-03	-0.6192E-04	0.1415E-03	-25.95
75	0.1032E-03	-0.4915E-04	0.1143E-03	-25.48	76	-0.3902E-03	0.1774E-03	0.4286E-03	155.5
77	-0.1000E-03	0.3718E-04	0.1067E-03	159.6	78	0.1252E-04	-0.1062E-05	0.1256E-04	-4.850
79	0.9977E-05	-0.3145E-06	0.9982E-05	-1.805	80	0.1037E-03	-0.4415E-04	0.1127E-03	-23.08
81	-0.1293E-03	0.6144E-04	0.1431E-03	154.6	82	-0.1342E-03	0.6420E-04	0.1487E-03	154.4
83	0.1259E-03	-0.6994E-04	0.1440E-03	-29.05	84	-0.7553E-04	0.2490E-04	0.7953E-04	161.8
85	-0.7761E-04	0.2496E-04	0.8153E-04	162.2	86	-0.4223E-04	0.4921E-04	0.6484E-04	130.5

Figure 15. Sample MOM Module Segment Current Data

```

TOTAL CPU TIME(SECONDS) =      35626.49

CHECKPOINT NUMBER      2 STARTED AT TIME      593.776 ON LOGICAL UNIT      7
COMMON BLOCK ADEBUG WRITTEN OUT TO      CKFL, 1337 WORDS
COMMON BLOCK AMPZIJ WRITTEN OUT TO      CKFL, 71 WORDS
COMMON BLOCK ARGCOM WRITTEN OUT TO      CKFL, 104 WORDS
COMMON BLOCK CSYSTM WRITTEN OUT TO      CKFL, 72 WORDS
COMMON BLOCK DEFDAT WRITTEN OUT TO      CKFL, 506 WORDS
COMMON BLOCK FLDCOM WRITTEN OUT TO      CKFL, 7 WORDS
COMMON BLOCK GEODAT WRITTEN OUT TO      CKFL, 120 WORDS
COMMON BLOCK IOFLES WRITTEN OUT TO      CKFL, 200 WORDS
COMMON BLOCK JUNCOM WRITTEN OUT TO      CKFL, 205 WORDS
COMMON BLOCK PARTAB WRITTEN OUT TO      CKFL, 3442 WORDS
COMMON BLOCK SCNPAR WRITTEN OUT TO      CKFL, 755 WORDS
COMMON BLOCK SEGMNT WRITTEN OUT TO      CKFL, 5531 WORDS
COMMON BLOCK SYMSTR WRITTEN OUT TO      CKFL, 102 WORDS
COMMON BLOCK SYSFIL WRITTEN OUT TO      CKFL, 36 WORDS
COMMON BLOCK TEMPO1 WRITTEN OUT TO      CKFL, 5502 WORDS
COMMON BLOCK GTDDAT WRITTEN OUT TO      CKFL, 14 WORDS
COMMON BLOCK MODULE WRITTEN OUT TO      CKFL, 13 WORDS
COMMON BLOCK INTMAT WRITTEN OUT TO      CKFL, 131 WORDS
PERIPHERAL FILE 8      SYMBOL PLANE NUMREC= 1
PERIPHERAL FILE 10     SYMBOL VIN NUMREC= 1
PERIPHERAL FILE 11     SYMBOL I NUMREC= 1
PERIPHERAL FILE 13     SYMBOL UPR NUMREC= 384
PERIPHERAL FILE 14     SYMBOL LWR NUMREC= 384
CHECKPOINT COMPLETE AT      595.832
ELAPSED TIME=      2.055
CURRENT FILE LENGTH=      2005748

```

Figure 16. End of MOM Module Checkpoint

OUTPUT Module. For this analysis, only segment current information was needed. As such, the OUTPUT module execution begins with a start-up procedure, lists the number of temporary files used, sets the operating frequency, and concludes with a module checkpoint. The main purpose of this module is to print and plot field patterns generated by previous modules, such as radar cross section patterns due to the predicted segment currents. Should the user wish further results from the same program file and geometry data (perhaps another pattern cut) he can begin execution from OUTPUT module checkpoint and not have to resolve the interactions matrix.

This chapter dealt with the actual GEMACS computations. It described the implementation and testing of the GEMACS program, GEMACS manuals, CV-580 wire grid model, lightning channel models, operation of the GEMACS program, and GEMACS output. The next chapter presents the results and conclusions of the analysis.

#### 4. Results and Conclusions

One of the two main objectives of this thesis was to qualitatively determine the ability of GEMACS to predict lightning induced EM skin current distributions on an aircraft. This determination was accomplished by comparing GEMACS predicted CV-580 wire grid segment current transfer functions to those aircraft frequency-domain transfer functions generated in previous studies (16; 36). Prior to this qualitative analysis, the accuracy of the Banded Matrix Iteration (BMI) approximation technique employed in conjunction with the GEMACS MOM module as well as the effects of adding a ground plane to the aircraft/lightning channel model were quantitatively investigated. It was found that the accuracy afforded by the BMI technique using a bandwidth (number of banded segments) of 161 segments is acceptable. Also, results justify the incorporation of a ground plane in the wire grid model. Finally, the results of the qualitative analysis, using a 384 segment CV-580 wire grid representation with grounded lightning channel, show that GEMACS, implemented under the conditions outlined in the previous chapter, is capable of predicting aircraft EM surface currents in the frequency range of dc to 5.0 Mhz.

The other main objective was to compare the relative efficiency of the frequency-domain GEMACS program to a time-domain three-dimensional finite difference (T3DFD) program. The T3DFD program had been previously implemented to

determine CV-580 EM surface currents as a function of time and space (15). The time domain information was transformed into the frequency domain for comparisons with the actual, measured data. Although the comparisons reveal good correlation, the GEMACS results provided additional information about lightning's EM interaction with aircraft which was not predicted by the time domain program, particularly near dc. Furthermore, the GEMACS program was found to be much more efficient than the T3DFD program, based on mainframe central processing unit (CPU) run times.

#### Segments of Interest

The current levels induced on several of the segments in the CV-580 wire grid model and present on the associated lightning channel models were investigated. In a wire representation of this size, it would be impractical to plot or graph the current response on each and every segment, although this information is available as output from the GEMACS program. Also, for the actual lightning measurements, current information was available at only 4 sensor locations on the CV-580. Predicted currents on selected segments other than where those sensors were located were inspected; however, no corresponding in-flight measurements are available to validate those predictions.

Twelve segments, labeled on Figure 17, were chosen as a selective representation of the overall current distributions

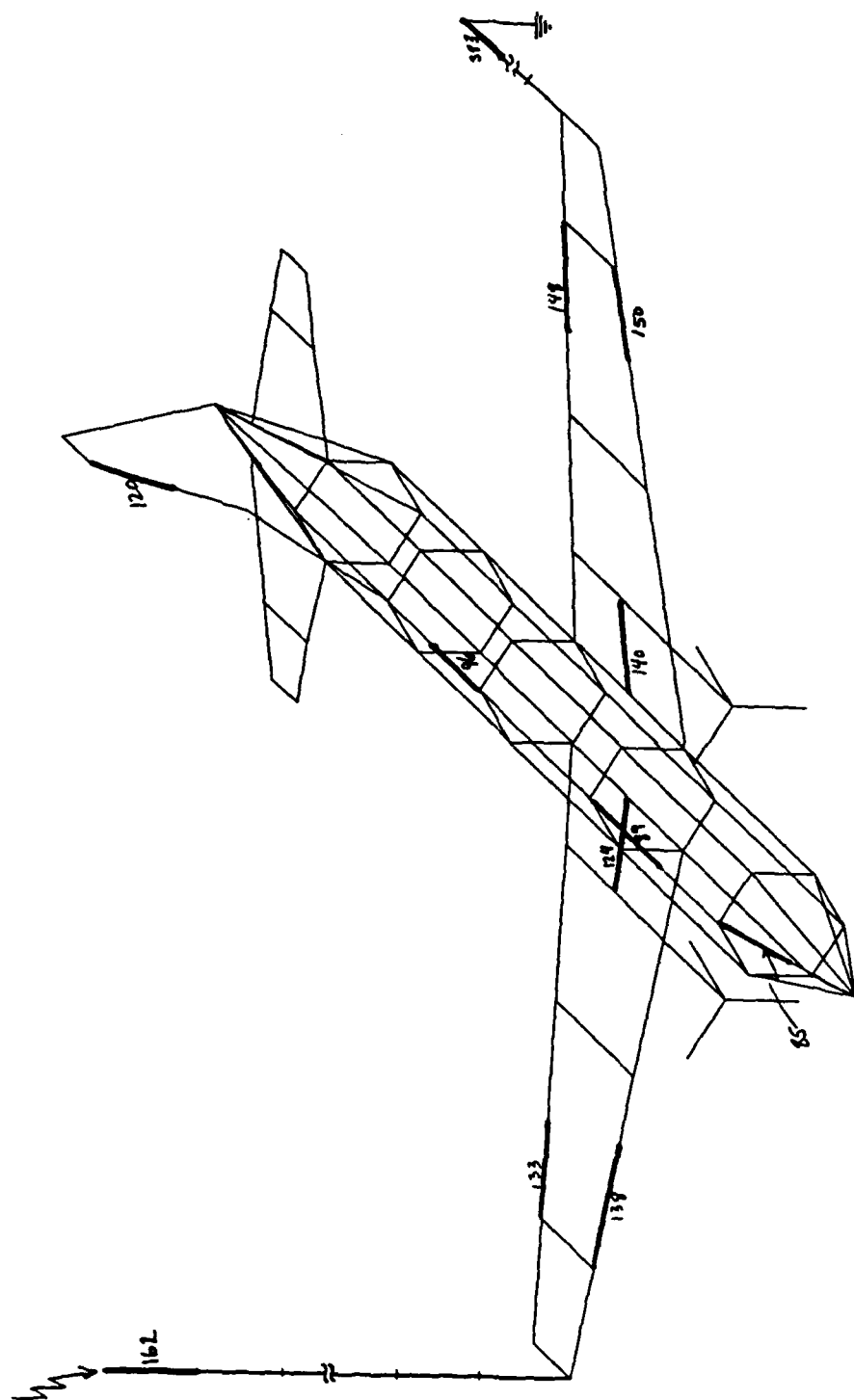


Figure 17. Segments of Interest

on the aircraft's surface. Predicted current information for four sensor locations (segments 89, 96, 124, and 140) and the excited segment 162 were used for the comparisons of GEMACS predictions to actual measurements and to the T3DFD predictions.

#### Ground Plane -vs- No Ground Plane

The analysis described in this report is a natural extension of the work described in the BDM Corp. report (12) in which GEMACS was implemented to predict the EM surface currents on a helicopter. In fact, the approach employed in this analysis paralleled the BDM analysis approach. However, actual lightning measurements were never performed to verify the GEMACS predicted skin currents. What remained was to actually validate GEMACS predictions with in-flight measured data. This validation became one of the thesis' objectives.

The lightning channels implemented in the BDM Corp. analysis were modelled as two long, thin conductors with the exiting channel terminated in free space. A more realistic representation of the lightning/aircraft interaction event is to terminate the exiting channel model into an infinite ground plane located in cartesian space at  $z = 0$ . This more closely models the actual physics of a lightning channel which terminates at the earth's surface. The effects of adding a ground plane to the aircraft/lightning wire grid model are discussed below.

GEMACS was operated with and without the inclusion of a ground plane located at  $z = 0$ , at frequencies of 0.5 MHz and 4.5 MHz. The method of determining the effect of the added ground plane consisted of calculating the percent error between predicted segment currents with and without a ground plane. The ground plane was assumed to have no effect if the percent error was less than 1. It was assumed to have little effect if the percent error was greater than 1 but less than or equal to 5. Otherwise, inclusion of the ground plane had more than negligible effect. The results of the ground plane -vs- no ground plane current comparisons are summarized in Table 1. The percent error was calculated as following:

$$\text{percent error} = \frac{\text{No Ground} - \text{Ground}}{\text{No Ground}} \times 100. \quad (4.1)$$

Table 1  
Comparison of Ground Plane and No Ground Plane  
Predicted Segment Currents

Seg.	0.5 MHz			4.5 MHz		
	No Ground	Ground	% Error	No Ground	Ground	% Error
85	0.129E-2	0.123E-2	4.7	0.116E-3	0.329E-4	71.5
89	0.200E-4	0.191E-4	4.8	0.412E-3	0.461E-4	88.8
96	0.121E-3	0.171E-4	85.9	0.353E-3	0.636E-3	80.4
120	0.116E-4	0.984E-5	15.3	0.369E-4	0.148E-3	301.7
124	0.108E-2	0.991E-3	7.8	0.169E-2	0.338E-2	99.9
133	0.178E-4	0.192E-4	7.6	0.113E-2	0.227E-2	101.2
138	0.522E-4	0.600E-4	15.0	0.157E-2	0.317E-2	101.6
140	0.326E-4	0.355E-4	8.8	0.893E-3	0.178E-2	99.7
148	0.652E-5	0.105E-4	60.7	0.372E-3	0.442E-4	88.1
150	0.605E-5	0.909E-5	50.3	0.220E-3	0.188E-3	14.5
162	0.307E-3	0.314E-3	2.0	0.295E-2	0.379E-2	28.4
383	0.324E-5	0.651E-5	100.9	0.142E-3	0.312E-3	119.4
Mean	0.245E-3	0.227E-3	7.6	0.824E-3	0.132E-2	59.8

The overall effect of adding a ground plane is that it resulted in a significant difference in predicted segment currents. At 0.5 MHz, the calculated percent error varied drastically between segments ranging from an acceptable 2.0% up to a gross 100.9%. The difference was even more apparent at 4.5 MHz where the "best" percent error was 14.5% and extended to over 300%. However, the arithmetic mean percent error at 0.5 MHz was 7.6%, only 2.6% out of acceptable range. This relatively low mean error existed because the highest errors at 0.5 MHz were associated with lower predicted current magnitudes. But, in order to justify the use of the no ground case for the entire GEMACS analysis, the predicted segment currents would have to have been similar to those obtained from the ground case for all of the analysis frequencies from 0.5 MHz to 5.0 MHz. Given the percent error calculations in Table 1, the no ground case cannot be used to accurately predict the aircraft segment currents. Therefore, the ground case, which more realistically models the actual lightning/aircraft interaction event, was used to perform the GEMACS frequency domain analysis.

#### MOM with BMI

A substantial CPU time reduction can be realized by implementing the Banded Matrix Iteration (BMI) technique to decompose the segment interaction matrix, but this technique should only be applied if it is found to be accurate within a

specified error limit. The Method of Moments (MOM) is implemented by GEMACS to solve for the currents on the 384 segments of the wire grid model of the CV-580 and lightning channels. The process includes the decomposition of a 384 by 384 segment interaction matrix. According to Dr. Coffey (4), 99% of the CPU time spent in the GEMACS MOM Module is devoted to decomposing this interaction matrix. GEMACS includes the optional BMI technique which can be used in conjunction with the moment method to reduce this time by as much as half. This provides an obvious cost-saving advantage, especially when the approximation method is accurate to within a desired error, say, 5% error, as suggested by Coffey.

GEMACS was operated with and without the BMI technique for frequencies of 0.5 MHz and 5.0 MHz. The predicted segment currents generated using the BMI method were considered valid and acceptable if the currents differed by no more than 5% from those currents predicted by the complete MOM. Table 2 presents the data used to make the assessment of the BMI method's accuracy. The equation used to compute percent error is analogous to Eq 4.1 and is shown below.

$$\text{percent error} = \frac{\text{MOM} - \text{BMI}}{\text{MOM}} \times 100. \quad (4.2)$$

The segment currents predicted with the BMI approximation technique varied only slightly from those obtained using the

Table 2  
Comparison of BMI and MOM Predicted Segment Currents  
(Relative Magnitudes Shown)

Segment	0.5 MHz			5.0 MHz		
	MOM	BMI	% Error	MOM	BMI	% Error
85	1224	1227	0.2	3396	3289	3.1
89	1857	1905	2.6	4780	4613	3.5
96	1759	1716	2.4	6408	6363	0.7
120	1002	984	1.8	1452	1483	2.1
124	1026	991	3.4	3401	3375	0.7
133	1961	1917	2.2	2288	2274	0.6
138	6089	6003	1.4	3191	3173	0.6
140	3612	3546	1.8	1796	1783	0.7
148	1074	1048	2.4	4637	4420	4.7
150	9250	9093	1.7	1916	1880	1.9
162	3135	3136	0.0	3796	3792	0.1
383	6602	6505	1.5	3169	3120	1.5
Mean	2294	2265	1.3	1325	1317	0.6

complete MOM solution. The currents shown in the table are relative; that is, the orders of magnitudes have been divided out so that even slight differences are more apparent. As shown, at 0.5 MHz, the percent error ranges from 0.0% (rounded to the nearest tenth) to 3.4%, with an arithmetic mean of 1.3%. Similarly, at 5.0 MHz, the percent error ranges from 0.1% to 4.7%, with mean 0.6%. All calculated errors are within 5% and were considered acceptable for this analysis. In fact, many errors are lower than 1% indicating that, based on the initial criteria, there is relatively no difference between MOM and BMI predicted segment currents.

The reason for the excellent correlation between the two cases is the size of the segment bandwidth employed in the BMI technique. As described in the theory chapter of this report, the bigger the bandwidth, the better the approximation. The 161 segment bandwidth represents nearly one-half of the entire

384 segment aircraft/lightning channel wire grid model and includes all of the segments which make up the complex geometrical model of the CV-580 aircraft.

The CPU time saved due to the implementation of the BMI technique coupled with the method's accuracy, relative to the complete MOM solution, justified the use of the BMI approximation in the GEMACS analysis. Had no CPU time been saved, the analysis would have been performed by using the complete MOM solution. The entire BMI analysis took 35626 CPU seconds or about 9 hours and 53 minutes. The MOM analysis for one frequency averaged 3990 CPU seconds or 1 hour and 6 minutes. For 10 frequencies, the MOM analysis would take about 11 hours and 5 minutes. The total CPU time saved by implementing the BMI technique would be approximately 1 hour and 12 minutes. This is a significant time reduction, given that this analysis was conducted for only 10 frequencies. Should GEMACS be used in future, similar analyses for a broader frequency range or smaller frequency increments, the CPU time reduction would provide a considerable cost advantage to the user.

### Results

The next three sections describe the results used to compare the GEMACS predicted segment currents to those obtained from in-flight, lightning measurements and to the T3DFD predictions. The actual lightning measurements and the

T3DFD study were performed by the USAF Atmospheric Electricity Hazards Group (AFWAL/FIESL). Several reports were generated which describe the measurement procedure, results, and T3DFD analysis (15; 16; 36). The two sections immediately following summarize the results of the actual lightning measurements and T3DFD analysis.

#### Actual Lightning Strike Results

During 1984 and 1985, a CV-580 aircraft was supplied by the FAA and instrumented by AFWAL/FIESL, who measured and recorded the electromagnetic fields and skin current distributions on the aircraft due to direct lightning attachments (16; 36). Lightning currents were measured at the base of booms equipped with current shunts installed at the wing tips. The shunts were oriented to produce a negative polarity waveform when conventional current flowed onto the aircraft.

The skin current distributions on the aircraft were measured by four Multi-gap Loop (MGL) derivative magnetic field sensors which were located under each wing between the engine and the fuselage, on the top forward fuselage, and on the top aft fuselage, as shown in Figure 18. These magnetic field sensors were oriented so that a negative output would occur for conventional current flow from nose to tail or from right wing tip to the left wing tip.

The electric fields present on the aircraft during the

lightning attachments were measured by three Flush Plate Dipole (FPD) derivative electric field sensors which were located under each wing tip and on the left surface of the vertical stablizer, also shown in Figure 18. The wing tip electric field sensors were oriented to produce a positive output in a negative electric field.

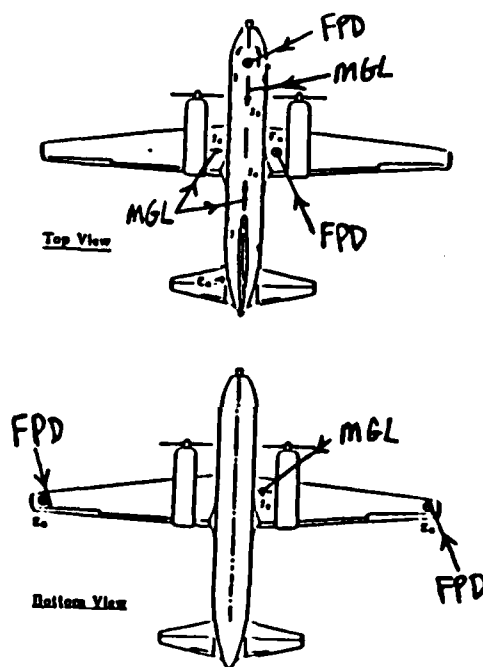
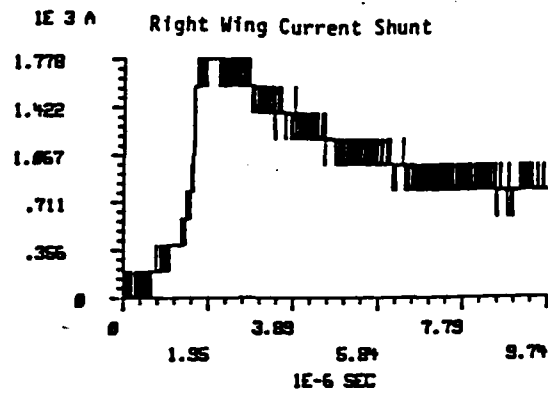


Figure 18. CV-580 MGL and FPD Sensor Locations

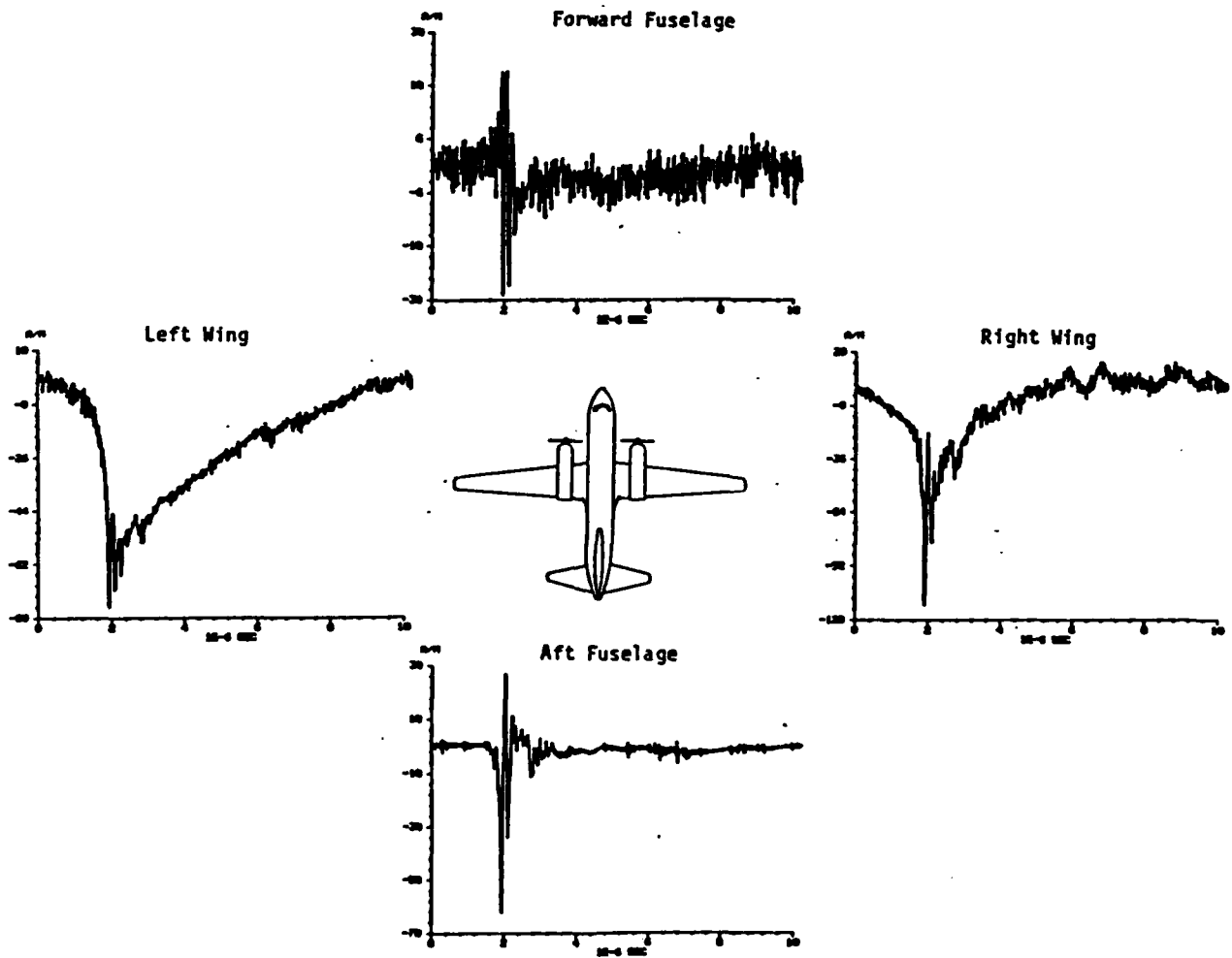
Video cameras viewed both wings and wide angle video cameras viewed the hemisphere above and below the fuselage surfaces. The cameras visually recorded the entry and exit locations during the lightning attachments. They were also used to verify the lightning current paths on the aircraft as determined by sensor measured polarities and delay times (36).

The CV-580 was flown for 50 hours below 20,000 feet in the vicinity of Florida thunderstorms. Time-domain skin current distributions were measured on the CV-580 for 21 lightning strikes. Figure 19 illustrates the current waveforms recorded on the aircraft by the skin current sensors during a typical wing-to-wing strike, recorded during a lightning strike measurement on September 5, 1984. Figure 19-A gives the injected current as measured at the right wing boom current shunt. The current response waveforms show that some of the current redistributes onto and excites resonances on those portions of the aircraft which are not in the direct path of the lightning current. That is, some current is distributed onto the fore and aft fuselage during a wing-to-wing strike (16:5).

Frequency domain techniques described earlier in this report were applied to the airborne data to derive aircraft transfer functions. The first step in the frequency domain conversion was to remove the effects of the measurement system. This process is described in detail in the airborne data collection reports (16; 36). The time domain measured airborne transient waveforms were transformed into the frequency domain by applying Fast Fourier Transforms (FFT) (16:5). The resulting waveforms are frequency domain representations of the time domain measured phenomena. This procedure is graphically illustrated for the current source (Figure 20) and the forward fuselage sensor response (Figure 21).



A.



B.

Figure 19. Measured Aircraft Surface Current Waveforms

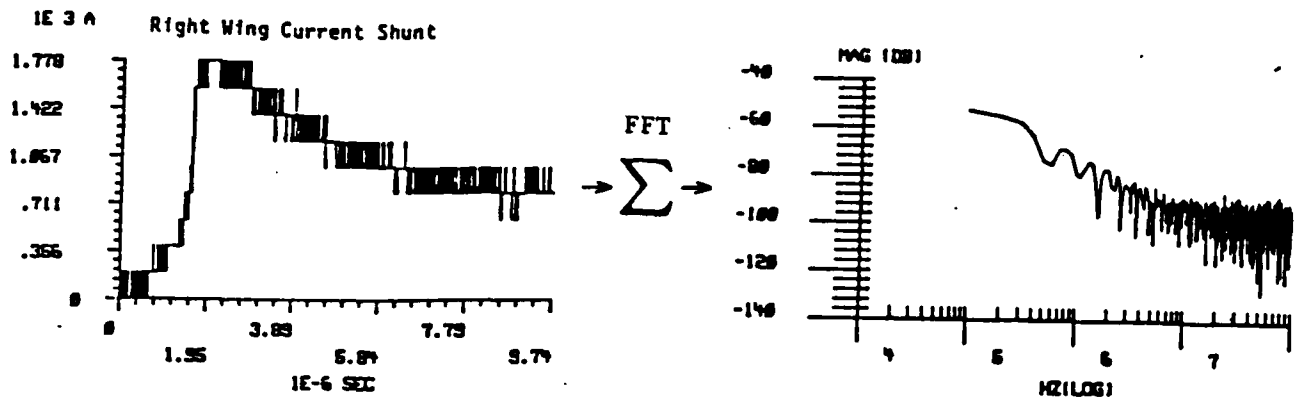


Figure 20. Transformation of the Source Current  
(16:11,16)

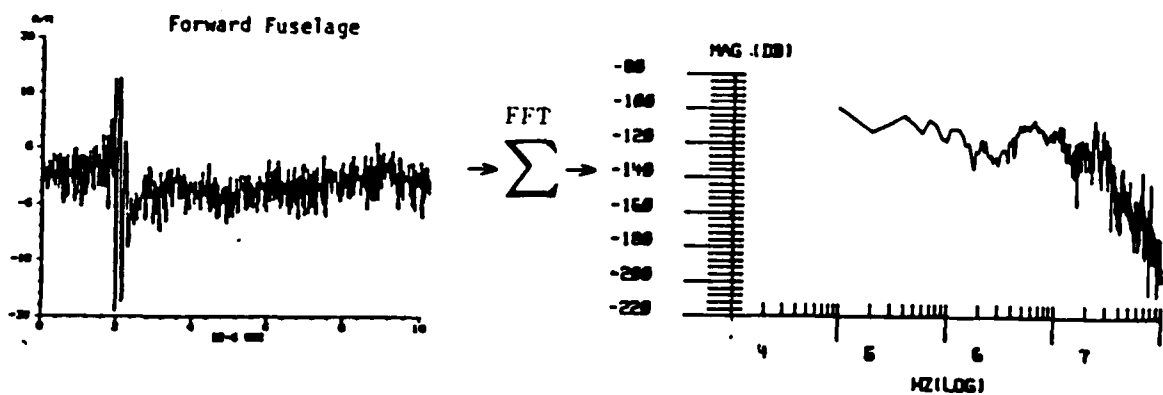


Figure 21. Transformation of the Forward Fuselage  
Sensor Response (16:11,16)

Next, the transfer function of the aircraft at the four sensor locations was produced (16:5). A transfer function in the frequency domain is defined as the FFT of the output divided by the FFT of the input. In the airborne data case, the output was the sensor response and the input was the measured right wing boom shunt current. The transfer functions were produced by dividing the calculated frequency-domain waveforms point by point. An example of the transfer function generation procedure is illustrated in Figure 22. Figure 23 shows a linear plot of the forward fuselage transfer function for 0 to 25 MHz. Figure 24 shows the aircraft transfer functions at the locations of each of the four MGL sensors during the airborne wing-to-wing strike (16:6).

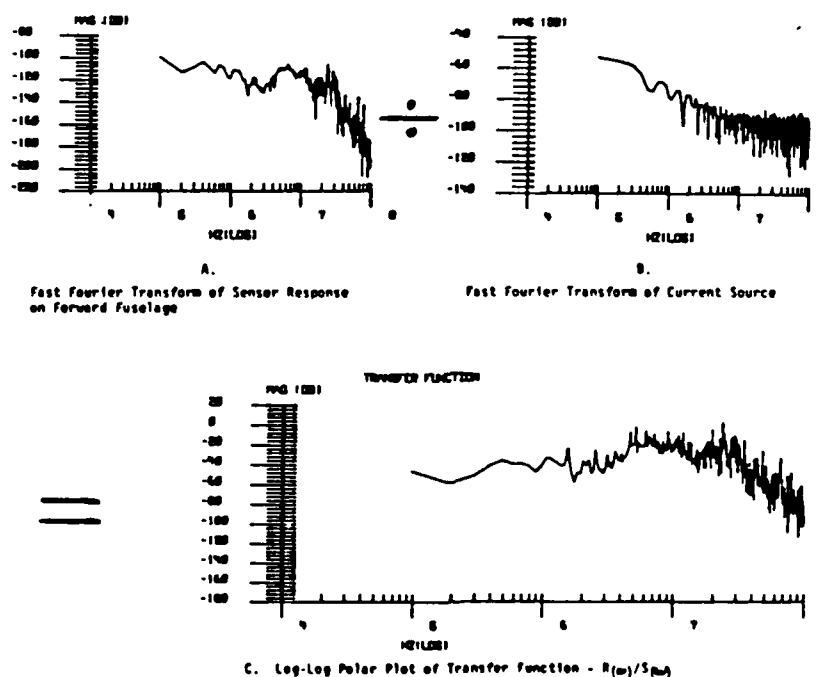


Figure 22. Example of the Transfer Function Generation Procedure

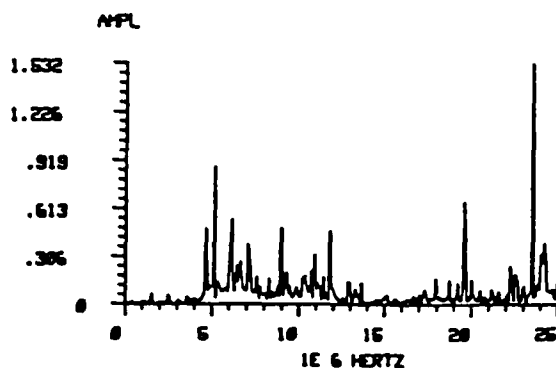


Figure 23. Linear Plot of the Forward Fuselage Transfer Function

In his report, Hebert suggests that many of the prominent peak magnitudes in these transfer functions occur at frequencies which can be related to dimensions of the aircraft (16:6). The forward fuselage transfer function spike at 4.7 MHz represents a half wavelength resonance of approximately 105 feet, the distance from wing tip to wing tip. Nine MHz (55 feet) is roughly the distance from the wing tip to the fuselage and 7.2 MHz (68 feet) corresponds to the distance from the wing tip to the far engine mount. The peaks at frequencies of 1.5, 2.5, and 3.6 MHz on the left wing, right wing, and aft fuselage transfer functions correspond well to frequencies which are multiples or combinations of aircraft dimensions. For example, 2.5 MHz is 197 feet or about twice the distance from the wing tip to the tail (16:6). Other resonant frequencies may be a combination of several aircraft dimensions.

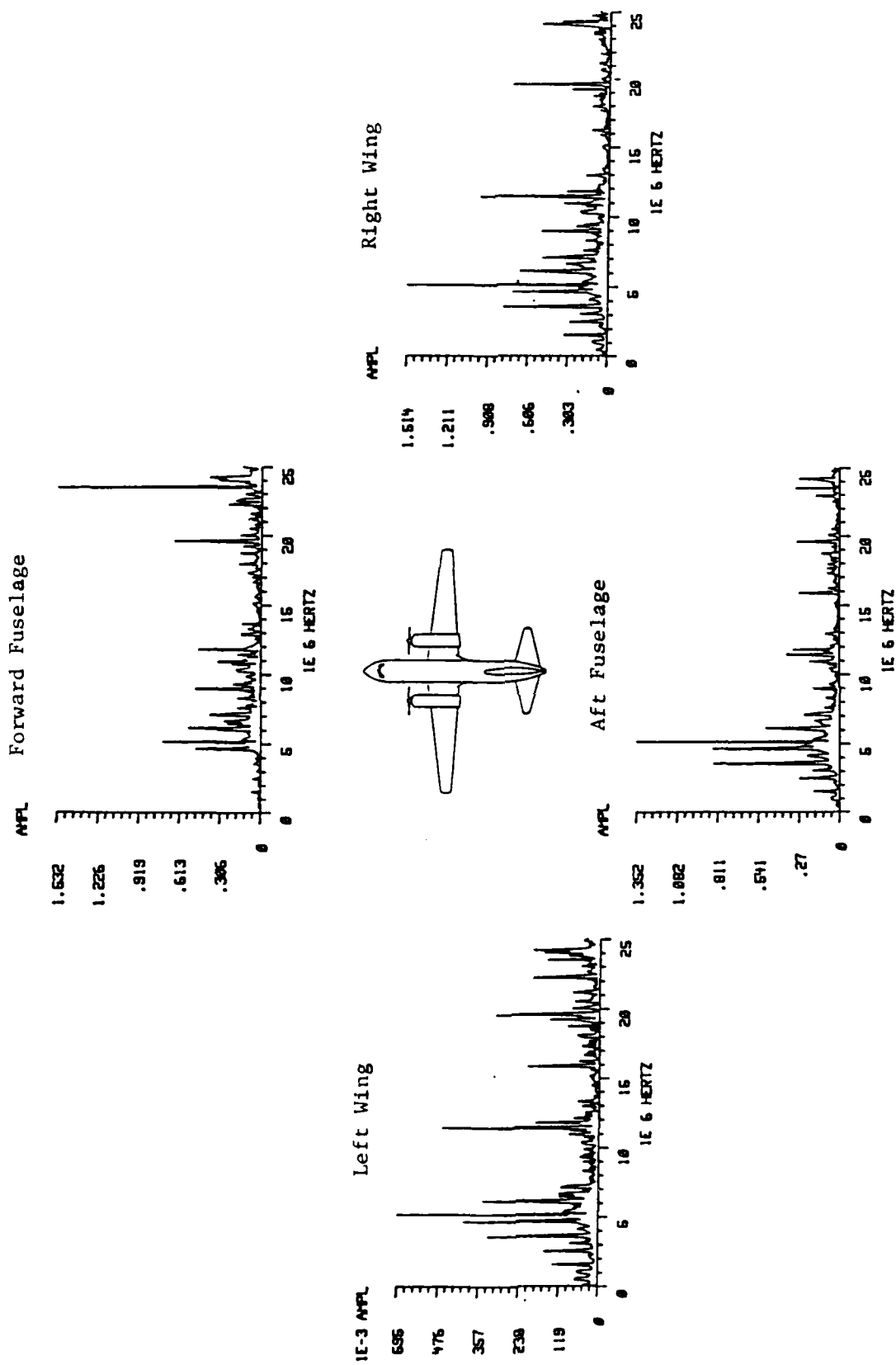
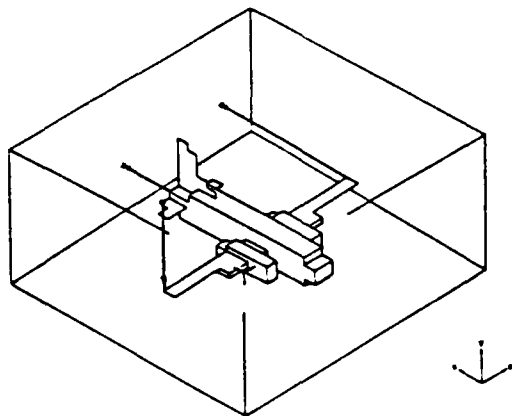


Figure 24. Actual Aircraft Transfer Functions

## T3DFD Results

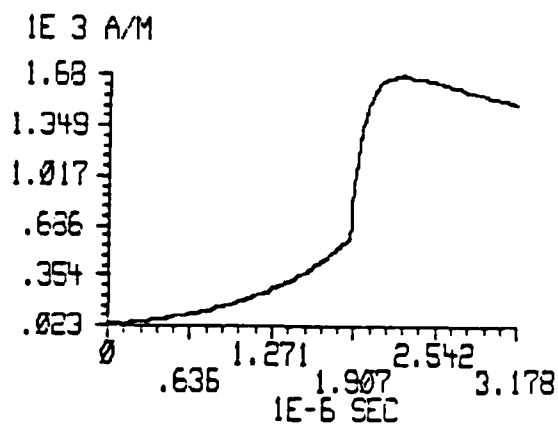
The T3DFD program was implemented for the analysis of lightning's EM interaction with a CV-580 aircraft (15). The time-domain results were transformed into the frequency domain to compare T3DFD predicted surface currents to in-flight lightning measurements. For these comparisons, only the forward fuselage frequency domain transfer function was derived.

The T3DFD analysis began with the construction of an appropriate CV-580 block model, as shown in Figure 25-A. Figure 25-B shows the source, Figure 25-C is the time domain predicted resonances on the forward fuselage during a wing-to-wing strike, and Figure 25-D is the FFT of this predicted signal. Figure 25-E is a log-log plot of the transfer function with the right wing boom current, Figure 21-B, taken as the source, and the forward fuselage taken as the response. Figure 25-F shows a linear plot of the same transfer function. In the actual lightning versus time domain comparisons, it was suggested that the high frequency spikes found in the actual aircraft transfer functions above 19 MHz were caused either by "noise, internal coupling, or resonances within the data acquisition coaxial wire networks rather than by natural modes on the aircraft's exterior" (16:6).



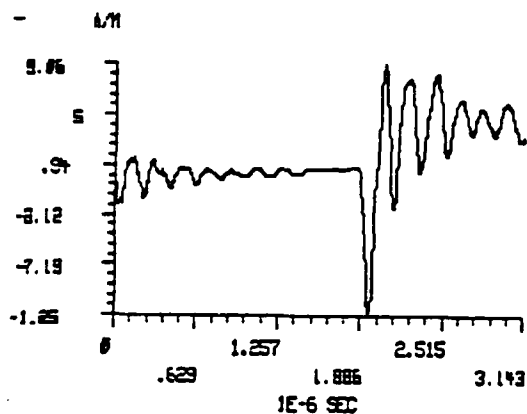
A.

T3DFD Code Model of the CV580 Aircraft



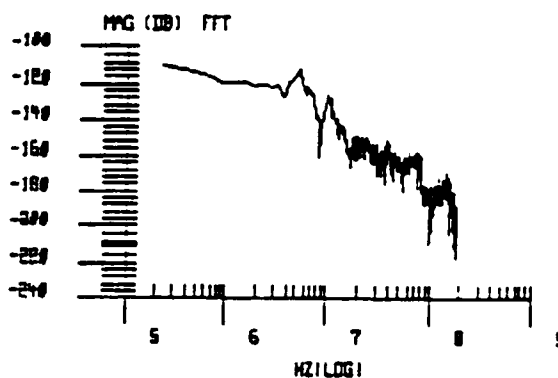
B.

Source Waveform for T3DFD Code Application



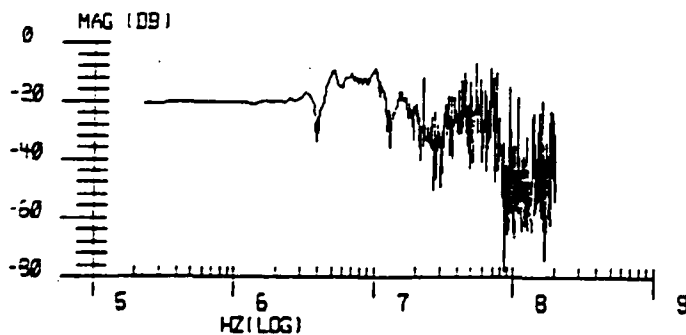
C.

Response at the Forward Fuselage Surface Current Sensor to the Source in 12B



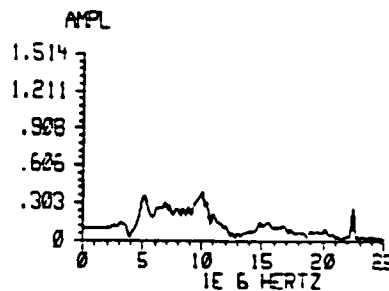
D.

FFT of Response in 12C



E.

Log-Log Plot of Transfer Function When Response in 12C is Divided by Source in 12B



F.

Linear Plot of 12E from 97 kHz to 25 MHz

Figure 25. T3DFD Generated Results

## GEMACS Results

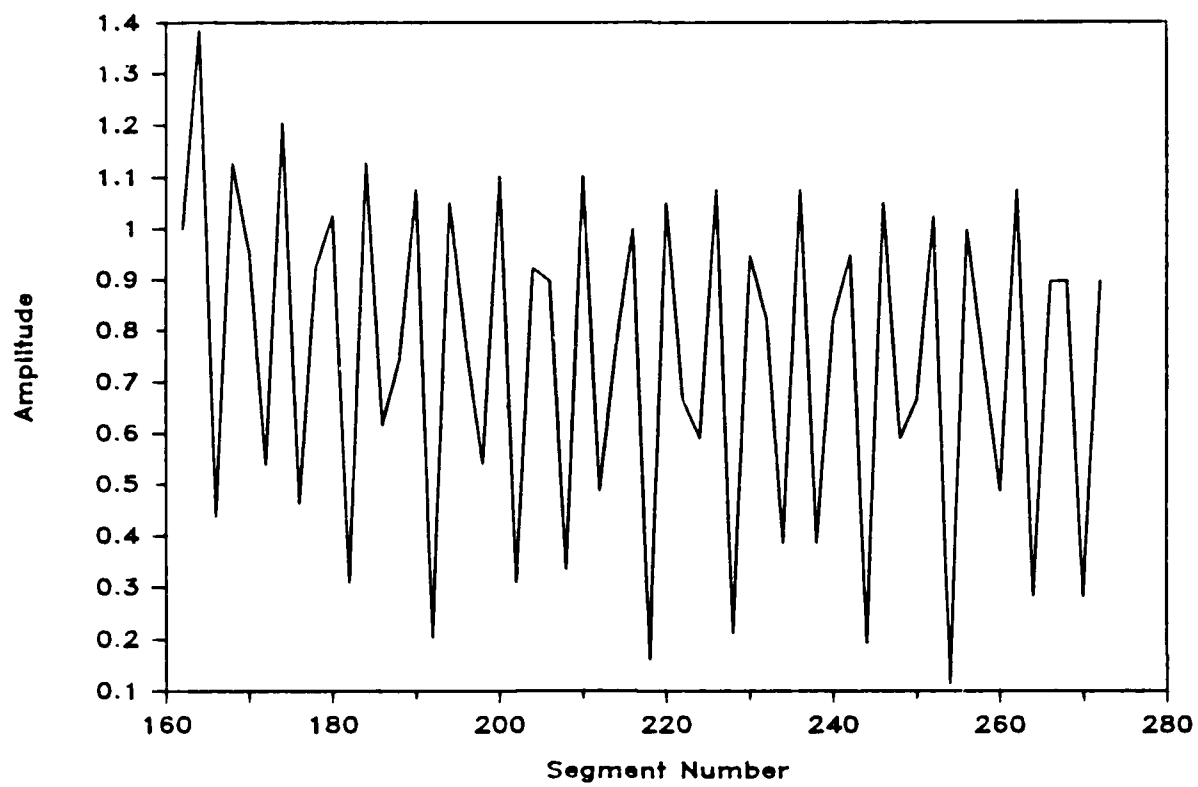
The GEMACS program generated predicted segment currents by implementing the MOM with BMI to solve the 384 element interaction matrix. The aircraft/lightning channel wire grid model was composed of 384 wire segments with a maximum segment length of 236 inches and with the exiting lightning channel model terminated into an infinite ground plane, representing earth, located at  $z = 0$ . The segment representing the top of the lightning channel was excited with a delta-gap voltage source of magnitude 1 V. The program was operated for a total of ten frequencies.

Analysis Frequency Bandwidth. The GEMACS analysis was accomplished for frequencies of 0.5 MHz to 5.0 MHz. The bandwidth boundaries were not selected at random, but rather were chosen after an inspection of the actual lightning results. First, implemented FFT technique described earlier is limited by the number of time sampled points available. It is impossible for the technique to be used to convert finite time-domain information into the entire frequency domain, especially in the low frequency range of dc to about 0.5 MHz. In fact, according to Hebert (14), for the amount of measured time-domain sample points available, any calculated frequency-domain data below 0.5 MHz should be considered invalid. As such, 0.5 MHz provides a lower bound for this analysis. Second, Figure 21-B, shown earlier, illustrates the FFT of the lightning threat. The measured current drops off

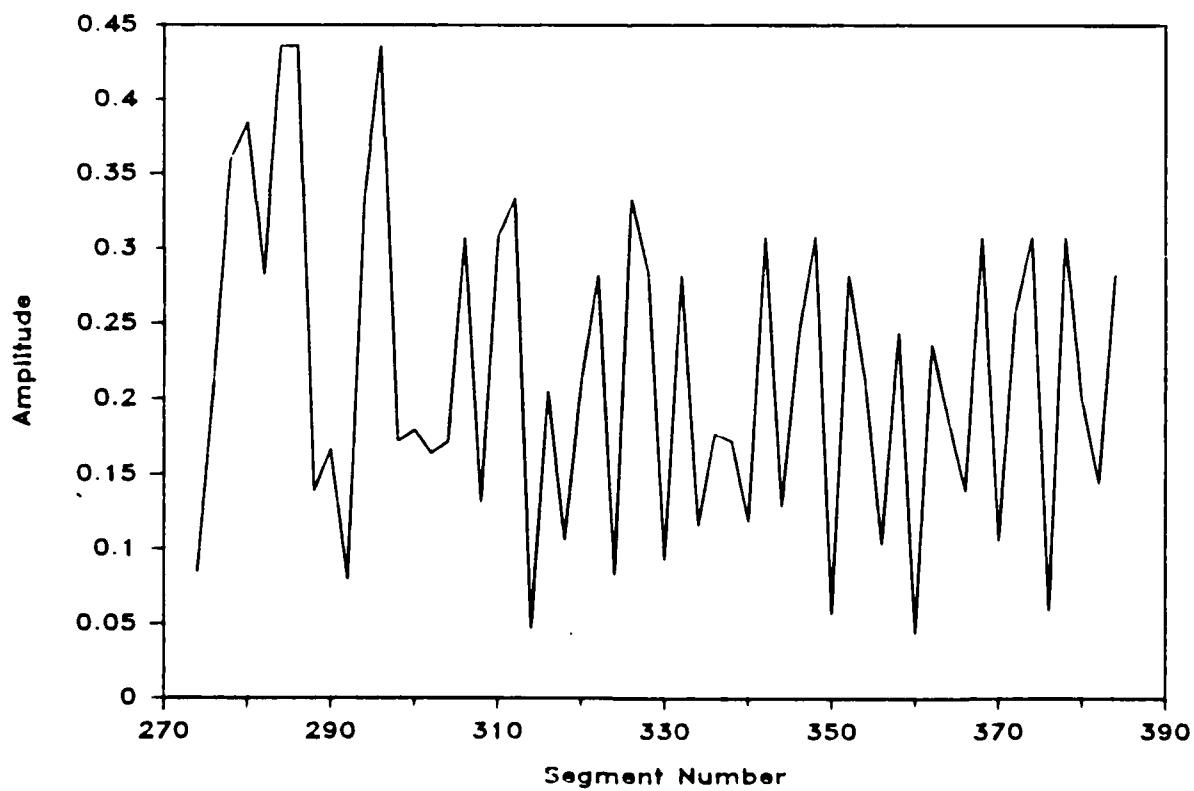
exponentially as the frequency increases. It was determined that, although the aircraft has a transfer function at frequencies greater than 5 MHz, the energy of the lightning threat above this frequency is considerably diminished. Therefore, the lower and upper bounds of the analysis frequency bandwidth were chosen to be 0.5 MHz and 5.0 MHz, respectively.

Lightning Channel Current Distribution. Before deriving predicted aircraft transfer functions, the predicted current distribution on the entry and exiting lightning channels was plotted for a frequency of 5 MHz. The purpose of this plot was to hopefully gain insight to the relationships between frequency, lightning channels, and segment lengths. The plotted distributions, as shown in Figure 26, were also normalized to the predicted current on the excited segment.

Two interesting conclusions can be hypothesized from the lightning channel current distributions. First, the waveforms have an inherent periodic nature which is related to the length of the lightning channel. The waveform in Figure 26-A has a period of 5 segments or a frequency of 1 cycle every 5 segments. One hundred and ten segments were used to model each of the two lightning channels for a total channel length of 25080 inches, which translates into a channel segment length of 228 inches. Hence, the entry channel waveform has a frequency of 1 cycle per  $228 \times 5 = 1140$  inches. The analysis operating wavelength is 2362 inches at 5 MHz. Therefore, the resonances seen in Figure 26-A are related to  $1140/2362 = 0.48$



(a) Entry Channel



(b) Exit Channel

Figure 26. Lightning Channels Current Distribution at 5 MHz

of a wavelength, which shows an approximate half-wavelength dependency. The exiting channel waveform in Figure 26-B has the same inherent periodicity except for segments 272 to 294. This leads to the next interesting conclusion.

The plotted lightning channel current distributions show that the direction of the lightning channel, as it enters or exits the aircraft wire grid model, may play an important role in the analysis of the predicted aircraft transfer functions. The exiting lightning channel model runs parallel to the aircraft wire grid aft fuselage. The direction of the entry channel model is completely orthogonal with respect to the wire grid's wings or fuselage. It is well known that two perfectly conducting objects, parallel to each other, exhibit a mutual coupling effect. The mutual coupling increases as the two parallel conductors get physically closer to each other, and decreases as they get farther apart. However, if the two perfect conductors are perpendicular to each other, no mutual coupling occurs.

The lightning channel waveforms demonstrate this mutual coupling phenomenon. In Figure 26-B, there are three peaks, occurring in the segment 272 to segment 294 interval, which are noticeably higher than the remaining waveform peaks. The segment interval containing these peaks is 24 segments or 54.2 inches. The parallel distance from the left aft wing tip to the end of the aft fuselage is 540 inches. This shows that the exiting channel and aft fuselage exhibit mutual coupling even as the channel length increases to ten times the length

of the aft fuselage.

In the entry channel waveform, mutually coupling is not readily apparent. This can be explained by the fact that this channel enters the aircraft in a direction orthogonal to the wings and fuselage. The higher spike located at segment 164 is due to the initial input current surge; all other waveform peaks and valleys appear relatively uniform. The important result is that entry and exiting lightning channel orientation strongly affect the overall EM interaction event; this observation is further supported by other thesis' results.

Derivation of Transfer Functions. The predicted segment currents were used to derive wire grid transfer functions which were then compared to actual aircraft transfer functions. The normalization process consisted of dividing the predicted current response by the entry segment current for a given frequency. Since the MOM method provides a linear solution of Maxwell's equations, the transfer functions can be used to linearly extrapolate the aircraft's response to a worst-case 100,000 ampere lightning threat.

The first step in obtaining the predicted transfer functions was to identify those wire grid segments which represented actual sensor locations, as shown in Figure 27. The segment numbers were given acronyms which better identified their location on the aircraft, as seen in Table 3. For the rest of the analysis, these segments of interest will be referred to by their identifying acronym. The next derivation step was to divide each of the predicted segment

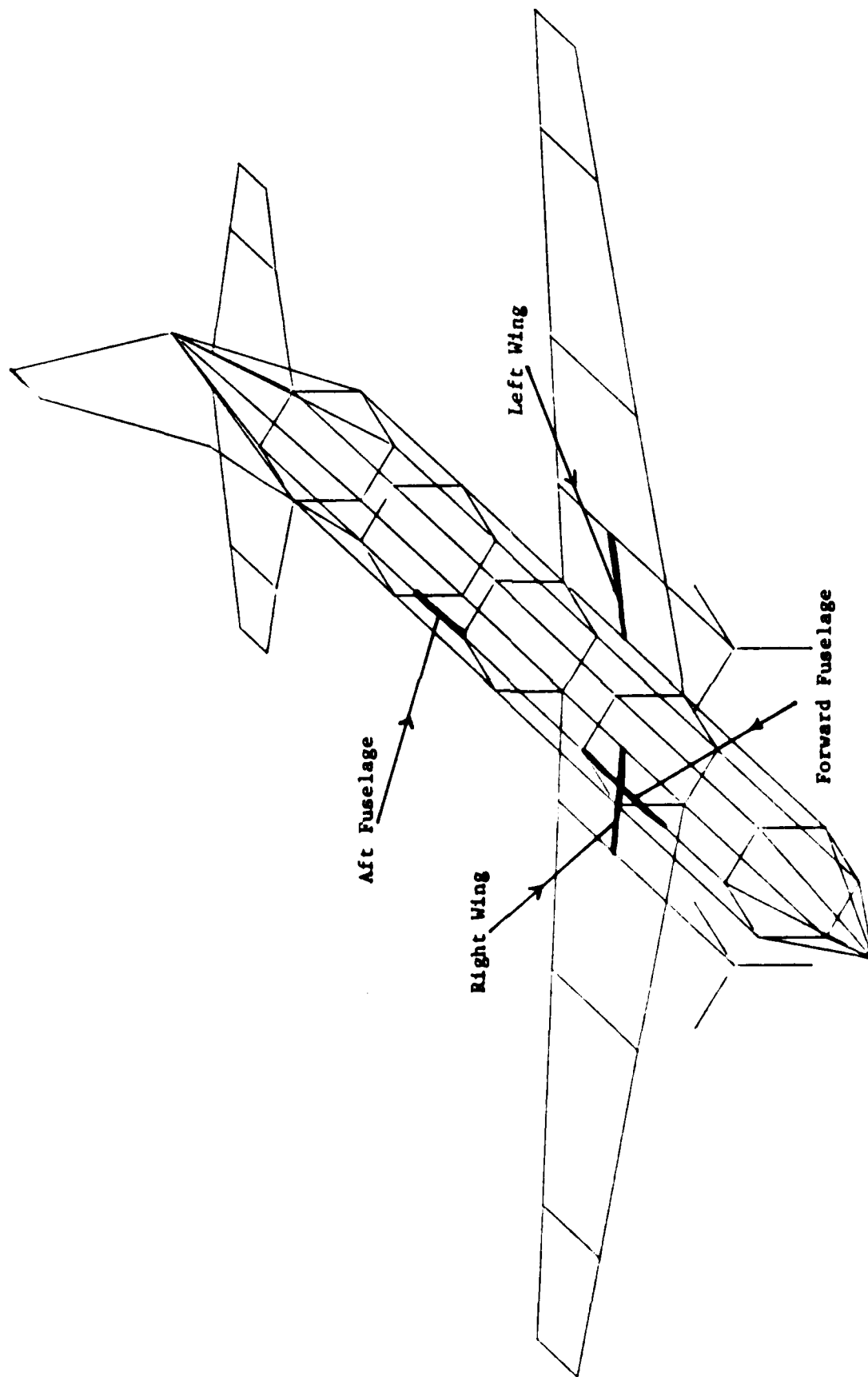


Figure 27. Segments Representing Actual Sensor Locations

Table 3  
Acronym Identifiers for Segments of Interest

Segment	Location	Identifier
89	top forward fuselage	FF
96	top aft fuselage	AF
124	right wing near fuselage	RW
140	left wing near fuselage	LW

currents by the predicted current on the excited (source) segment, for each analysis frequency. Finally, the normalized segment currents were plotted as a function of analysis frequency, yielding predicted aircraft transfer functions.

Resulting Transfer Functions. Many observations can be made by inspecting the resulting transfer functions, graphed in Figures 28, 29, 30, and 31. In all cases, natural half-wavelength resonances due purely to the aircraft dimensions were noted. In one case, the mutual coupling effect described earlier was observed. Other similarities were detected between pairs of transfer functions.

The lengths of various aircraft wire grid dimensions were responsible for many of the half-wavelength resonant spikes found in the transfer functions. The AF and FF transfer functions, Figures 28 and 29, both have resonances existing at 3.5 MHz, which corresponds to a half-wavelength of 1688 inches or very close to the combination of the fuselage and aft stabilizers' lengths. These functions also show a peak at 5 MHz which is contributed by the fuselage and tail lengths. The RW transfer function, Figure 30, exhibits a resonance at 4.5 MHz equal to a half-wavelength of 1312 inches or about 3

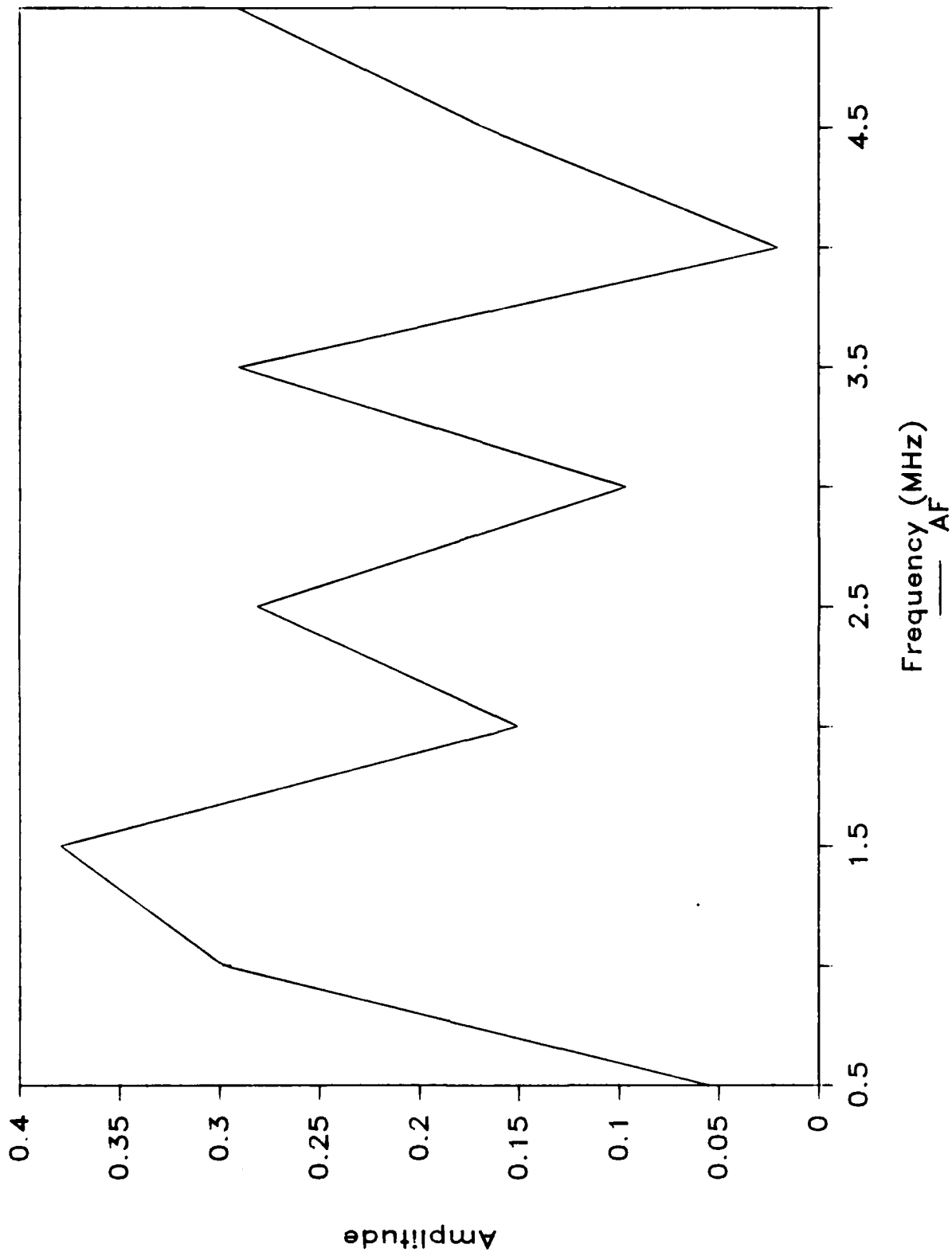


Figure 28. Aft Fuselage Transfer Function

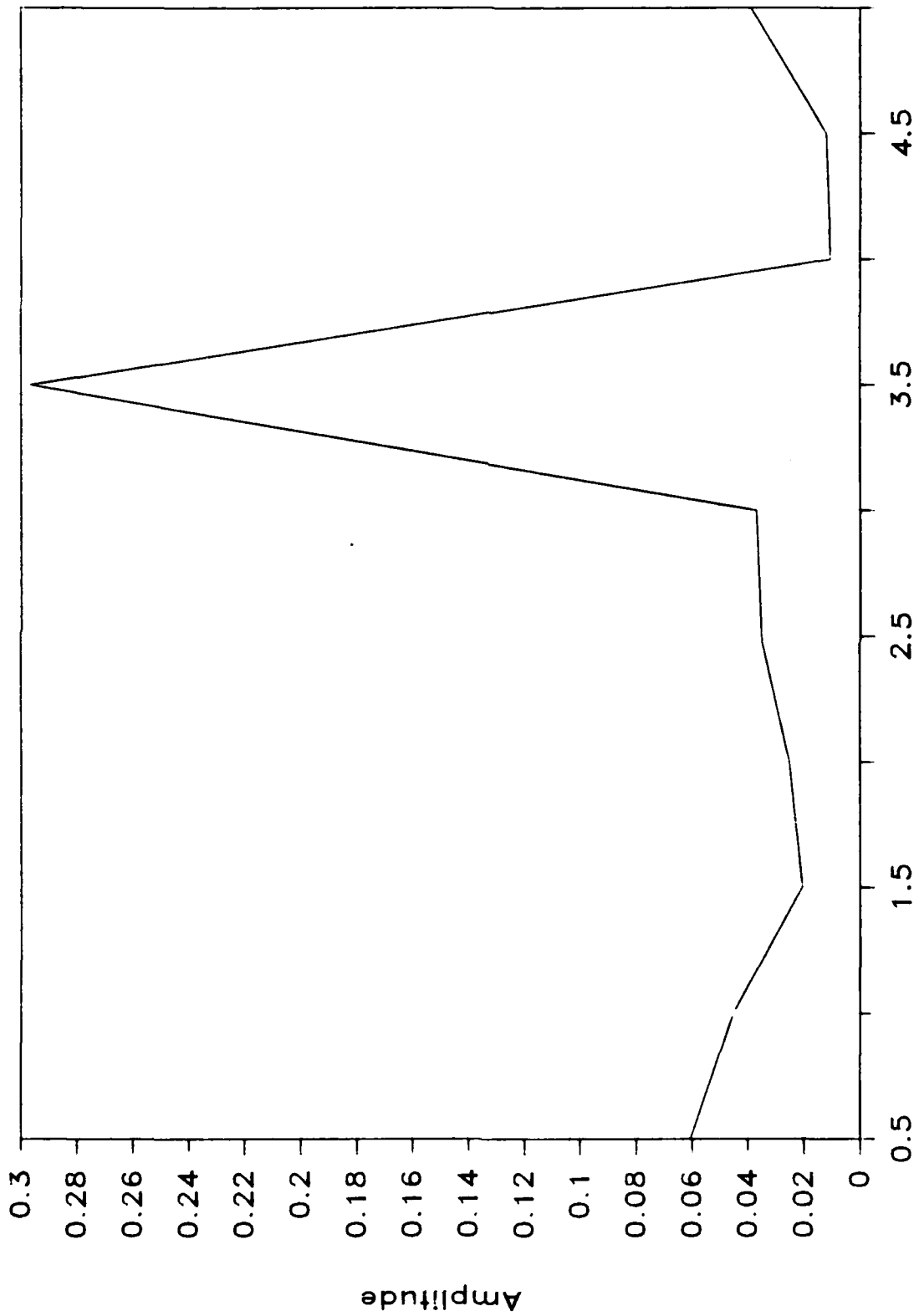


Figure 29. Forward Fuselage Transfer Function

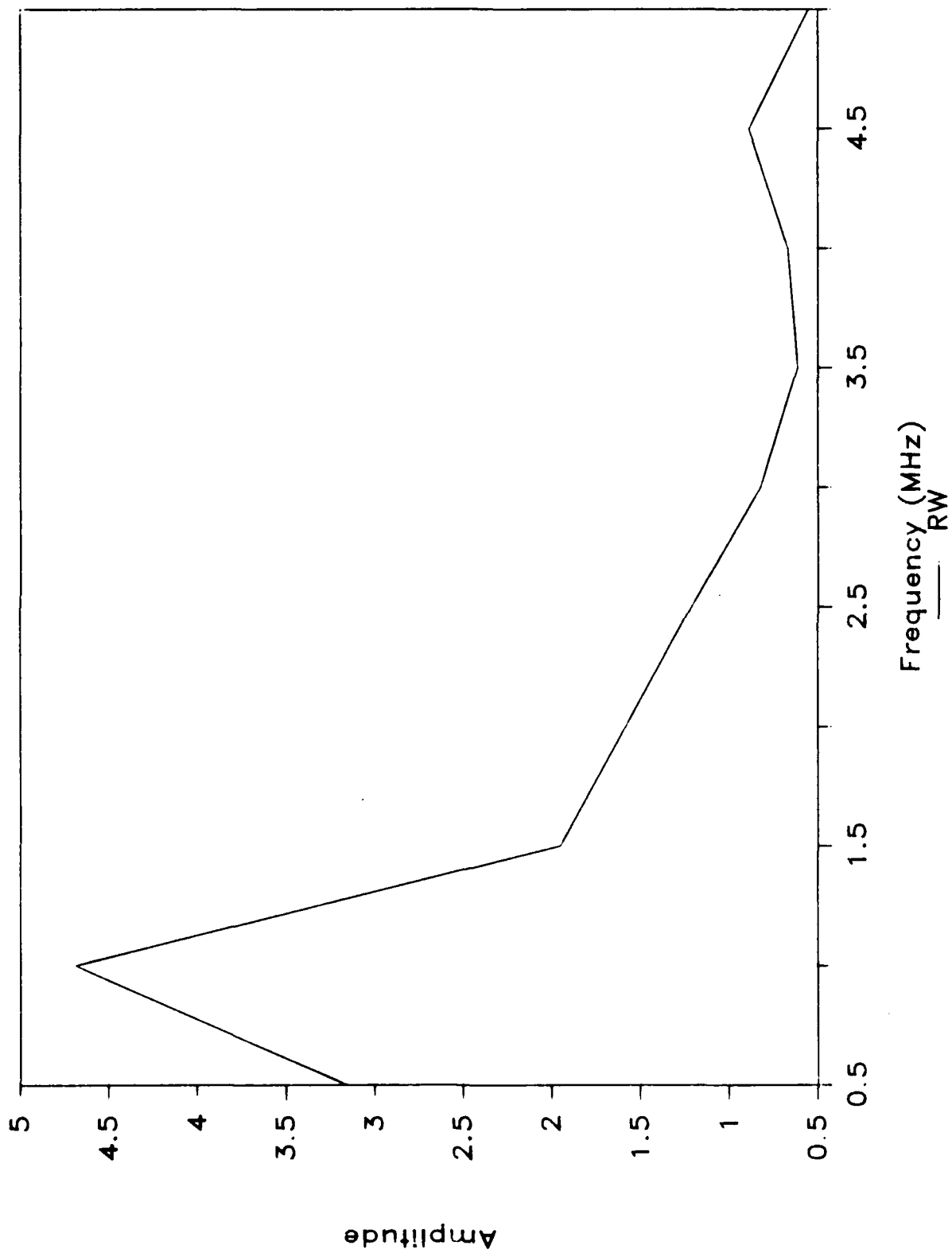


Figure 30. Right Wing Transfer Function

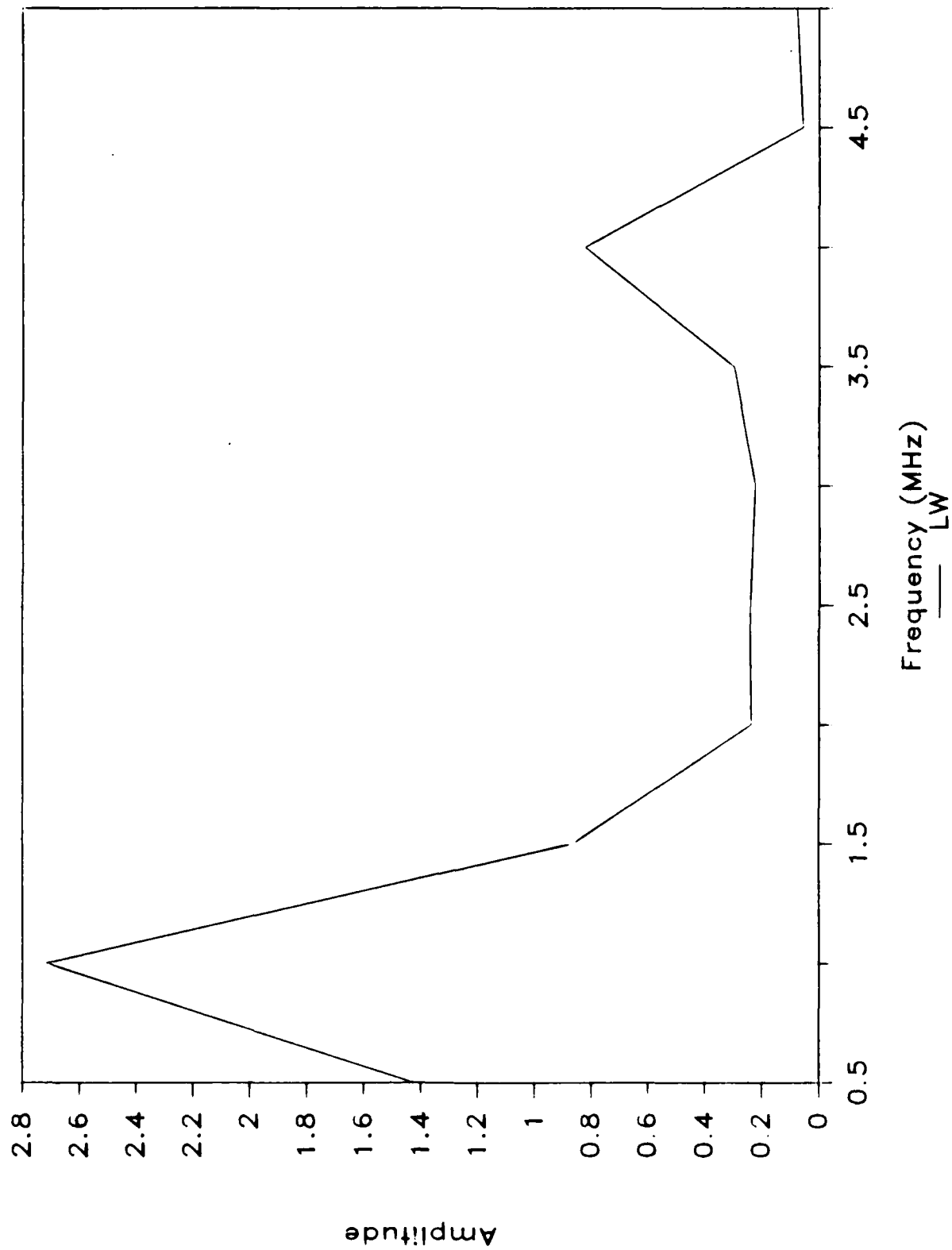


Figure 31. Left Wing Transfer Function

feet short of the exact wing span. A related spike is found at 4.0 MHz on the LW transfer function, Figure 31, which corresponds to a half-wavelength of 1476 inches, precisely the wing span plus lengths of the segments representing the left and right engine mounts. The four transfer functions also yield other resonances at lower frequencies which probably do not relate to natural aircraft half-wavelength resonances.

Predicted transfer function spikes at frequencies of 1.0 MHz to 2.5 MHz are due to a variety of reasons. The AF transfer function has many prominent peaks which are more than likely a result of the mutual coupling phenomena taking place between the aft fuselage and the exiting lightning channel. The large spike found on the RW and LW transfer functions is not a result of mutual coupling, but rather illustrates a different phenomenon. The right and left wing are in the direct line of entry and exiting energy. As such, near dc, at the relatively low frequency of 1.0 MHz, the current flows in a more direct path and the result approaches a static current distribution. In other words, the aircraft wings' current response more closely resembles the input current surge. The noticeable similarity between the RW and LW transfer functions is a direct result of the symmetry inherent to the winged portion of the aircraft wire grid model.

This section described three sets of results: Airborne, T3DFD, and GEMACS. The following sections compare the results and present the analysis conclusions.

## Comparisons with Airborne Results

The transfer functions derived and described above were compared to the CV-580 transfer functions derived from actual lightning measurements. The comparisons were qualitative in nature; that is, only shapes of the curves and locations of resonances were compared with no regard to peak magnitudes. The GEMACS predictions closely resembled the actual data for one of the transfer functions. In other cases, many of the actual aircraft transfer function spikes were not evident in the predicted aircraft transfer functions. Figure 32 shows the actual and predicted transfer functions side-by-side for easy comparisons.

The predicted AF transfer function was an excellent representation of the actual aft fuselage transfer function. All other predictions were adequate representations. The GEMACS AF transfer function and the actual AF waveform show resonances at 1.5 MHz, 2.5 MHz, 3.5 MHz, and 5 MHz. The actual AF waveform shows additional spikes at 4.5 MHz and 6 MHz not used in this analysis. The GEMACS EF transfer function is a skewed version of the actual EF waveform. The first prominent spike is noted at 3.5 MHz on the GEMACS EF transfer function, whereas the first prominent spike on the actual EF waveform occurs at 4.5 MHz. The spike at 5 MHz is also present on both transfer functions. The actual RW and LW waveforms are also shown for comparison.

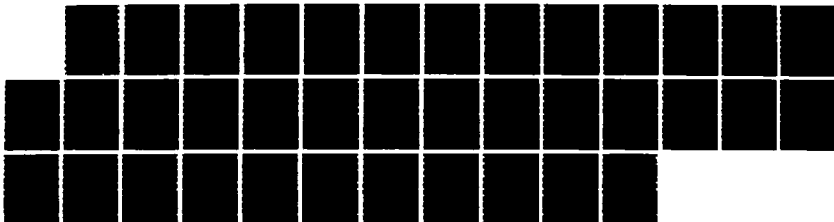
AD-A178 854

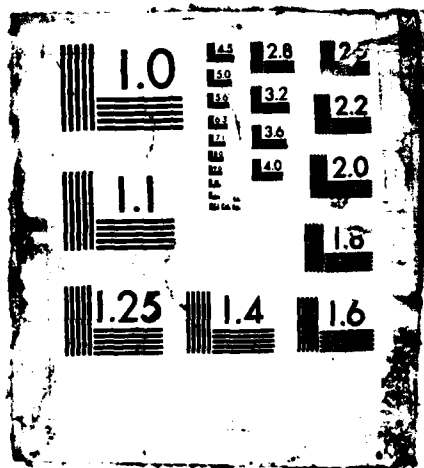
GEMACS (GENERAL EM MODEL FOR THE ANALYSIS OF COMPUTER  
SYSTEMS) FREQUENCY- (U) AIR FORCE INST OF TECH  
WRIGHT-PATTERSON AFB OH SCHOOL OF ENGI F G TOMKO  
DEC 86 AFIT/GE/ENG/86D-10 F/G 1/3

2/2

UNCLASSIFIED

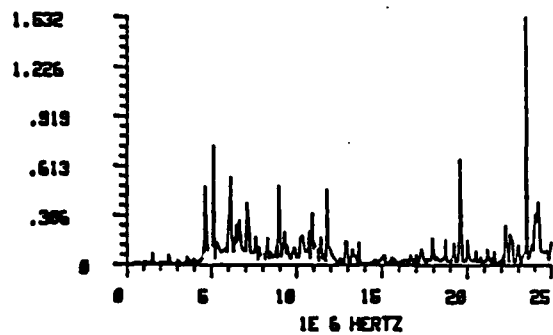
NL



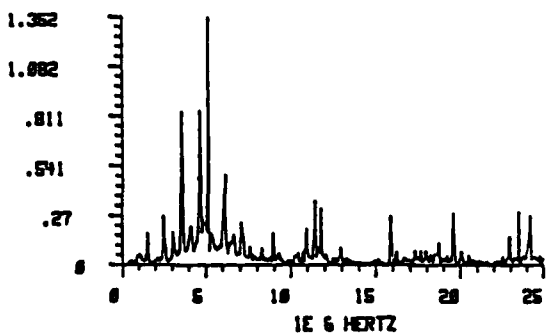
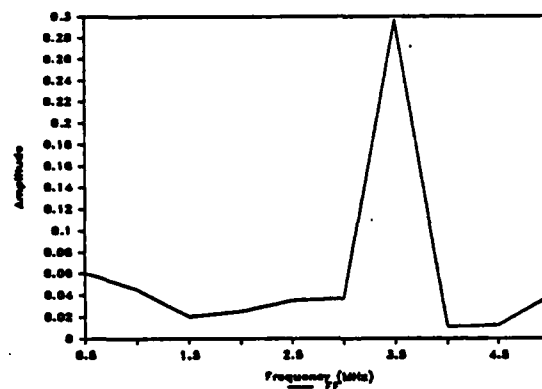


# ACTUAL

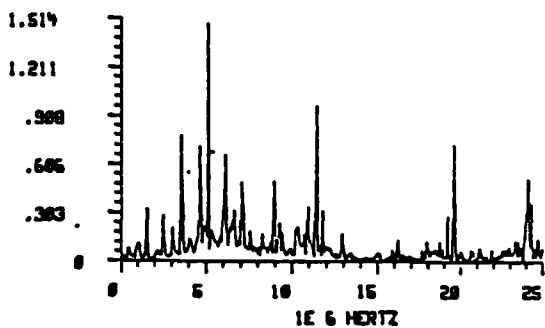
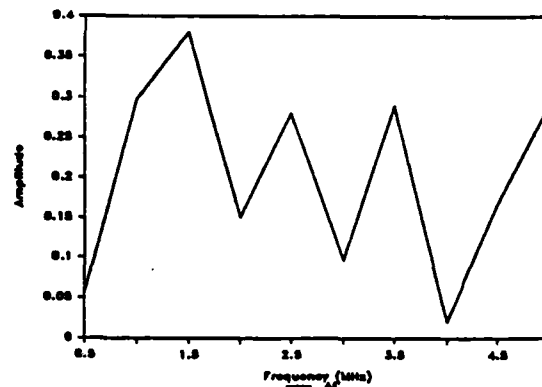
# PREDICTED



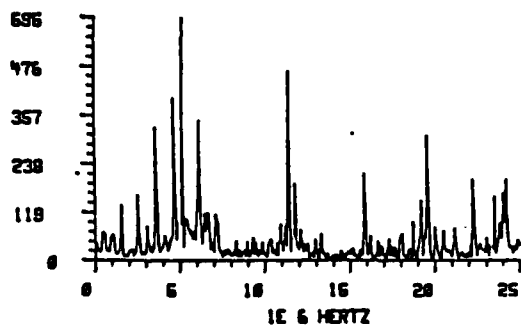
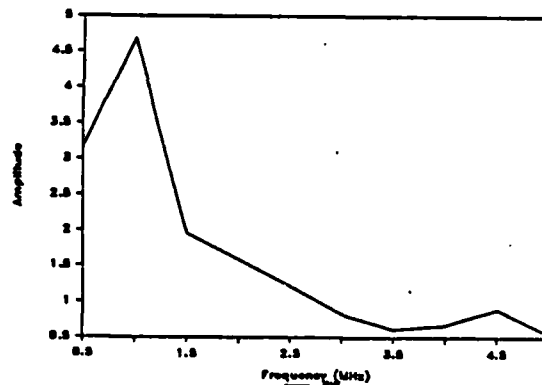
FF



AF



RW



LW

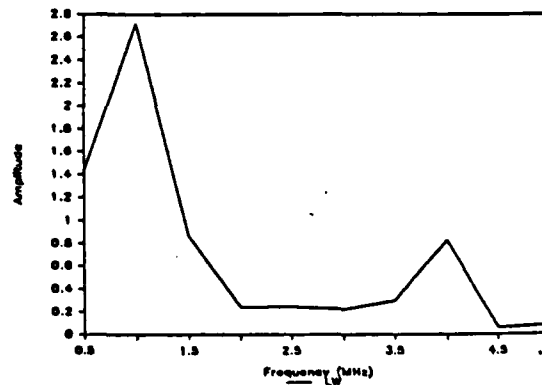


Figure 32. Actual and Predicted Transfer Functions

The differences found in the predicted and actual transfer functions may be attributed to three different aspects employed in this analysis. First, the 161 segment aircraft wire grid model allowed the AF and FF transfer functions to be more representative of the actual waveforms than the RW and LW predictions. Of the total 161 segments, only 40 segments were used to grid both wings and engine mounts, leaving 141 segments for the remaining portion of the aircraft. Of those 141 segments, 130 wire grid segments represent the fuselage. As such, this portion of the wire grid model more closely resembles the actual aircraft fuselage. Had more segments been used to model the aircraft wings, the RW and LW transfer functions would probably have yielded more information. Second, although the analysis frequency bandwidth was justified, additional frequencies in the bandwidth would have provided more transfer function resonances at higher frequencies, as suggested by the actual waveforms. Third, the aircraft/lighting channel was assumed to be perfectly conducting and modelled as such. GEMACS offers the user the option of loading some or all of the segments and to choose the conductivities of those loads. Although use of this feature was beyond the scope of this effort, the addition of resistive, inductive, or capacitive loadings on the wire segments would have influenced the predicted transfer functions to show a more complex interaction between the channel and the aircraft. These additional predicted resonances may account for the additional

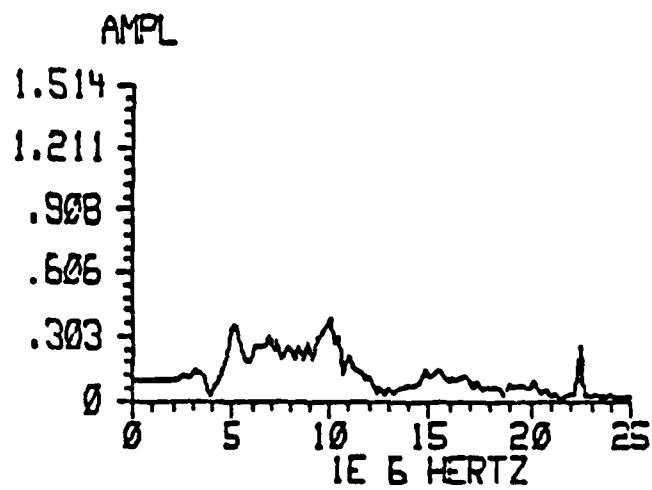
resonances found in the actual aircraft transfer functions. Overall, the predicted waveforms were adequate representations of the actual waveforms, given the caveats explained above.

#### Comparisons with T3DFD Results

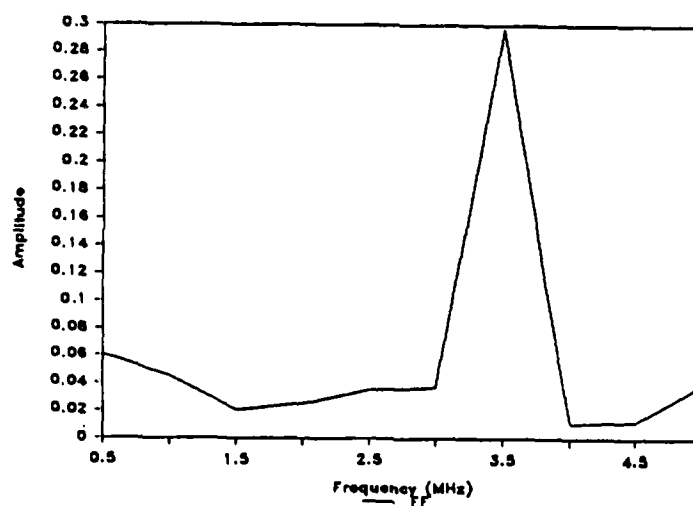
The main purpose of including the T3DFD results in this analysis was to assess the overall efficiency of the GEMACS program and not to provide another validation scheme. Of course, given the relative success of the time-domain program in predicting aircraft resonant regions, it is advantageous to show that GEMACS did at least as good a job, besides the fact that GEMACS did the job more efficiently.

The GEMACS predicted FF transfer function was compared to the FF transfer function generated from the results of the T3DFD analysis. As can be seen in Figure 33, the GEMACS predicted waveform resembles the T3DFD predicted waveform in the frequency region 2 MHz to 5 MHz. The low frequency limitations associated with the FFT technique forced the predicted T3DFD time-sampled, point-limited waveform to be relatively meaningless below 2 MHz. Thus, GEMACS not only predicts aircraft resonances as well as the T3DFD program, but also provides more information at lower frequencies.

The GEMACS program is a much larger program, in terms of lines of code and memory requirements. The T3DFD program is written in 1500 lines of FORTRAN code, much less than the



(a) T3DFD



(b) GEMACS

Figure 33. GEMACS and T3DFD Predicted Transfer Functions

100,000 lines needed for the GEMACS program. A 27x27x27 decentralizing mesh used in the time-domain analysis requires over 2 million separate memory locations to store the calculated fields and constituent parameters. The total memory locations required by this GEMACS analysis was well over 10 million.

Memory requirements aside, the measure of the two programs' efficiencies was based strictly on the amount of CPU time the programs needed to execute. The GEMACS program on the VAX computer took 32.97 seconds to run the INPUT module, 85.30 seconds for the OUTPUT module, and 35626.45 seconds for the MOM module, for a total run time of 35744.72 CPU seconds or about 9 hours and 55 minutes. The T3DFD program was run on a CDC Cyber 845 computer, which is about 1.5 times faster than the ISL VAX. The CPU execution time for one pass through the program was 4341.2 seconds (50:71). Twenty passes were needed to compute the required time-domain EM fields bringing the total CPU run time to 86824 seconds or about 24 hours and 7 minutes, not including the time it takes to convert the data to the frequency domain. Had this program been run on the slower VAX machine, the execution time would have been extended to about 36 hours. The CPU time reduction afforded by GEMACS is over 26 hours. This significant reduction in program execution time demonstrates that the use of GEMACS by future lightning EMP analysts can result in a savings of thousands of dollars. Therefore, the GEMACS program was determined to be much more efficient than the T3DFD program.

## Conclusions

The following is a digest of the conclusions drawn from the results presented in this thesis:

1. The predicted transfer functions adequately represent the actual aircraft transfer functions at most of the frequencies in the 0.5 MHz to 5.0 MHz bandwidth.
2. The GEMACS program is much more efficient, in terms of mainframe CPU run time, than the T3DFD program.
3. The lightning/aircraft EM interaction problem must be well posed. Actual lightning channel entry and exit orientations strongly affect the overall interaction; some orientations can result in mutual coupling between the channel and aircraft. In order for a model to predict the coupling phenomena, channel orientations must be known. Also, the wing-to-wing configuration implemented for this analysis yielded results that would differ considerably from those that would be obtained from a nose-to-tail scenario.
4. The GEMACS predicted transfer functions offer more resonance information at lower frequencies than the transfer functions derived from the previously performed T3DFD analysis results.
5. The FFT technique used to convert time-domain

information is limited by the number of time-sampled points. The technique cannot transform discrete time-domain information into the entire frequency spectrum, especially at frequencies below 0.5 MHz.

6. The termination of the exiting lightning channel model into an infinite ground plane more accurately represents the actual lightning/aircraft interaction event. Termination of the channel in free space, as was performed in the BDM helicopter analysis, may lead to erroneous results. However, no investigation was performed to determine the optimum location of the ground plane with respect to the aircraft.

7. The MOM including the BMI technique is a very accurate and efficient solution method relative to the general MOM solution, although it should be carefully implemented and tested against the complete solution method whenever it is used.

8. The prominent peak magnitudes found in the actual aircraft transfer functions occur at frequencies related to the dimensions and combinations of dimensions of the aircraft.

9. The derived transfer functions show resonant frequencies that correspond to half-wavelengths equal to aircraft lengths and combinations of lengths.

10. Plotted lightning channel current distributions

at 5 MHz show that the periodic nature of the distribution is related to the length of the corresponding lightning channel model.

11. Actual transfer functions show resonant spikes at other frequencies not used in the analysis, suggesting that a more refined frequency band (closer spaced frequencies) should have been used.

12. Other differences noted between actual and predicted waveforms could most likely have been accounted for if

a. more segments had been included in the wings and rear stabilizer sections of the aircraft wire grid model and

b. the actual aircraft surface/channel impedances had been incorporated into that model.

The overall conclusion is that GEMACS, implemented under the conditions outlined in this report, can adequately predict lightning induced EM skin current distributions as a function of frequency on the CV-580 aircraft and that GEMACS can make these predictions more efficiently than the corresponding time-domain three-dimensional finite difference program. The GEMACS frequency-domain analysis and results are summarized and recommendations for follow-on efforts are given in the next chapter.

## 5. Summary and Recommendations

The process whereby lightning induced EM fields penetrate and/or diffuse through aircraft apertures and joints is not well understood and is presently being investigated. With the increased use of low current level semiconductor circuits in many mission critical subsystems, and with the trend towards completely fly-by-wire aircraft, inadequate protection from the lightning environment could jeopardize both mission capability and aircrew safety. The amount of added external and internal lightning protection required has yet to be quantitatively determined. Once the exterior protection is provided, engineers will be able to determine the amount of interior shielding and circuit surge protection necessary to protect the aircraft from the lightning hazard. Without this knowledge, aircraft designers must overprotect the electronic circuits at a substantial monetary and weight cost.

This thesis took a first step towards determining the external protection requirements by implementing the General EM Model for the Analysis of Complex Systems (GEMACS) frequency-domain program to analyze lightning's EM interaction with the surface of a CV-580 aircraft. The aircraft and lightning channels were represented by a 384 segment wire grid model. The GEMACS' Method of Moments (MOM) Module provides an approximate solution to Maxwell's integral equations. Wire grid segment currents were solved as a function of frequency. Predicted frequency-domain current transfer functions were

derived and compared to actual CV-580 transfer functions derived from in-flight, measured lightning data.

The two main objectives of this thesis were as follows:

(1) to determine the capability of the GEMACS program to predict aircraft skin current distributions as a function of frequency and (2) to assess the GEMACS program's efficiency relative to the efficiency of the time-domain three-dimensional finite difference (T3DFD) program. The GEMACS program yielded acceptable skin current predictions in the frequency band 0.5 MHz to 5.0 MHz. Also, the results of the GEMACS analysis provided more information in this bandwidth than the corresponding results of the previously performed T3DFD analysis. Finally, the GEMACS program was found to be much more efficient than the T3DFD program, in terms of mainframe CPU program execution time.

The GEMACS is by no means a finished product. In fact, the GEMACS Version 4 is completed but is as yet unpublished. The new version will yield a tremendous increase in GEMACS capabilities by the inclusion of modules which will allow the finite difference (FD) analysis of cavities and apertures and a MOM/GTD/FD hybridization "to allow the self-consistent analysis of the EM interaction from the source to the aperture, through the aperture, and inside the compartments of aerospace vehicles" (5:4). Also, Rome Air Development Center is planning a self-training tutorial book which will present examples of how to apply GEMACS to a variety of problems.

There are several follow-on efforts which could further

define the need for an aircraft's external protection from a lightning strike. The first recommendation is to perform another GEMACS analysis similar to the one described in this thesis. The starting point of the new analysis would be to refine the aircraft wire grid model by adding more segments, especially to the sections of the grid which represent the wings, rear vertical and horizontal stabilizers, and engine mounts. An alternate lightning channel offered in the analysis chapter should be implemented to determine if it is an accurate method of simulating the lightning induced current surge. The impedance conductivity of the CV-580 surface material and lightning channels should be incorporated into the analysis. The new analysis should be performed for more frequencies, possibly 100 or 200, in a 0.5 MHz to 10.0 MHz bandwidth. The results of the new analysis added to the results of this thesis would certainly show the GEMACS program's potential capability to precisely predict aircraft skin currents as a function of frequency.

Another related recommendation is to determine if the various aircraft resonant regions can be determined by using a lumped parameter circuit approach. Since the frequency of lightning is relatively low, it may be possible to construct a circuit model, representing the surface of the aircraft, with nothing more than lumped circuit parameters of resistance, capacitance, and inductance loads, much like the manner a transmission line is modelled in circuit components. Then, for a given lightning induced current surge, elementary

circuit analysis, using standard circuit analysis programs such as SPICE or SCEPTRE, could be used to determine the inherent resonant frequencies associated with the RLC representation. Since these resonances relate well to dimensions of the aircraft, a first-order approximation of the skin current distributions may be possible from such a simple analysis approach. Also, knowledge of the aircraft's resonant frequencies can lead to the determination of the half-wavelengths which may correspond to areas on the aircraft needing the most protection from a threatening lightning strike.

## Appendix

### Constructing Wire Grid Models in GEMACS

The process of constructing a wire grid model in GEMACS is relatively straightforward. However, depending on the size of the object to be modelled, the procedure can be tedious and time consuming. The purpose of this section is to provide a step-by-step modelling algorithm to assist future GEMACS users. The algorithm is applicable to strict wire grid models to be used in conjunction with the GEMACS method of moments module. The process does not apply to the construction of those types of geometries (solids, plates, non-wire elements) needed for GEMACS GTD and GTD/MOM hybrid analyses.

In essence, a GEMACS MOM wire grid model is a finite set of user defined points connected by wire segments in a coordinate space. It is basically a dot-to-dot game in which the user determines the location of the dots and how the dots will be connected. Like all games, the wire model must be constructed according to a set of "rules". The rules for constructing a wire grid model in GEMACS are given in the Engineering and User Manuals and are listed below:

1. Segments must be short compared to the highest operating wavelength. One-tenth of a wavelength is adequate for most purposes.

2. Actual wires should be modelled with the actual wire radius. Grid models should use a wire radius of approximately one-fifth of the segment length.

3. Grid mesh perimeters (distance around any given closed loop of adjacent segments) should not be greater than one-half wavelength. Larger perimeters may lead to loop resonances and poor results.

4. Joined segments' lengths should not differ by more than a factor of two.

5. Small angles (less than 20 degrees) between joined segments should be avoided.

6. The maximum number of segments at any given junction is limited to 50.

7. The maximum number of segments is 20,000.

The GEMACS User and Engineering Manuals provide additional guidelines for GTD structure geometries.

The following step by step modelling procedure is only one way of obtaining the desired wire grid pattern. Depending on the size and complexity of the object being modelled, it may be convenient to skip some of the steps. An example is provided which illustrates the procedure.

Step 1. Obtain a drawing, schematic, or any type of diagram that gives the overall dimensions of the object. For large objects, it is best to have a three-view drawing which shows a top, front, and side view.

Step 2. Convert all dimensions to a common measurement unit. That is, if the dimensions are metric, convert them all to meters, centimeters, etc.

Step 3. Determine the maximum frequency at which GEMACS will be operated. Calculate the corresponding wavelength. One-tenth of this wavelength will be the model's maximum segment length.

Step 4. On one of the drawings, place dots on the surface of the object, bearing in mind the maximum segment length. Connect the dots so that the resulting wire pattern is a fairly good representation of the object.

Step 5. Choose a convenient location for the origin of an "appropriate" coordinate system (this procedure was developed with the cartesian coordinate system regarded as appropriate.)

Step 6. Plot a top, side, and front view of the dot/segment representation on engineering graph paper. In order to maintain coherence between the three drawings, it may be convenient to round off the object's overall dimensions. The actual dimensions can be included later. It is at this point that the user should check to see that the guidelines offered above are followed. In particular, assure that (a) no segment is longer than one-tenth wavelength, (b) closed loop perimeters are shorter than one-half wavelength, and (c) joined segments differ by no more than a factor of two. Other guideline criteria will be met/verified in a later step.

Step 7. From the three-view plots, draw a 3-D

representation of the object. This may be the hardest step for some users; however, it is necessary to be able to see all segments in relation to each other. Also, the 3-D drawing will allow the user to determine if joined segments have an angle of greater than 20 degrees between them.

Step 8. Number the dots and segments. If the object is relatively small (e.g. FM antenna, simple loop antenna) the user can simply specify the geometry in the most convenient manner and then use the GEMACS "renumber" command to subsequently renumber the wire segments to locate the near-neighbor interactions close to the diagonal of the interaction matrix (see GEMACS User Manual, p57). However, for large objects, especially those in which the user is only interested in the current or voltage data associated with few of the segments, the GEMACS Banded Matrix Interaction (BMI) technique should be employed. In this case, it is necessary to number and connect the points in a way such that the segments of interest lie within the desired banded portion of the interaction matrix. The user should reference the User and Engineering Manuals for a complete description of the BMI technique. The best choice of numbering is obvious in some cases and not in others; also, more than one choice may be apparent. The following suggestions may be helpful in numbering the wire model in a logical, practical manner:

- a. Number the points/segments of greatest interest first to assure that they are within the banded portion of the interaction matrix. All other "uninteresting" segments can be

numbered in any convenient manner.

b. Locate the two most extreme points on the wire grid. These points will be the start and finish points of the numbering scheme.

c. There are two ways to number the remaining points/segments:

1. Number the points in a left-to-right fashion until the finish point is reached. Then, draw arrowheads from point to point until all segments have been marked. For ease of future code entry, use a logical and consistent method of directing the arrowheads (e.g. direct all arrowheads from the smaller numbered point to the larger numbered point.)

-or- 2. Draw arrowheads from point to point. Direct the arrowheads in such a way as to simulate the probable current path from the start point to the finish point. After all segments have been marked, place numbers on the points such that the arrowhead points from the smaller number to the larger one.

Step 9. Once all points have been numbered and segments marked, the structure geometry must be coded for GEMACS use. For strict wire grid models, only four GEMACS Geometry Input Processor (GIP) commands are needed: SC (scale), PT (point), RA (radius), and CP (connect point). The easiest, most careful, but less direct, method of getting the wire grid information into code is as follows:

a. Set up a table for the points in coordinate

space. Using the 3-D drawing, three-view plots, and basic analytical geometry, determine the coordinate components of every point on the wire grid model (this sub-step is the reason that the  $x,y,z$  system is preferred.)

b. Set up a table for point connection information. The table should include the point at which the segment begins and ends, how many segments there are between any two points, and the length of each segment.

c. Set up another table for calculation of segment radii. In one column, list all segment lengths in ascending order of magnitude. Recall the guideline concerning the length-to-radius proportion. Set a minimum radius proportion of about one-sixth of a segment length ( $L$ ). Calculate  $L/6$  and  $L/5$  for each  $L$ . Now the table contains radius windows for each segment length. Since the maximum number of radius values supported by GEMACS is 10, separate the segment lengths into no more than 10 ranges of lengths. Choose the largest radius in any given range of segment lengths to be used as the segment radius for those lengths.

All of the information needed to code the wire grid model is now easily accessible and applicable. Follow the GEMACS User Manual instructions for entering the information in the required format. The following example demonstrates the step-by-step wire grid modelling procedure for a CV-580 aircraft as the structure geometry of interest.

### Example

The CV-580 wire grid used for this GEMACS analysis will be used as an example of the above step-by-step procedure. A CV-580 drawing showing the overall dimensions of the aircraft is obtained (step 1) and is shown in Figure A1. All of the dimensions are converted to inches (step 2). The maximum operating frequency is chosen to be 5 MHz (step 3) and one-tenth of an operating wavelength is calculated to be approximately 236 inches. This value is the maximum allowable segment length. The dots are placed on Figure A1 with the maximum segment length in mind (step 4). A cartesian coordinate system is chosen such that the tail of the aircraft just touches the y-z plane, the edge of the right wing just touches the x-z plane, and the entire aircraft is above the x-y plane ( $z=0$ ), which represents the ground (step 5). A front, top, and side view are plotted on graph paper, Figure A2, and the geometry guidelines have been checked (step 6). A 3-D view of the CV-580 wire grid representation is drawn (step 7) and the segments and points are then numbered in accordance with step 8.c.1. The numbered wire grid is illustrated in Figure A3. Steps 9a, 9b, and 9c are shown in Tables A1, A2, and A3, respectively. Figure A4 gives the wire grid pattern and radii data in GEMACS code. The 2-D and 3-D plots, Figures A5 and A6, were obtained using a Hewlett-Packard HP-9000.





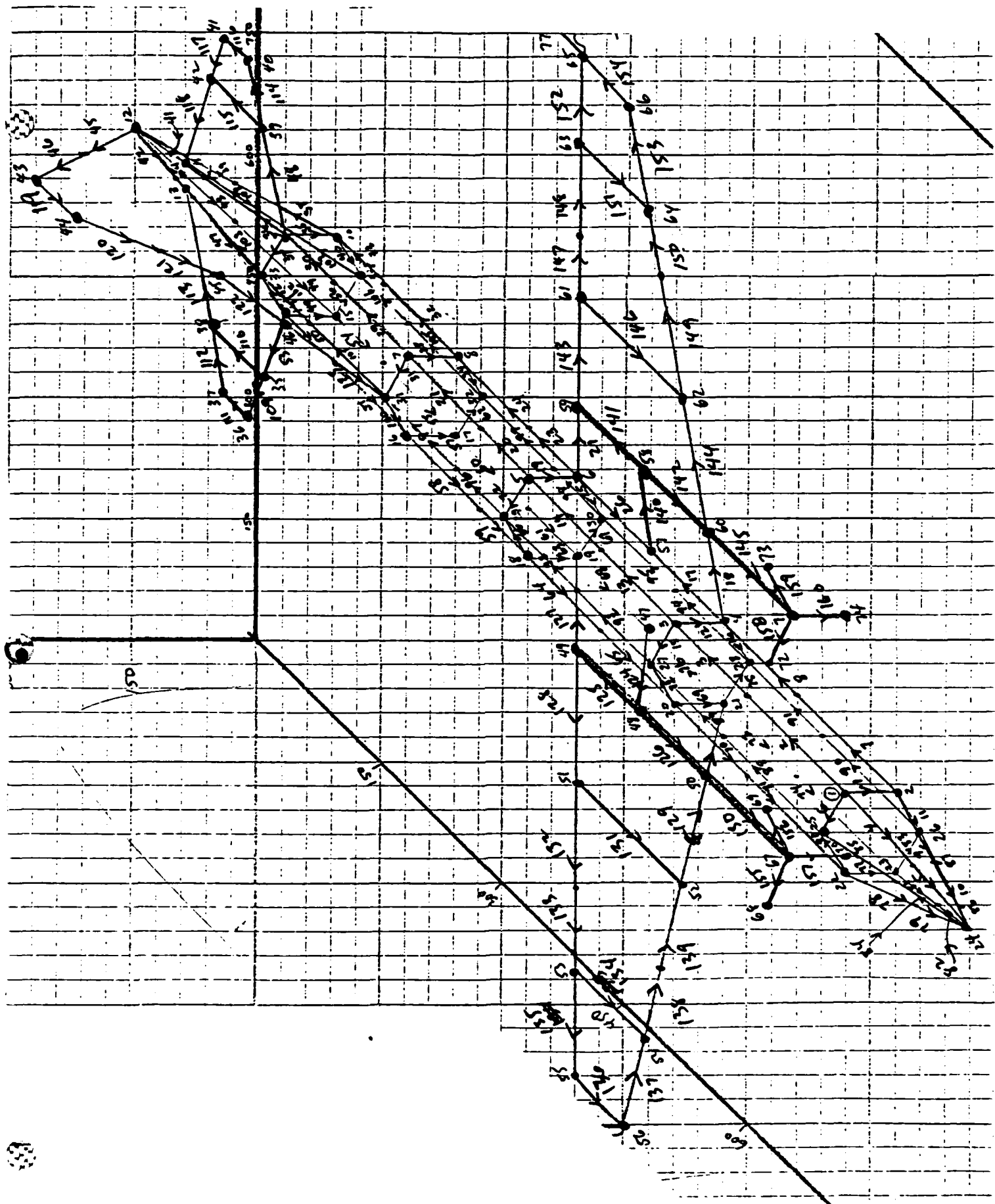


Figure A3. 3-D Plot of CV-580 Wire Grid Model

Table A1  
Example of Coordinate Components  
of Wire Grid Points

Point	X	Y	Z
1	870.0	682.0	150.0
2	870.0	682.0	90.0
3	660.0	682.0	150.0
4	660.0	682.0	90.0
5	480.0	682.0	150.0
6	480.0	682.0	90.0
⋮	⋮	⋮	⋮
78	-24660.0	1260.0	0.0

Table A2  
Example of Point Connections

Segment Number	Start Point	End Point	Number of Segments	Segment Length
1	1	2	1	60
2,3	1	3	2	105
4,5	1	24	2	65
6	1	25	1	60
7,8	2	4	2	105
9,10	2	24	2	65
11	2	26	1	60
⋮	⋮	⋮	⋮	⋮
274-383	76	77	110	228
384	77	78	1	150

Table A3  
Example of Segment Radii

Segment Lengths	Radius	Radius Number
40,45	7.16	1
60,62,64.5,65,68	10.82	2
70,71,75	11.94	3
80,100	16.0	4
⋮	⋮	⋮
228	36.29	10

SC IN	PT 71 750.0 750.0 100.0	CP 22 25 1 0 2
PT 1 870.0 682.0 150.0	PT 72 750.0 720.0 135.0	CP 23 24 2 0 2
PT 2 870.0 682.0 90.0	PT 73 750.0 640.0 135.0	CP 23 26 1 0 2
PT 3 660.0 682.0 150.0	PT 74 750.0 750.0 30.0	CP 24 25 2 0 2
PT 4 660.0 682.0 90.0	PT 75 600.0 0.0 270.0	CP 24 26 2 0 2
PT 5 480.0 682.0 150.0	PT 76 600.0 0.0 25350.0	CP 25 27 2 0 7
PT 6 480.0 682.0 90.0	PT 77 420.0 1260.0 150.0	CP 26 28 2 0 7
PT 7 330.0 682.0 150.0	PT 78 -24660.0 1260.0 150.0	CP 27 29 2 0 5
PT 8 330.0 682.0 90.0	PT 79 -24660.0 1260.0 0.0	CP 28 30 2 0 5
PT 9 180.0 682.0 150.0	RA 7.16 10.82 11.94 16.0	CP 29 31 2 0 3
PT 10 180.0 682.0 90.0	RA 14.48 15.68 16.71 19.87	CP 30 32 2 0 3
PT 11 60.0 647.0 150.0	RA 24.03 36.29	CP 31 16 1 0 2
PT 12 0.0 630.0 150.0	CP 1 2 1 0 2	CP 31 33 2 0 3
PT 13 60.0 613.0 150.0	CP 1 3 2 0 7	CP 33 12 2 0 5
PT 14 180.0 578.0 150.0	CP 1 24 2 0 2	CP 32 34 2 0 3
PT 15 180.0 578.0 90.0	CP 1 25 1 0 2	CP 34 12 2 0 7
PT 16 330.0 578.0 150.0	CP 2 4 2 0 7	CP 35 26 1 0 3
PT 17 330.0 578.0 90.0	CP 2 24 2 0 2	CP 35 38 1 0 2
PT 18 480.0 578.0 150.0	CP 2 26 1 0 2	CP 36 37 1 0 1
PT 19 480.0 578.0 90.0	CP 3 4 1 0 2	CP 37 38 1 0 3
PT 20 660.0 578.0 150.0	CP 3 5 2 0 5	CP 38 13 1 0 9
PT 21 660.0 578.0 90.0	CP 3 27 1 0 2	CP 39 40 1 0 3
PT 22 870.0 578.0 150.0	CP 4 28 1 0 2	CP 39 42 1 0 2
PT 23 870.0 578.0 90.0	CP 4 57 1 0 5	CP 40 41 1 0 1
PT 24 970.0 630.0 120.0	CP 4 60 1 0 6	CP 41 42 1 0 3
PT 25 870.0 630.0 180.0	CP 5 6 1 0 2	CP 42 11 1 0 9
PT 26 870.0 630.0 60.0	CP 5 7 2 0 3	CP 43 44 1 0 1
PT 27 660.0 630.0 180.0	CP 5 29 1 0 2	CP 44 45 2 0 2
PT 28 660.0 630.0 60.0	CP 6 8 2 0 3	CP 45 46 1 0 2
PT 29 480.0 630.0 180.0	CP 6 30 1 0 2	CP 46 31 1 0 6
PT 30 480.0 630.0 60.0	CP 6 57 1 0 5	CP 47 48 1 0 6
PT 31 330.0 630.0 180.0	CP 6 59 1 0 6	CP 48 49 1 0 4
PT 32 330.0 630.0 60.0	CP 7 8 1 0 2	CP 48 50 1 0 4
PT 33 180.0 630.0 180.0	CP 7 9 2 0 3	CP 49 19 1 0 6
PT 34 180.0 630.0 60.0	CP 7 31 1 0 2	CP 49 51 1 0 9
PT 35 154.0 480.0 150.0	CP 8 10 2 0 3	CP 52 50 1 0 9
PT 36 140.0 410.0 150.0	CP 8 32 1 0 2	CP 50 21 1 0 6
PT 37 100.0 410.0 150.0	CP 9 10 1 0 2	CP 50 67 1 0 4
PT 38 86.0 480.0 150.0	CP 9 11 1 0 8	CP 51 52 1 0 9
PT 39 154.0 780.0 150.0	CP 9 33 1 0 2	CP 51 53 2 0 7
PT 40 140.0 850.0 150.0	CP 10 12 2 0 6	CP 53 54 1 0 5
PT 41 100.0 850.0 150.0	CP 10 34 1 0 2	CP 53 55 1 0 8
PT 42 86.0 780.0 150.0	CP 11 12 1 0 2	CP 55 56 1 0 2
PT 43 60.0 630.0 330.0	CP 12 13 1 0 2	CP 56 54 1 0 8
PT 44 105.0 630.0 330.0	CP 12 15 2 0 6	CP 54 52 2 0 7
PT 45 180.0 630.0 225.0	CP 12 43 2 0 6	CP 57 58 1 0 6
PT 46 240.0 630.0 210.0	CP 13 14 1 0 6	CP 58 59 1 0 4
PT 47 570.0 578.0 90.0	CP 9 39 1 0 7	CP 58 60 1 0 4
PT 48 570.0 480.0 100.0	CP 14 15 1 0 2	CP 59 61 1 0 9
PT 49 470.0 480.0 100.0	CP 14 16 2 0 3	CP 60 62 1 0 9
PT 50 650.0 480.0 100.0	CP 14 33 1 0 2	CP 60 71 1 0 4
PT 51 506.0 330.0 116.0	CP 14 35 1 0 7	CP 61 62 1 0 9
PT 52 634.0 330.0 116.0	CP 15 17 2 0 3	CP 61 63 2 0 7
PT 53 527.5 120.0 137.5	CP 15 34 1 0 2	CP 62 64 2 0 7
PT 54 612.5 120.0 137.5	CP 16 17 1 0 2	CP 63 64 1 0 5
PT 55 540.0 0.0 150.0	CP 16 18 2 0 3	CP 63 65 1 0 8
PT 56 600.0 0.0 150.0	CP 17 19 2 0 3	CP 64 66 1 0 8
PT 57 570.0 682.0 90.0	CP 17 32 1 0 2	CP 66 65 1 0 2
PT 58 570.0 780.0 100.0	CP 18 19 1 0 2	CP 67 66 1 0 3
PT 59 490.0 760.0 100.0	CP 18 20 2 0 5	CP 67 69 1 0 3
PT 60 650.0 780.0 100.0	CP 18 29 1 0 2	CP 67 70 1 0 3
PT 61 506.0 930.0 116.0	CP 19 30 1 0 2	CP 71 72 1 0 3
PT 62 634.0 930.0 116.0	CP 19 47 1 0 5	CP 71 73 1 0 3
PT 63 527.5 1140.0 137.5	CP 20 21 1 0 2	CP 71 74 1 0 3
PT 64 612.5 1140.0 137.5	CP 20 22 2 0 7	CP 76 75 110 0 10
PT 65 540.0 1260.0 150.0	CP 20 27 1 0 2	CP 75 56 1 0 8
PT 66 600.0 1260.0 150.0	CP 21 23 2 0 7	CP 65 77 1 0 8
PT 67 750.0 480.0 100.0	CP 21 28 1 0 2	CP 77 78 110 0 10
PT 68 750.0 420.0 135.0	CP 21 47 1 0 5	CP 78 79 1 0 9
PT 69 750.0 540.0 135.0	CP 22 23 1 0 2	
PT 70 750.0 480.0 30.0	CP 22 24 2 0 2	END

Figure A4. Geometry Input Data for CV-580 Wire Grid Model

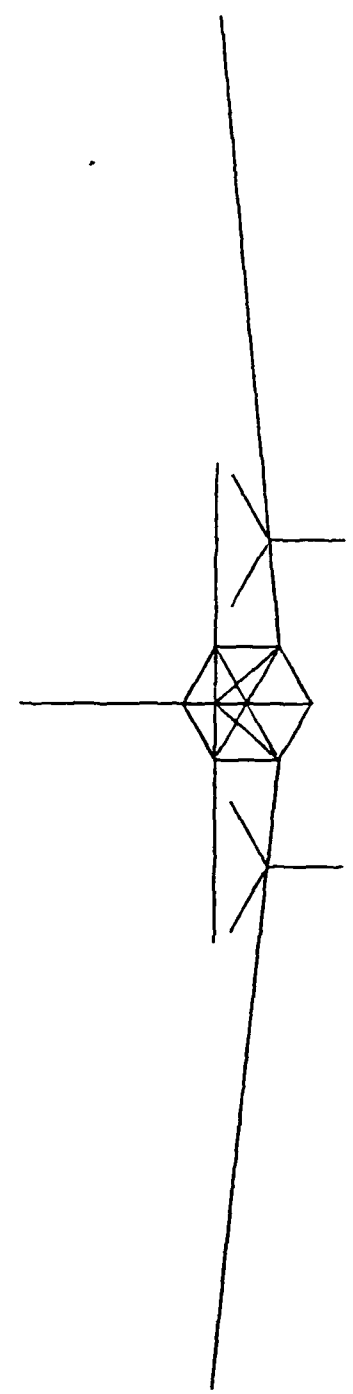
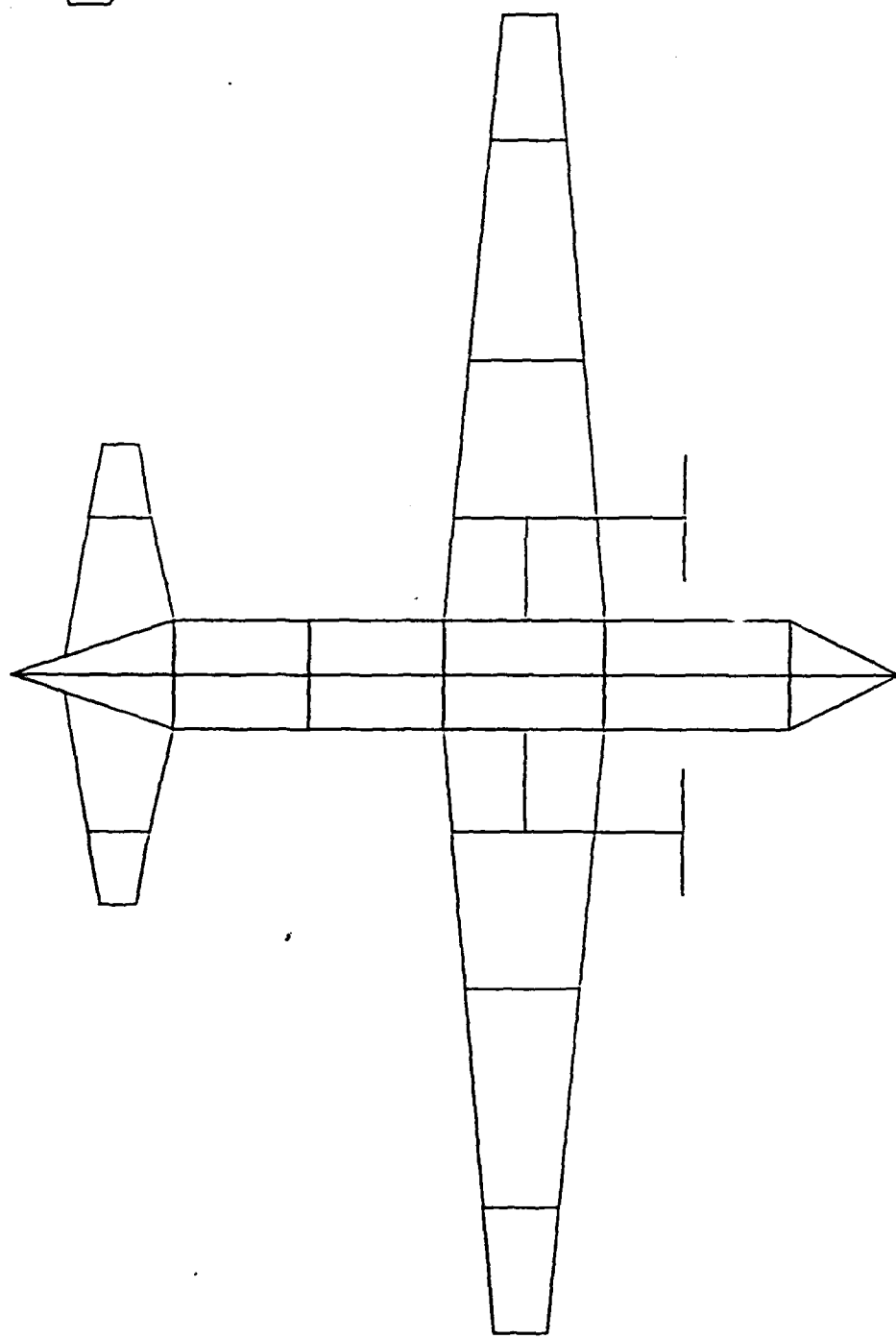
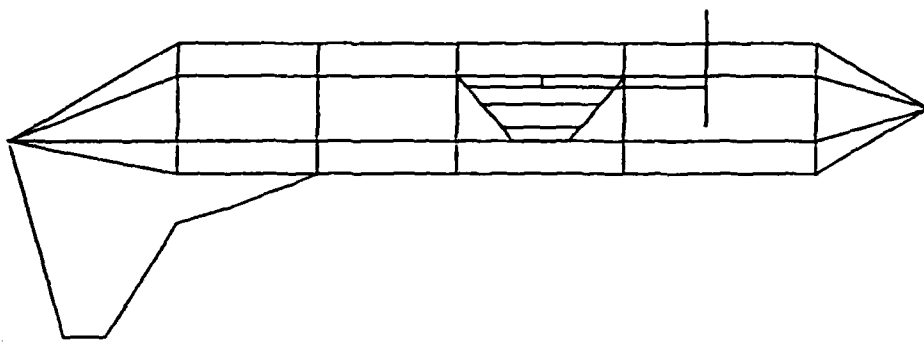


Figure A5. 2-D Wire Representations of CV-580

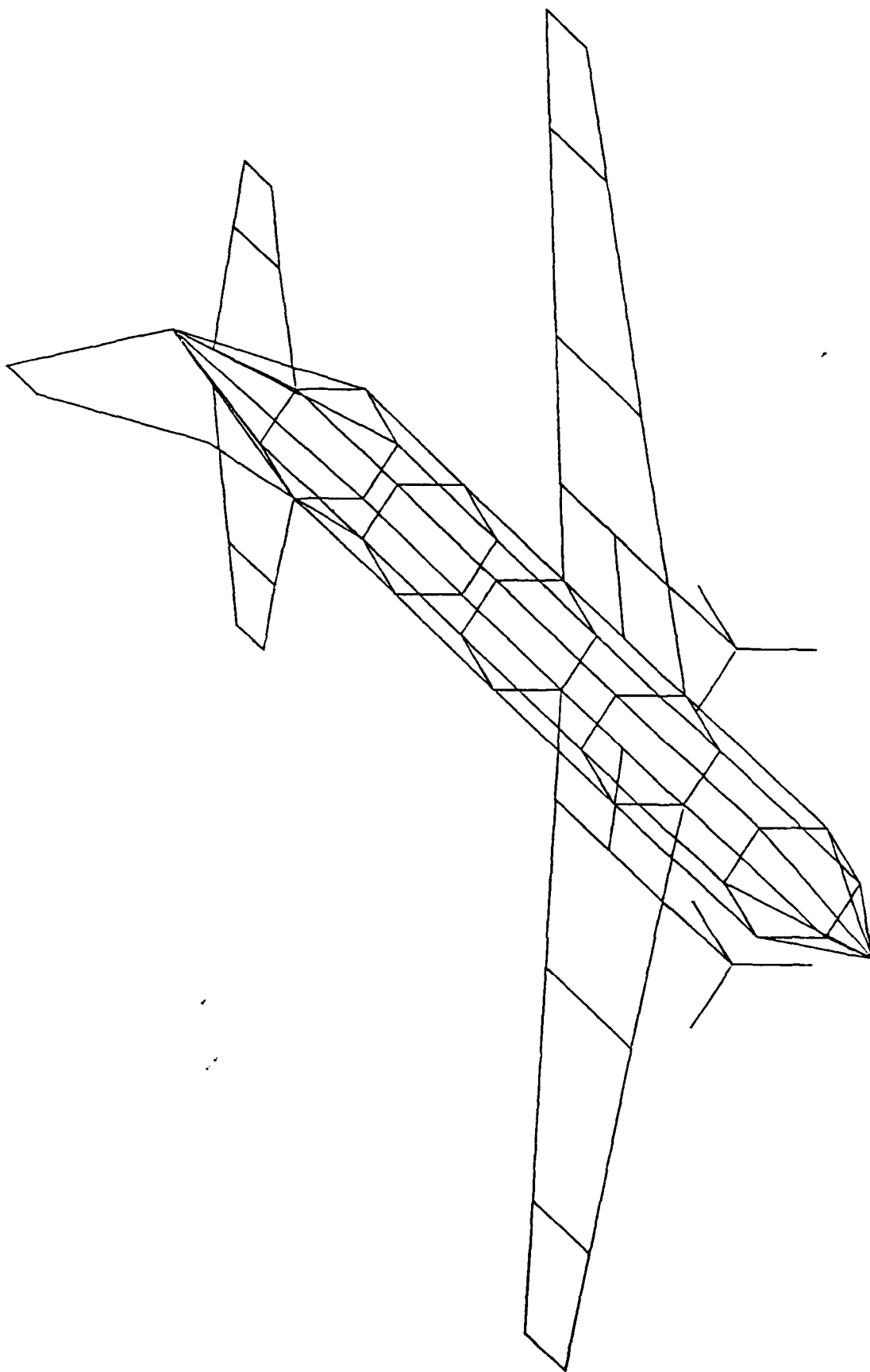


Figure A6. 3-D Wire Representation of CV-580

Overall, the process of constructing a wire grid model is not hard but can be very tedious and time consuming. One suggestion for making the process even smoother would be the inclusion of a Computer Aided Design (CAD) capability to the front end of the GEMACS code. This capability would allow users to define and construct the desired wire grid models at a terminal and to actually visualize the construction taking place. Besides the obvious advantages of being able to reconstruct the wire geometry at the stroke of a key, the CAD feature would allow users to apply the results to a wide case of problems, including EMC, EMI, NEMP, and LEMP, with the same geometry set.

## Bibliography

1. Abrams, C.R. EMP (Electro-Magnetic Pulse) Protection of Advanced Flight Control Systems: Final Report. Project Number F41423. Naval Air Development Center, Aircraft and Crew Systems Technology Directorate, Warminster, PA, November 1984 (AD-B088966L).
2. Beavin, R.C., J.R. Lippert, and J.E. LaVoie. "Progress of the Atmospheric Electricity Hazards Protection Program," Proceedings of the 9th International Aerospace and Ground Conference on Lightning and Static Electricity. Paper No 13: 1-14. Orlando FL, June 26-28, 1984.
3. Bevensee, R.M. et al. "Computer Codes for EMP Interaction and Coupling," IEEE Transactions on Electromagnetic Compatibility, EMC-20, No 1: 156-165 (February 1978).
4. Coffey, E.L. Electromagnetics Analyst. Telephone Interview. Advanced Electromagnetics, Albuquerque NM; 1 October 1986.
5. Coffey, E.L. and J.L. Hebert. "Implementation of GEMACS for Lightning Interactions Analysis," Proceedings of the 11th International Aerospace and Ground Conference on Lightning and Static Electricity. Dayton OH, June 24-26, 1986.
6. Conte, Samuel D. and Carl de Boor. Elementary Numerical Analysis: An Algorithmic Approach (Third Edition). New York: McGraw-Hill Book Company, 1980.
7. Cukr, Jeffrey M. An Analysis and Comparison of Lightning Return Stroke Models at Altitude. Master's Thesis. Air Force Institute of Technology, Wright-Patterson AFB, OH, December 1981 (AD-A151841).
8. DuBro, Gary A. Atmospheric Electricity-Aircraft Interaction. Lecture Series. Advisory group for Aerospace Research and Development. Neuilly-Sur-Seine, France, May 1980 (AD-A087976).
9. Edwards, V.E. et al. Distributed and Embedded, Pulse-Tolerant, Hierarchical Flight Control System (DEPTH-FCS): Final Report, October 1982 - August 1983. Contract Number N62269-82-C-0274. Honeywell Systems and Research Center, Minneapolis, MN, August 1983 (AD-B089827L).

10. Eriksen, E.J., T.H. Rudolph and R.A. Perala. Atmospheric Electricity Hazards Analytical Model Development and Application; Vol III: Electromagnetic Coupling Modelling of the Lightning/Aircraft Interaction Event: Final Report, August 1979 - June 1981. Electro Magnetic Applications Inc, Denver CO, June 1981 (AD-A114017).
11. Fisher, Frank A. Analysis and Calculations of Lightning Interactions with Aircraft Electrical Circuits: Final Technical Report, 16 May 1976 - 21 February 1978. Contract F33615-76-C-3122. General Electric Company Corporate Research and Development, Schenectady, New York, August 1978 (AD-A062606).
12. Gindelberger, B.E., G. Salo, and G.H. Lamb. GEMACS Modification, Implementation, and Analysis for AFWAL/FIEA: Final Report. The BDM Corporation, Air Force Wright Aeronautical Laboratories Technical Report (in publication), AFWAL/FIEA, Wright-Patterson AFB, OH.
13. Harrington, Roger F. Field Computation by Moment Methods. Malabar, Florida: Roger E. Krieger Publishing Company, 1983.
14. Hebert, James L. Lightning Analysis and Characterization Engineer. Personal Interviews. AFWAL/FIESL, Wright-Patterson AFB, OH; 22 February 1986 - 15 November 1986.
15. Hebert, James L. and Carlos Sannchez-Castro. Implementation of a Three-Dimensional Finite Difference Electromagnetic Code for Analysis of Lightning Interaction with a FAA CV-580 Aircraft. Final Technical Report, April 1984 - January 1985. Wright-Patterson AFB, OH: Flight Dynamics Laboratory, Air Force Wright Aeronautical Laboratories (AFWAL/FIESL).
16. Hebert, James L. and J.G. Schneider. "Current Levels and Distributions on an Aircraft During Ground Lightning Simulation Tests and In-Flight Lightning Attachments," Proceedings of the 11th International Aerospace and Ground Conference on Lightning and Static Electricity. Dayton OH, June 24-26, 1986.
17. Holland, R. "THREDE: A Free-Field EMP Coupling and Scattering Code," IEEE Transactions on Nuclear Science, Volume NS-24. (December 1977).
18. Jaeger, D. Increasing Significance of Electromagnetic Effects in Modern Aircraft Development. Messerschmitt-Boelkow-Blohm GMBH Military Aircraft Division, Munich, Germany F R, October 1983 (AD-P002844/AD-A135100).

19. Kadlec, D.L. and E.L. Coffey. GEMACS User Manual (Version 3). The BDM Corporation, RADC-TR-83-217, Volume I, September 1983 (AD-A137461).
20. Kadlec, D.L. and E.L. Coffey. GEMACS Engineering Manual (Version 3). The BDM Corporation, RADC-TR-83-217, Volume I, September 1983 (AD-A137462).
21. Kadlec, D.L. and E.L. Coffey. GEMACS Computer Code Documentation (Version 3). The BDM Corporation, RADC-TR-83-217, Volume I, September 1983 (AD-A137463/AD-A137464/AD-A137509/AD-A137510).
22. Kreyszig, Erwin. Advanced Engineering Mathematics (Fourth Edition). New York: John Wiley and Sons, Inc., 1979.
23. Kuhlman, B.P. and M.J. Reazer. "Characterization of Fast-Risetime Electromagnetic Field Pulses Recorded in Airborne Measurements during Florida Thunderstorms," Proceedings of the 9th International Aerospace and Ground Conference on Lightning and Static Electricity. Paper No 23: 1-13. Orlando FL, June 26-28, 1984.
24. Kunz, Karl S., B.W. Torres, R.A. Perala, J.M. Hamm, M.L. Van Blaricum, and J.F. Prewitt. "Surface Current Injection Techniques: A Theoretical Investigation," IEEE Transactions on Nuclear Science, Volume NS-25, Number 6: 1422-1427 (December 1978).
25. Kurzhals, P.R. and R. Onken. Integrity in Electronic Flight Control Systems: Advisory Report. Advisory Group for Aerospace Research and Development, Neuilly-Sur-Seine, France, July 1979 (AD-A074614).
26. Lee, K.S.H. (Editor) et al. "EMP Interaction: Principles, Techniques and Reference Data," EMP Interaction Note 2-1. Technical Report AFWL-TR-80-402. Air Force Weapons Laboratory, Kirtland AFB NM, December 1980.
27. Lippert, J.R. "Vulnerability Assessment of Electricity/Electronic Subsystems and Equipment to Atmospheric Electricity," Proceedings of the 8th International Aerospace and Ground Conference on Lightning and Static Electricity. Paper No 77: 1-8. Fort Worth TX, June 21-23, 1983.
28. Longmire, Conrad L. "State of the Art in IEMP and SGEMP Calculations," IEEE Transactions on Nuclear Science, Volume 22, Number 6: 2340-2344 (December 1975).

29. Maxwell, K.J., F.A. Fisher, J.A. Plummer, and P.R. Rogers. Computer Programs for Prediction of Lightning Induced Voltages in Aircraft Electrical Circuits: Final Report, 1 February 1974 - 30 November 1974. Contract F33615-74-C-3068. General Electric Corporate Research and Development, Schenectady, New York, April 1975 (AD-A015174).
30. Mazur, V., B.D. Fisher, J.C. Gerlach. Conditions Conducive to Lightning Striking an Aircraft in a Thunderstorm. Cooperative Institute for Mesoscale Meteorological Studies, Norman OK, 1983 (AD-P002235/AD-A135100).
31. McGlasson, Allan J. Forecasting the Lightning Strike Hazard to Aircraft, Student Research Report, ACSC-1665-81. Air Command and Staff College, Maxwell AFB, AL, May 1981 (AD-B057560L).
32. Muhleisen, R. and H.J. Fisher. Lightning Danger to Jet Aircraft, Part I. Report Number FTD-ID(RS)T-1382-77. Foreign Technology Division, Wright-Patterson AFB, OH, September 1977 (AD-B025455L).
33. Perala, R.A., T. Rudolph, and F. Eriksen. "Electromagnetic Interaction of Lightning with Aircraft," IEEE Transactions on Electromagnetic Compatibility, EMC-24, No 2: 173-203 (May 1982).
34. Pierce, Edward T. Triggered Lightning and Some Unsuspected Lightning Hazards: Scientific Note Number 15. Stanford Research Institute, Menlo Park CA, January 1972 (AD-735917).
35. Rasch, Nickolus O. A Compendium of Lightning Effects on Future Aircraft Electronic Systems: Final Report. Federal Aviation Administration Technical Center, Atlantic City NJ, February 1982 (AD-A114117).
36. Reazer, Jean S. and A.V. Serrano. "Spatial and Temporal Description of Strikes to the FAA CV-580 Aircraft," Proceedings of the 11th International Aerospace and Ground Conference on Lightning and Static Electricity. Dayton OH, June 24-26, 1986.
37. Robb, John D. and J.R. Stahmann. Aircraft Protection from Thunderstorm Electromagnetic Effects. Lightning and Transients Research Institute, Minneapolis MN, May 1963 (AD-414903).
38. Rustan, Peter L. and James L. Hebert. "Lightning Measurements on an Aircraft Flying at Low Altitude," Second International Conference on the Aviation Weather System: 220-225 (June 1985).

39. Rustan, P.L., B.P. Kuhlman, and M.J. Reazer. "Airborne Measurements of the Risetimes in Lightning Return Stroke Fields," Proceedings of the 8th International Aerospace and Ground Conference on Lightning and Static Electricity. Paper No 17: 1-9. Fort Worth TX, June 21-23, 1983.
40. Rustan, P.L. and J. Moreau. "Aircraft Lightning Attachment at Low Altitudes," Proceedings of the 10th International Aerospace and Ground Conference on Lightning and Static Electricity. Paris, France, June 10-13, 1985.
41. Rymes, M.D. T3DFD User's Manual: Final Technical Report, August 1979 - June 1981. Prepared for Air Force Flight Dynamics Laboratory (FES), Wright-Patterson AFB, OH. Contract number F-33615-79-C-3412. Electro Magnetic Applications, Inc. (EMA-81-r-24), Denver CO, April 1981.
42. Schowalter, Jeffrey S. Direct Lightning Strikes to Aircraft. Master's Thesis. Air Force Institute of Technology, Wright-Patterson AFB, OH, June 1982 (AD-A118075).
43. Shaeffer, John F. and Gustave L. Weinstock. Aircraft Related Lightning Mechanisms: Technical Report. Contract F33615-71-C-1581. McDonnell Aircraft Company, St Louis MO, October 1972 (AD906805).
44. Siarkiewicz, K.R. "An Introduction to the General Electromagnetic Model for the Analysis of Complex Systems (GEMACS)," RADC-TR-78-181, September 1978 (AD-060319).
45. Siarkiewicz, K.R. "GEMACS - An Executive Summary," Conference on Electromagnetic Compatibility, 1985.
46. Stutzman, Warren L. and Gary A. Thiele. Antenna Theory and Design. New York: John Wiley and Sons, 1981.
47. Tesche, F.M. "Topological Concepts for Internal EMP Interaction," IEEE Transactions on Electromagnetic Compatibility, EMC-20, No 1: 60-64 (February 1978).
48. Uman, Martin A. Lightning. New York: McGraw-Hill Book Company, 1969.
49. Weinstock, G.L. A Realistic Approach to Aircraft Lightning Protection. McDonnell Aircraft Company, St Louis MO, 1983 (AD-P002189/AD-A135100).

50. Williford, Clifford F. Comparison of Absorption and Radiation Boundary Conditions Using a Time-Domain Three-Dimensional Finite Difference Electromagnetic Computer Code. Master's Thesis. Air Force Institute of Technology, Wright-Patterson AFB, OH, November 1985.

VITA

Captain Frank G. Tomko was born on 28 June 1958 in Sommerville, New Jersey. He graduated from Socastee High School, Myrtle Beach, South Carolina, in 1976. He attended the University of South Carolina, graduated Magna Cum Laude in 1980, and received a Bachelor of Science in Applied Mathematics. He attended the AF Officer Training School, Medina Annex, Lackland AFB, Texas, and was commissioned on 6 May 1981. After commissioning, he was selected to attend Auburn University, Auburn, Alabama, until March 1983 when he graduated Magna Cum Laude and received a Bachelor of Science in Electrical Engineering. From Auburn, he was assigned to the Electro-Optics Sensors and Atmospheric Science Group of the Avionics Laboratory, Wright Patterson AFB, Dayton, Ohio. He entered the AFIT School of Engineering in June 1985.

Permanent Address: 237 Pine Street, Myrtle Beach, S.C., 29577

ADH 170 844

# REPORT DOCUMENTATION PAGE

Form Approved  
OMB No. 0704-0188

1a. REPORT SECURITY CLASSIFICATION <b>UNCLASSIFIED</b>			1b. RESTRICTIVE MARKINGS		
2a. SECURITY CLASSIFICATION AUTHORITY			3. DISTRIBUTION/AVAILABILITY OF REPORT Approved for public release; distribution unlimited		
2b. DECLASSIFICATION/DOWNGRADING SCHEDULE					
4. PERFORMING ORGANIZATION REPORT NUMBER(S) AFIT/GE/ENG/86D-10			5. MONITORING ORGANIZATION REPORT NUMBER(S)		
6a. NAME OF PERFORMING ORGANIZATION School of Engineering	6b. OFFICE SYMBOL (if applicable) AFIT/ENG	7a. NAME OF MONITORING ORGANIZATION			
6c. ADDRESS (City, State, and ZIP Code) Air Force Institute of Technology Wright-Patterson AFB, Ohio 45433		7b. ADDRESS (City, State, and ZIP Code)			
8a. NAME OF FUNDING/SPONSORING ORGANIZATION See Box 19	8b. OFFICE SYMBOL (if applicable) AFWL/FIESL	9. PROCUREMENT INSTRUMENT IDENTIFICATION NUMBER			
8c. ADDRESS (City, State, and ZIP Code) Wright-Patterson AFB, Ohio 45433		10. SOURCE OF FUNDING NUMBERS			
		PROGRAM ELEMENT NO. 62201F	PROJECT NO. 2402	TASK NO. 02	WORK UNIT ACCESSION NO. 23
11. TITLE (Include Security Classification) See Box 19					
12. PERSONAL AUTHOR(S) Frank G. Tomko, B.S., Captain, USAF					
13a. TYPE OF REPORT MS Thesis	13b. TIME COVERED FROM _____ TO _____	14. DATE OF REPORT (Year, Month, Day) 1986 December		15. PAGE COUNT 130	
16. SUPPLEMENTARY NOTATION					
17. COSATI CODES			18. SUBJECT TERMS (Continue on reverse if necessary and identify by block number)		
FIELD	GROUP	SUB-GROUP			
09	03		Electromagnetic Scattering		
09	02		Electromagnetic Computer Program		
			Lightning		
			Method of Moments		
19. ABSTRACT (Continue on reverse if necessary and identify by block number)					
Sponsoring Organization: Atmospheric Electricity Hazards Group (AEHG) Flight Dynamics Laboratory					
Title: GEMACS FREQUENCY-DOMAIN ANALYSIS TO DETERMINE THE LIGHTNING INDUCED ELECTROMAGNETIC SKIN CURRENT DISTRIBUTIONS ON AN AIRCRAFT					
Thesis Advisor: Randy Jost, Captain, USAF					
Abstract: See Back					
Approved for public release: LAW AFB 186-1 Lynn E. WOLAVER Dean for Research and Professional Development Air Force Institute of Technology (AFIT) Wright-Patterson AFB OH 45433					
20. DISTRIBUTION/AVAILABILITY OF ABSTRACT <input checked="" type="checkbox"/> UNCLASSIFIED/UNLIMITED <input type="checkbox"/> SAME AS RPT. <input type="checkbox"/> DTIC USERS			21. ABSTRACT SECURITY CLASSIFICATION UNCLASSIFIED		
22a. NAME OF RESPONSIBLE INDIVIDUAL Randy Jost, Captain, USAF			22b. TELEPHONE (Include Area Code) 513/255-3576		22c. OFFICE SYMBOL AFIT/ENG

A frequency-domain electromagnetic (EM) analysis of an aircraft's EM interaction with lightning is performed by using the General EM Model for the Analysis of Complex Systems (GEMACS) to determine the EM skin current distributions on the surface of a FAA CV-580 aircraft. The Method of Moments (MOM) is incorporated in GEMACS to provide an approximate solution to Maxwell's integral equations and to determine the aircraft surface currents. A 384 segment wire grid model of the CV-580 and lightning channels is constructed for the analysis; two variations of modelling the channels are implemented. The GEMACS analysis is performed for frequencies of 0.5 MHz to 5.0 MHz, in 0.5 MHz increments. The GEMACS' predicted segment currents are used to derive wire grid frequency-domain transfer functions which are compared to: (1) actual aircraft transfer functions obtained from in-flight lightning measurements, and (2) transfer functions generated from a previously performed time-domain three-dimensional finite difference (T3DFD) EM program analysis. Results show that GEMACS can be implemented to adequately predict lightning induced aircraft skin current distributions and associated aircraft resonant frequencies. Also, GEMACS provides more EM interaction information than T3DFD and, based on CPU run times, predicts this information much more efficiently.

END

5-87

DTIC